UNIVERSITY OF MINES AND TECHNOLOGY

TARKWA

FACULTY OF GEOSCIENCES AND ENVIRONMENTAL STUDIES

DEPARTMENT OF GEOLOGICAL ENGINEERING

A THESIS REPORT ENTITLED

PETROGRAPHY AND GEOCHEMISTRY OF TARKWAIAN QUARTZITES AT AMOANDA PIT AND BANKET CONGLOMERATES AT SADDLE PIT AND THEIR RELATIONSHIP WITH MAFIC INTRUSIVES IN THE AREA

BY

EMMANUEL KOFI TEYE

SUBMITTED IN PARTIAL FULFILLMENT OF THE REQUIREMENT FOR THE AWARD OF THE DEGREE OF MASTER OF SCIENCE IN GEOLOGICAL ENGINERRING

THESIS SUPERVISOR

……

DR G. M. TETTEH

TARKWA, GHANA

OCTOBER, 2021

DECLARATION

I declare that this thesis is my own work. It is being submitted for the Degree of Master of Science in Geological Engineering at the University of Mines and Technology (UMaT), Tarkwa. It has not been submitted for any degree or examination in any other University.

…….

(Signature of Student)

Submitted this …… day of …….. 2021

ABSTRACT

Thin and polished sections of thirty-six rock samples from Amoanda Pit in the Tarkwaian showed that the banket footwall quartzites contain mainly quartz, chlorite, plagioclase, amphibole and minor sericite, epidote, chalcopyrite, pyrite, magnetite, hematite and trace gold. The protoliths of the rock were probably sublitharenite, feldspathic litharenite and litharenite. Overlying banket conglomerate at the Saddle Pit is oligomictic or polymictic with large rounded pebbles and moderately sorted quartz, chert, schist, and hornstone; the matrix is made up of quartz, plagioclase feldspars, sericite, chlorite, garnet and amphiboles. At the Saddle Pit, diorite sills and dykes contain mainly plagioclase feldspars, amphibole, chlorite, sericite and quartz with minor epidote, biotite, garnet, pyroxene, pyrite, pyrrhotite and chalcopyrite. Pyrite is partially altered to secondary hematite and magnetite. The intrusive heat might have introduced secondary amorphous gold other than the palaeoplacer granular gold in the banket footwall quartzite and the conglomerate. Post placer gold was secondary mainly at the contacts with diorite and associated with second generation hematite and magnetite. Generally the rocks were affected by greenshist facies metamorphism which post-date peak amphibolite facies. Whole rock XRF analyses show Al_2O_3 range from 6.86 to 26.6 wt% possibly due to plagioclase which is partially altered to sericite and quartz. Eu anomaly values are greater than 1 probably due to plagioclase accumulation while high total REE could be due to high alteration of the rocks.

DEDICATION

To my wife, Ida and my children, Briana and Emmanuel.

ACKNOWLEDGEMENT

First and foremost, praises and thanks to God, the Almighty, for His protection to complete this research successfully.

I would like to express my deep and sincere gratitude to my supervisor, Dr George Mensah Tetteh for his supervisory roles and invaluable support during this work. His patience and coaching enabled me to complete this thesis successfully.

I am also grateful to the lecturers and staff of the Department of Geological Engineering, UMaT and most especially to Assoc Prof Anthony Ewusi and Dr Kofi Adomako Ansah for their support by way of provision of materials and advice. Mr Clement Benyarko assisted with the thin and polished section preparation.

Finally, my sincere thanks goes to the entire workforce of Aboso Goldfields Limited (AGL), Damang Gold Mine for their support towards the success of this work.

TABLE OF CONTENTS

LIST OF FIGURES

LIST OF TABLES

CHAPTER ONE

INTRODUCTION

1.1 Problem Definition

Examples of Palaeoplacer gold deposits formed by sedimentary processes are the Witwatersrand deposits in South Africa, the Jacobina deposits in Brazil and the Tarkwaian deposit in Ghana. Gold bearing pebble conglomerate and related arenaceous rock were formed in fluviatile to deltaic environment (Robert *et al.,* 1997). Mineralogy and trace element geochemistry of the shale units show post-burial alterations of chloritoid and pyrophyllite (Phillips and Powell, 2015). The pyrophyllite-rich material formed sub-parallel to bedding, commonly at lithological contact. Most intense alteration zone especially at the base or top of the conglomerate units containing pure pyrophyllite are marked by compressional deformation, muscovite, chlorite, pyrite and quartz overgrowth (Barnicoat *et al.*, 1997).

The Jacobina deposit in Brazil is made up of pyritic quartz-pebble metaconglomerates and quartzite intercalations of the Serra do Corrego Formation (Batista *et al.,* 2001). The basin contains structurally-controlled hydrothermal orebodies, and gold occurrences in quartzites (Batista *et al.,* 2001). There is high concentration of gold within the pyrite-Cr bearing mineral and tourmaline assemblages that crystallised over andalusite (Milesi *et al.,* 2001). The conglomerate matrix has been entirely recrystallised to fine-grained quartzite with sulphides, fuchsite, fine chromiferous rutile, tourmaline and chromite in the pore spaces with andalusite, accessory kyanite and sillimanite along foliations; phlogopite and fuchsite occur at the contact with ultrabasic dykes (Ledru *et al.,* 1997).

In Ghana metamorphosed Palaeoproterozoic (2300-1900 Ma) rocks of the volcano-sedimentary rocks of Birimian Supergroup and the overlying clastic sedimentary Tarkwaian Group (Oberthür *et al.,* 1998 and Griffis *et al.,* 2002). The Tarkwaian sandstones, conglomerates and argillites found within many of the volcanic belts especially the Ashanti Belt and occurrences have also been found on the eastern margin of the Sefwi Belt, in the Kibi-Winneba belt and the Nangodi Belt (Fig. 1.1) (Griffis *et al.,* 2002). The clastics are erosion products of the Birimian supracrustal rocks and the belt-type plutons and deposited in long, narrow intramontane grabens, which formed as the result of rifting preferentially in the central portions of the volcanic belts (Leube *et al.,* 1990).

The Tarkwaian rocks from the youngest include: the Huni Sandstone; the Tarkwa Phyllite; the Banket Series (also referred to as Banket Formation); and the Kawere Group (Kesse, 1985). Banket Series made-up of placer gold bearing quartz-pebble conglomerate with pebbles derived from the Birimian; it is interbedded with cross-bedded sandstones. Contained within the Banket Series, are four quartz-lithic pebble metaconglomerate horizons that host high grades of palaeoplacer-type gold mineralisation. Gold within the metaconglomerates is associated with other heavy mineral grains and occurs between clasts of vein quartz, quartzite and Birimian metavolcanic rocks (Junner *et al.*, 1942 and Leube *et al.*, 1990). Birimian metasedimentary rocks are divided into volcanoclastic rocks, turbidite-related wackes, argillitic rocks and chemical sediments with gradational boundaries (Leube *et al.*, 1990). The Tarkwaian rocks unconformably overly, or are faulted against, Birimian metavolcanic rocks metamorphosed to green-schist facies. (Leube *et al.*, 1990).

Amoanda resource is located 7 km south-west of Damang on the west limb of the Damang Anticline. Mineralisation is in the banket footwall quartzite and strata defines a north plunging antiform with an axial plane that plunges north. Gold mineralisation is associated with flat-lying, planar, narrow quartz veins that are carbonate ± pyrite ± pyrrhotite bearing (Leube *et al.*, 1990). Veins occur predominantly in banket footwall quartzite but also occur within the late stage diorite porphyry that intrudes the Western Birimian Fault. Although the mineralogy of the mineralised veins is dominated by quartz, accessory gangue minerals also include carbonate, albite and tourmaline; all associated with oxidised fluid sources. In addition, mineralised veins in diorite also contain minor chalcopyrite and sphalerite suggestive of a base-metal bearing fluid source (Leube *et al.*, 1990). Mineralised veins are typically not well-developed within Birimian volcaniclastic units or Kawere Conglomerate (Sharpe, 2005).

Saddle Pit, which is the immediate north extension of the main Saddle Pit at the eastern limb of the Damang anticline contains Tarkwaian metasedimentary and Birimian metavolcanic units, with the latter occupying the core of the Damang anticline (Tunks *et al*, 2004). Matrices of pebbles in the Tarkwaian conglomerates are enriched in heavy minerals such as hematite, magnetite, ilmenite, rutile, zircon and gold (Strogen, 1988; Marston *et al.*, 1992). In the Tarkwa and Damang regions, mafic sills and dykes are found within the Tarkwaian stratigraphic section (Junner *et al.*, 1942). These mafic rocks are metamorphosed dolerite, gabbro, microdiorite and tonalite (Brabham, 1998). There are two distinct styles of mineralization at Damang - the first is solely associated with the conglomerate horizons

within the Banket Series where there is free gold (Tunks *et al.*, 2004). And the second is associated with quartz veins associated with alteration halos (Tunks *et al.*, 2004). Mineralisation at Damang Gold Mine is found in the Tarkwaian banket conglomerate and dolerites affected by mid-amphibolite facies metamorphism with temperature estimates of 550^{o}C based on garnet–biotite geothermometry (Pigois *et al.*, 2003).

Studies at Damang shows sedimentary planar or cross bedded structures in the banket footwall quartzite are preserved but the concentrations of heavy minerals (magnetite) are significantly reduced due to the sulphidation of the detrital magnetite (Sharpe, 2005). In addition, quartz-sericite-pyrite is the main alteration type in banket footwall quartzite with abundant disseminated sulphides and quartz veining (Sharpe, 2005). The sulphides are mainly pyrite with minor to trace levels of pyrrhotite and chalcopyrite (White, 2010).

The purpose of this research is to investigate the petrography, geochemistry of the Tarkwaian Palaeoplacer quartzite at Amoanda Pit and the banket conglomerate of the Saddle Pit and their intrusives to relate to variable gold grade.

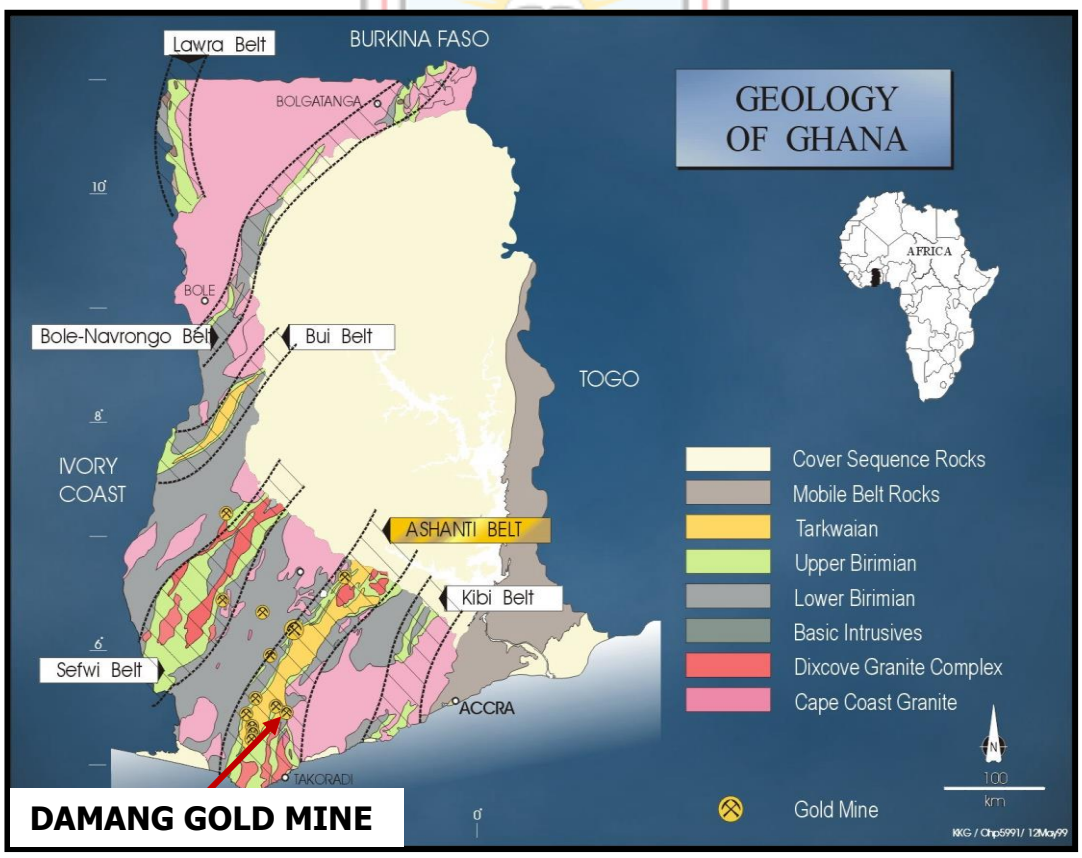

Fig. 1.1 Geology Map of Ghana showing the location of the Study Area (after, Leube *et al.*, 1990)

1.2 Research Objectives

The objectives of this thesis are:

- To deduce the mineralogical and textural changes of the rocks;
- To deduce the types of metamorphism and alteration of the rocks;
- To study the major and trace elements geochemistry in relation to protoliths and alterations of the rocks;
- To relate the mineralogy, metamorphism, alteration and geochemistry to the counterpact rocks at the neighboring Tarkwa mine.

1.3 Methods Used

Methods used in this research include:

- Review of relevant literature;
- Pit mapping;
- Petrographic description of rocks;
- Whole rock X-Ray Fluorescence analysis;
- Plots on geochemistry variation diagrams using excel.

1.4 Facilities Used

Facilities that were employed include;

- Library and Internet facilities at University of Mines and Technology (UMaT), Tarkwa;
- MapInfo software to plot the location of samples collected;
- Australian Laboratory Services (ALS) in Canada for major/minor and trace element analysis;
- AAS analysis for gold at SGS laboratory in Ghana;
- SM Lux Leitz 7000 microscope at the Petrology Laboratory UMaT, Tarkwa;

1.5 Thesis Organisation

The thesis is organised into six (6) chapters with each chapter addressing main headings as follows:

Chapter one is the introduction of the thesis containing the problem definition, research objectives, methods and facilities used.

Chapter two entails the literature review of the West Africa Craton, the geology of the Birimian, the geology of the Tarkwaian Group and the metamorphism of the Tarkwaian.

Chapter three deals with the various methods used for the research.

Chapter four is about the results presentation.

Chapter five discusses the results from the petrological and geochemical investigations.

Chapter six draws conclusions and gives recommendations on the research work.

CHAPTER TWO

LITERATURE REVIEW

2.1 West African Craton

The West African Craton is one of the five cratons of the Precambrian basement of Africa which make up the African plate, the others being the Kalahari craton, Congo craton, Saharan Metacraton and Tanzania craton (Jessell and Liégeois, 2015). These land masses came together to form the African continent in the late Precambrian to early Paleozoic eras (Doblas *et al.*, 2002). The West African craton stretches from the Little Atlas mountains of Morocco to Gulf of Guinea, underlies countries of Morocco, Algeria, Mauritania, Senegal, Gambia, Guinea Bissau, Guinea, Mali, Burkina Faso, Sierra Leone, Liberia, La Cote D'Ivoire, Ghana, Togo and Benin. The West African craton, comprises rocks of the Birim Supergroup, covers an extensive region in West Africa. This succession is considered to represent a late Palaeoproterozoic juvenile crust forming event, lasting from about 2.25 to 2.05 Ga, which was accompanied by the Eburnean orogenesis at about 2.1 Ga. The metasedimentary rocks were grouped into unclear upper and lower Birimian strata, while the igneous bodies were classified as belt and basin types (de Kock *et al.,* 2011). The West African craton presents two principal zones of outcrop: the Reguibat shield in the north and the Man shield (also called Leo shield or Guinea Rise) in the south. The southern part of the West African craton, i.e. the Man Shield, stretches over several countries, namely: Côte d'Ivoire, Ghana, Mali, Burkina Faso, Guinea, Liberia, Sierra Leone, west Niger, and north Togo (Fig. 2.1).

The Man shield is made up of two domains: (1) an Archean nucleus, called Kenema-Man domain, which is composed of geological formations structured during the Leonian and the Liberian orogenies and thus known as Leonian and Liberian formations; (2) a Palaeoproterozoic domain or Baoulé-Mossi domain, with relics of Archean basement. In this domain occur Birimian and Tarkwaian rocks (Assie, 2008).

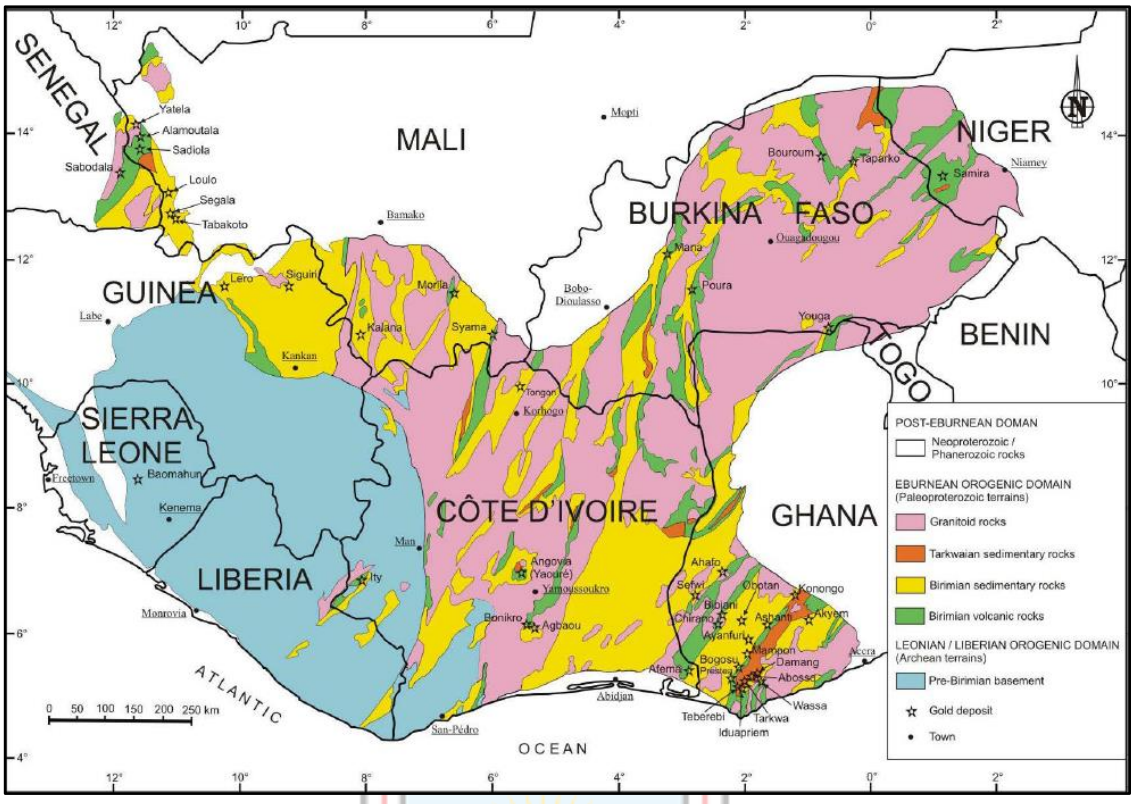

Fig. 2.1 Regional Geology of Man Shield and location of Major Known Gold Deposits (modified after Milési *et al.*, 1992)

2.2 The Birimian of Ghana

The Birimian (also termed Birimian Supergroup) represents geological formations deposited during the Eburnean orogeny over a maximum time interval of ca. 2.27 Ga to 2.05 Ga (Abouchami *et al.,* 1990; Boher *et al.,* 1992; Hirdes *et al.,* 1992; Hirdes *et al.,* 1996; Oberthür *et al.,* 1998; Hirdes and Davis, 2002; Pigois *et al.,* 2003). It extends across the western half of Ghana, Cote D'Ivoire, southern Mali, Burkina Faso, Senegal and the west of Niger.

Birimian rocks are made up of metamorphosed sedimentary and volcanogenic rocks with metamorphosed pyroclastic members (Dzigbodi - Adjimah, 1988). The meta-sedimentary rocks (formerly referred to as Lower Birimian) are regarded as "basin" deposits and are separated by "belt" deposits which are sub-parallel series of northeast trending volcanogenic rocks (formerly referred to Upper Birimian), (Allibone *et al.,* 2002a). The volcanic belts are typically 15- 40 km wide and about 60 - 90 km apart. These volcanics belts from southwest to northeast of Ghana are; the Kibi-Winneba, Ashanti, Sefwi, Bui, Bole-Navrongo and the

Lawra belt which trends N-S (Leube *et al.*,1990). Figure 2.2 shows the six (6) volcanic belts in Ghana.

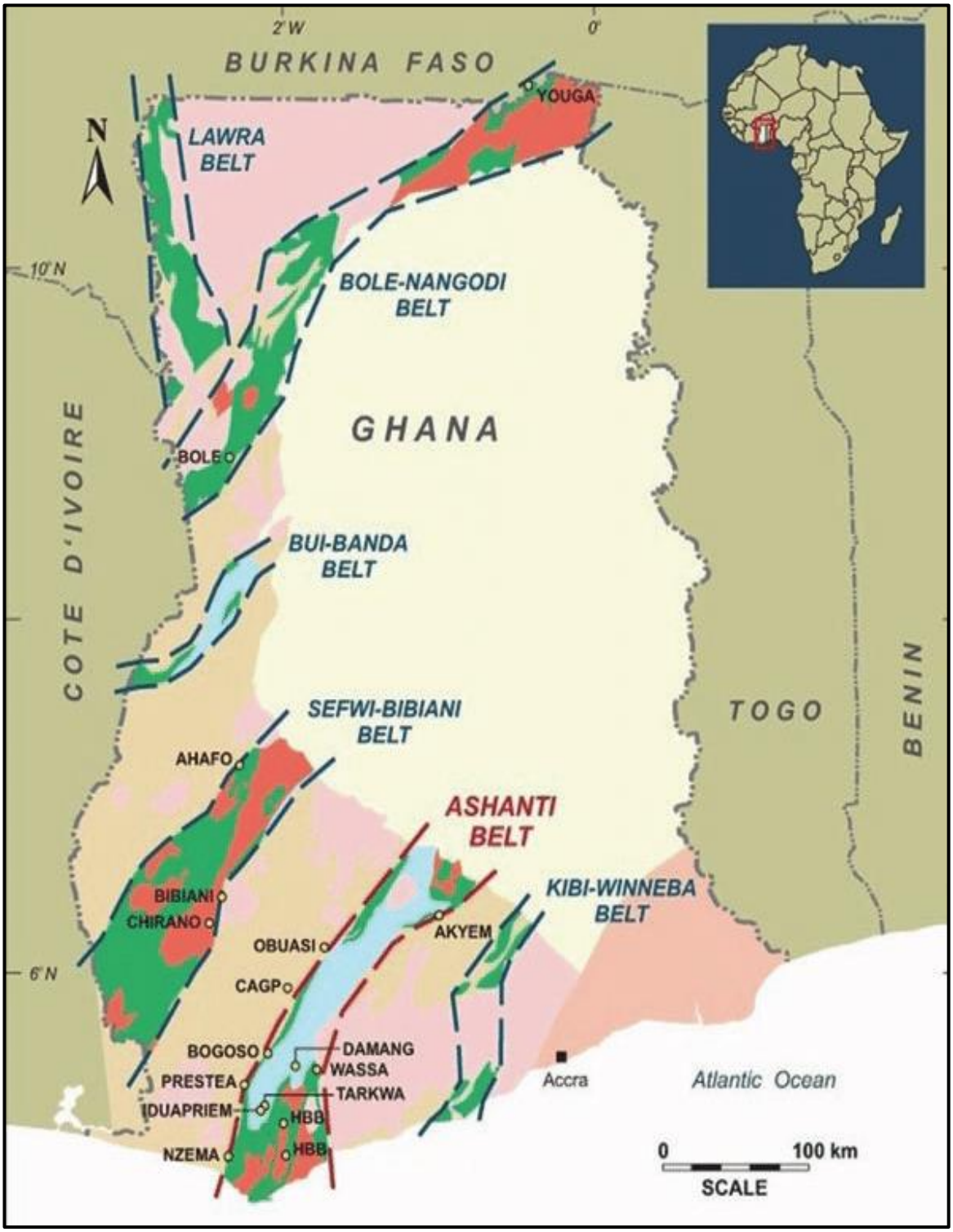

Fig. 2.2 A Geological Map of Ghana showing the Gold Belts and location of Damang (Kesse, 1985)

Though Trashliev (1972) and Asihene and Barning (1975) suggested a stratigraphic break between the metasedimentary and metavolcanic rocks, Leube *et al.,* (1990) proposed a lateral facies between Birimian metavolcanic rocks and metasedimentary rocks which together are related in origin. These put to rest an earlier controversy about the evolution of the Birimian rocks of Ghana where the Anglophone geologists were of the opinion that the metasedimentary rocks were older than the metavolcanic rocks but reversed by the Francophone geologists (Tagini, 1971; Papon, 1973; Bessoles, 1977 and Attoh, 1980). Leube *et al.,* (1990) and Hirdes *et al.,* (1993) based on plate tectonic concepts, regard the Birimian metasedimentary rocks as having evolved from volcanic island arcs and ridges within old Archaean sialic crust whilst the volcanic rocks were derived from contemporaneous igneous activity within volcanic belts that were located at the edges of the depositional basins. Milési *et al.,* (1991) viewed the evolution of the Birimian as having formed from volcanic belts and sedimentary basins within the West African Craton and subsequent collision.

The metasedimentary rocks and metavolcanic rocks of the Birimian have been folded, metamorphosed and intruded by various granitic bodies grouped into basin and belt granitoids. The basin granitoids are post-Birimian and pre-Tarkwaian and were classified as G1 or Cape Coast granitoids. The belt granitoids are younger and commonly found within the volcanic belts and were referred to as Dixcove or G2 granitoids (Kesse, 1985; Leube *et al.,* 1990). The belt granitoids occur in concordant batholiths accompanied by pegmatites and quartz veins (Kesse, 1985).

2.3 Tarkwaian Group

The Damang concession is located on the Man-Leo Shield within the southern Ashanti Belt. In order to understand the local geology of the Damang property, it is important to consider the geology of the Tarkwaian which is located in the Ashanti belt of which Damang forms part.

The Tarkwaian is one of four major palaeoplacers in the western world of late Archaean to Palaeoproterozoic age from which mineral commodities such as gold, uranium, thorium, platinum group elements and diamonds are produced. The others are the Witwatersrand goldfields of South Africa (Anon, 1990), the Elliot Lake uranium field of Canada (Roscoe and Card, 1992), and the Sierra de Jacobina goldfields of Brazil (Molinari and Scarpelli, 1988). While these latter deposits all carry as major constituents heavy minerals which are

stable under reducing, or at least oxygen-deficient, atmospheric conditions (pyrite, uraninite), the palaeoplacer ores of the Tarkwaian comprise a gold-magnetite-hematite-(ilmenite) paragenesis which is largely comparable to the "black sand paragenesis" encountered in the present-day placers (Davis *et al.*,1994).

The term Tarkwaian (or Tarkwaian Group) refers to clastic sedimentary rocks representing erosional products of Birimian provenance. In Ghana, the Tarkwaian Group is best developed within the Ashanti Belt and occurrences have also been found on the eastern margin of the Sefwi Belt, in the Kibi-Winneba belt and the Nangodi Belt (Griffis *et al.*, 2002). The sediments of the Tarkwaian Group consist of conglomerates, sandstones and minor argillites metamorphosed to low grade. The clastic sedimentary rocks were deposited in a basin, which is isoclinally folded with volcaniclastics, wackes, argillite and conglomerate (Leube *et al.*, 1990; Hirdes *et al.*, 1992; Davis *et al.*, 1994). They are thought to be erosion products of the Birimian supracrustal rocks and the belt-type plutons and to have been deposited in long, narrow intramontane grabens, which formed as a result of rifting preferentially in the central portions of all the five Birimian volcanic belts (Leube *et al.*, 1990). The Tarkwaian rests unconformably on the Birimian (Ntiamoah-Agyakwa, 1979; Leube *et al.*, 1990; Milesi *et al.*, 1989, 1992). The Tarkwaian consists of a subordinate arenaceous and conglomeratic sequence occurring among the Birimian Supergroup (Wright *et al.*, 1985; Milési *et al.*, 1992). Davis *et al.*, (1994) indicated that the maximum age of Tarkwaian sedimentation is 2132 ± 3 Ma.

Classification of the Tarkwaian Group was first devised by Junner (1940) who subdivided the sedimentary succession into four major units: the Kawere Group, Banket Series, Tarkwa Phyllite and Huni Sandstone. The best exposure and preservation of Tarkwaian Group rocks occurs within the Ashanti Belt, with equivalent successions from volcanic belts reported elsewhere within West Africa (Griffis *et al.*, 2002). Table 2.1 shows the stratigraphy of the Tarkwian System by Kesse (1985). Stratigraphic correlation of Tarkwaian strata at Damang is given in Fig. 2.3.

Table 2.1 Stratigraphy of the Tarkwaian System (After Kesse, 1985)

Unit	Thickness (m)	Composite Lithology
Huni Sandstone	1370	Sandstone, grits, quartzite, phyllite (Dompim type)
Tarkwa Phyllite	120 - 400	Phyllite and schists
Banket Series	120 -160	Quartzite, grits, breccia and banket quartz conglomerates
Kawere Group	250 - 700	Sandstone, quartzite, grits, and polymictic conglomerate

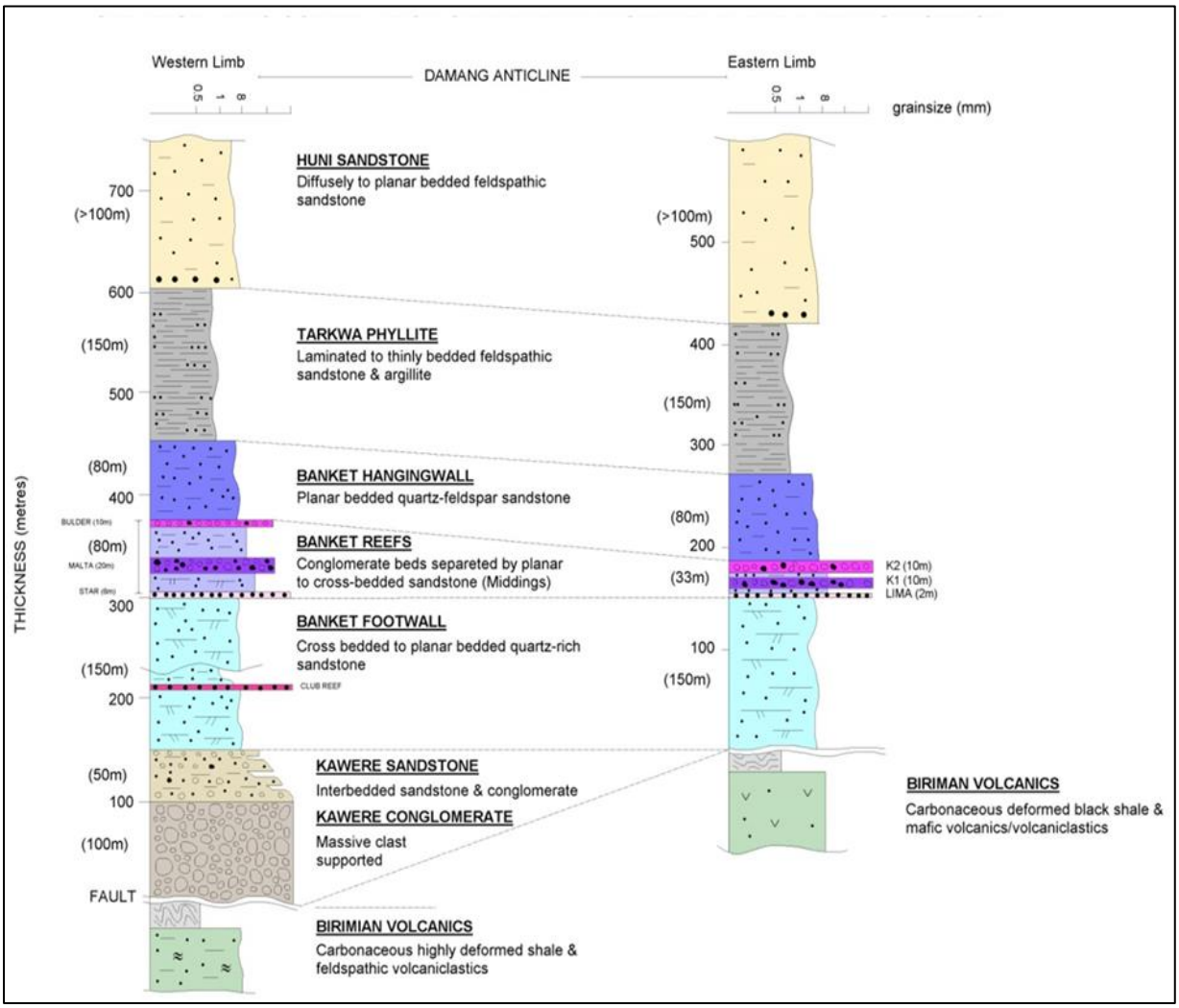

Fig. 2.3 Stratigraphic Correlation of Tarkwaian Strata between East and West Limbs of the Damang Anticline (Sharpe, 2005)

Kesse (1985) reports that the Tarkwaian is characterised by the predominance of coarse grained, immature sedimentary units. The stratigraphy of the Tarkwaian from oldest to youngest is as follows:

2.3.1 Kawere Group

The Kawere Group consist of poorly sorted, polymictic conglomerates and quartzites with no significant mineralisation and typically of shallow water greenish grey, feldspathic, carbonate-spotted quartzites, grits, breccias and conglomerates. The most conspicuous of the group are the conglomerates with inter-bedded grits and quartzites. The conglomerates normally consist predominantly of closely packed pebbles of very fine grained, silicified Birimian greenstones in a matrix of quartz, feldspar, chlorite, carbonate, epidote and magnetite. The quartzite and grits are normally greenish grey and poorly bedded (Junner, 1940).

2.3.2 Banket Series

They consist of well-sorted conglomerates and quartzites with clasts generally considered to be Birimian in origin and containing significant gold mineralisation, hosting the Damang ore-body; represents a fluviatile series with a thickness varying between 120-160m being greater south and west of Tarkwa. It is essentially an accumulation of high energy, coarse clastics, represented by conglomerates, grits and quartzites which have suffered low-grade metamorphism. Three of the units are persistent made up of breccia reef, middle reef and a unit of basal conglomerates which host the majority of the mineralization. The basal conglomerate is generally better sorted than the other reefs and more uniform in thickness, composition, size and in distribution of pebbles. The matrix of the conglomerates consists principally of quartz and sand (mainly hematite with ilmenite, magnetite and rutile). Minor constituents are sericite, chlorite, tourmaline, garnet, zircon and gold. Epidote and pyrite are rare except near dykes, faults and quartz veins.

2.3.3 Tarkwa Phyllite Series

They are fine grained chloritic siltstones, mudstones and schists with no significant mineralisation and are divided into those with and without chloritoid. The chloritoid phyllites may or may not contain porphyroblasts of carbonate. The phyllites without chloritoid vary from sandy to fine-grained lustrous types and may contain abundant magnetite and/or hematite. Colour banding is common and is due to alternating bands of

sericite or chlorite. Another type of banding is due to alternating sandy and fine-grained material.

2.3.4 Huni Sandstone

They are fine grained massive quartzites with no significant mineralisation. The sandstone is the weathered representation of feldspathic quartzites, which are in general finer than the Banket Series quartzites. They are grey, greenish or bluish in outcrops and weather to pale grey and green. They often show distinct magnetite banding and may be cross-bedded. Dompim phyllites and Dompim quartzites are now known to form part of Huni Sandstone and the whole formation. The Dompim phyllites are separated from the Tarkwa Phyllites by quartzites and sandstones.

2.4 Metamorphism of the Tarkwaian Group

There is a general consensus that the predominant metamorphic assemblage of SW Ghana is widely retrograde from peak amphibolite facies metamorphism representing peak conditions least 500º to 650ºC at 5-6 k.bar (Griffis *et al.,* 2002; Brabham, 1998, Pigois et al., 2003, Tunks et al., 2004). At Damang, peak metamorphism is recorded in more argillic units to have a garnet, biotite, plagioclase, ±staurolite, ±epidote, ±kyanite, ±cordierite assemblage that is retrograde to chlorite-muscovite-quartz (Sharpe, 2005). This metamorphic assemblage supports peak metamorphic temperatures in the range of 500º to 600ºC and pressures >5kbar, with garnet-biotite geothermometry by Pigois *et al.,* (2003) indicating an average peak metamorphic temperature of 550ºC. Age constraints on peak metamorphism (Oberthür *et al.,* 1998 in Pigois *et al.,* 2003) yield a minimum age of metamorphism between 2110 and 2080 Ma.

CHAPTER THREE

METHODS USED

This chapter outlines the various procedures and methods that were used in the selection of samples, their preparation and analyses. These methods include

- Pit mapping of the study area
- Thin and polish section preparation
- Whole rock geochemical analysis

3.1 Pit Mapping

Pit mapping aided in field description and hand specimen description of banket footwall quartzite, banket conglomerate and mafic intrusives at the Damang mine gold deposit. Locations of samples that were collected were marked and later collected by surveyors and descriptions of samples recorded. Measurements of structures such as bedding and foliations were also carried out (Fig. 3.1).

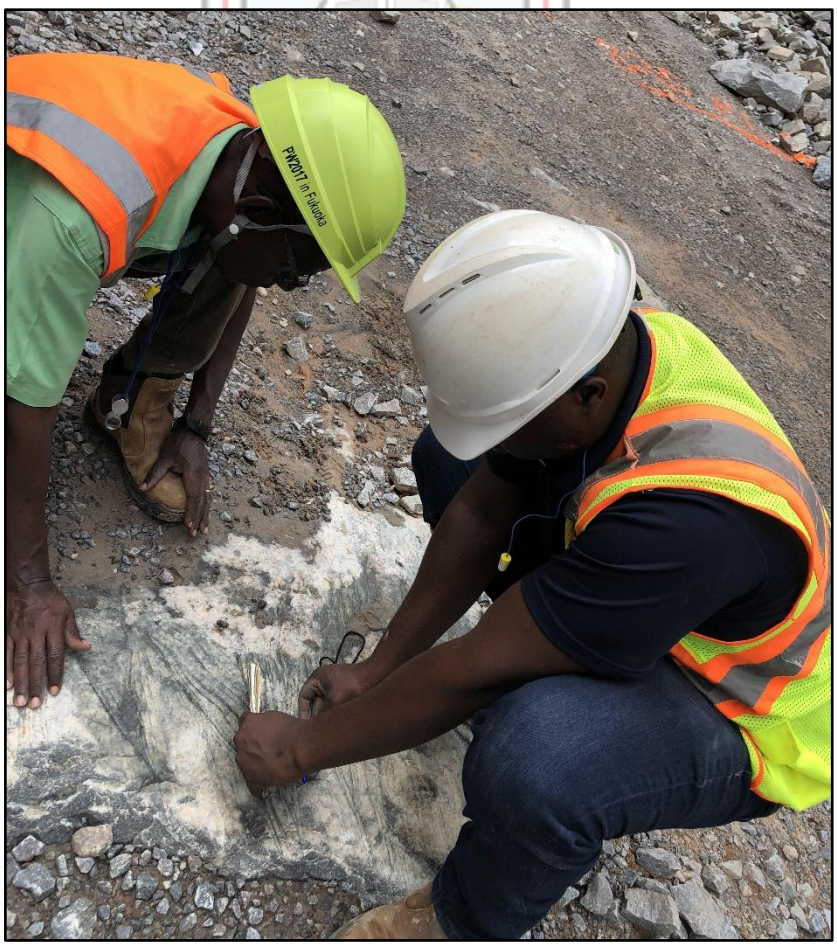

Fig. 3.1 Measurement of bedding and foliation in Banket Footwall Quartzite

A total of thirty-six (36) samples were collected from both the Amoanda and Saddle Pits and described accordingly in Appendix A. The samples for petrographic and geochemical studies were sampled for the three (3) rock types. MapInfo software was used to plot the sample points that were obtained from the pit (Fig. 3.2 and Fig. 3.3)

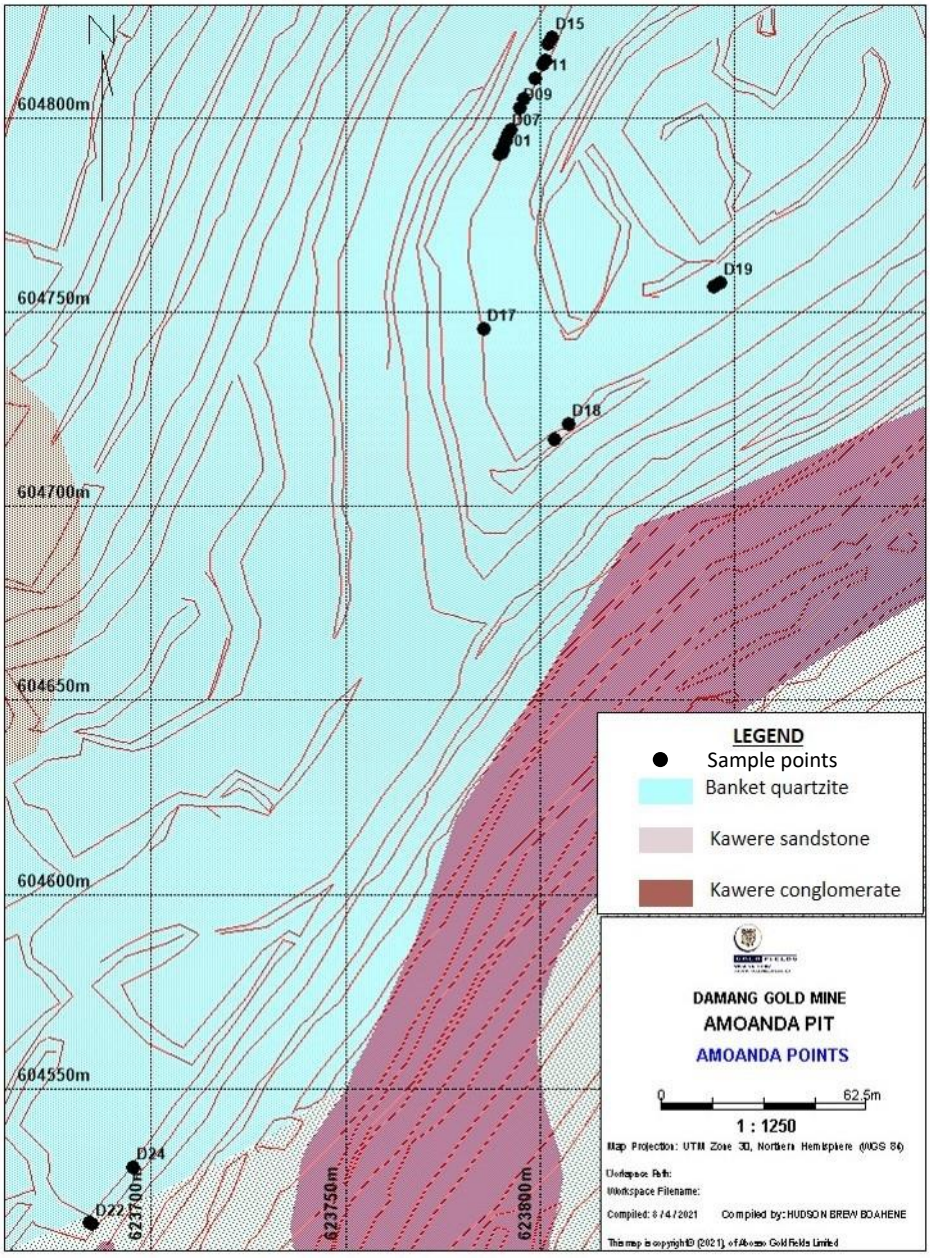

Fig. 3.2 Geology Map showing Sample Points at Amoanda Pit

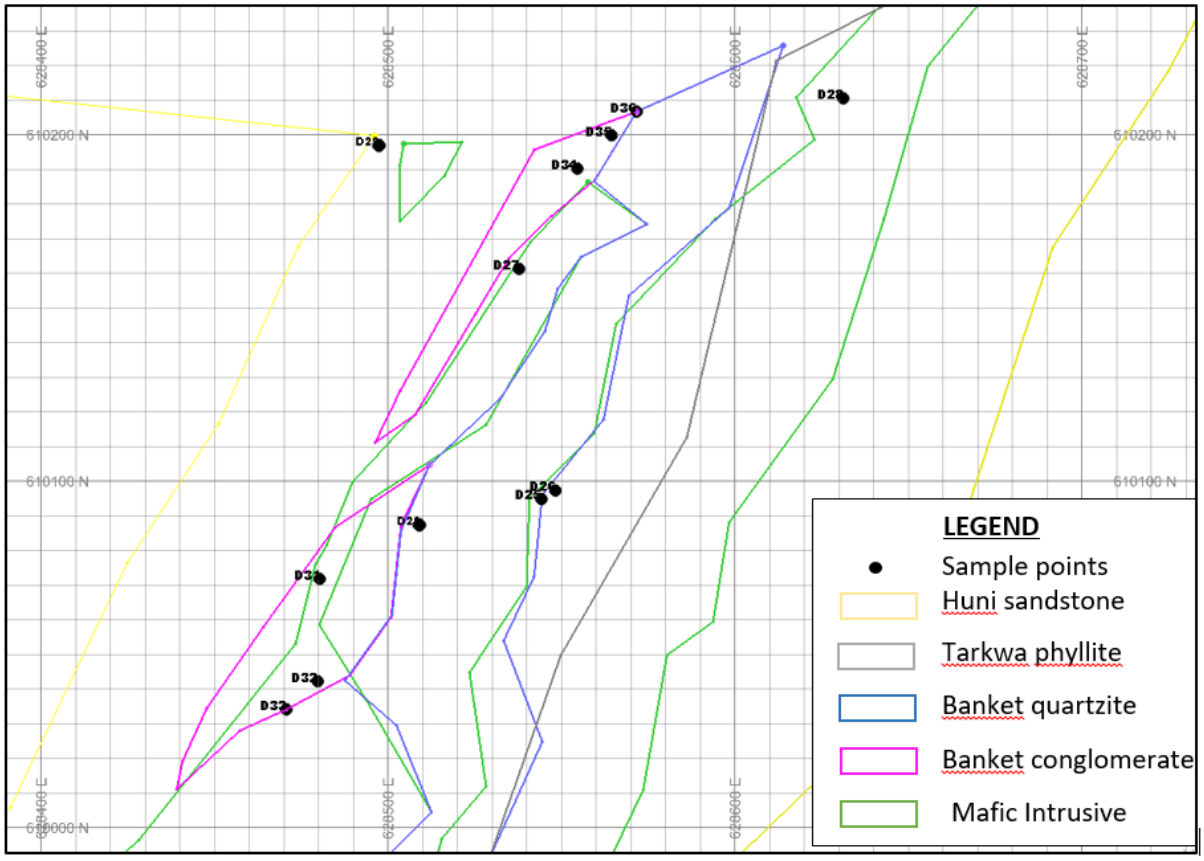

Fig. 3.3 Geology Map showing Sample Points at Saddle Pit

3.2 Thin and Polish Section Preparation

Rock samples from the Amoanda and Saddle pits collected were cut with the use of electric core cutting machine such that they will be a true reflection or representation of the entire rock types. Thin and polished sections of the rock samples were prepared at the Geological Engineering Laboratory of the University of Mines and Technology (UMaT), Tarkwa. Preparation of the thin and polished sections was carried out according to the guidelines of Hutchison (1974).

The thin and polished sections were studied for mineral composition and textures with the use of SM Lux Leitz microscope at the Geological Engineering Laboratory at UMaT, Tarkwa. References were made to Elsevier's Mineral and Rock Table during the polished section investigation (Lof, 1982). Minerals were identified using their colour, pleochroism, reflectivity, hardness, texture, bireflectance, internal reflection and anisotropy compiled by Picot *et al.*, (1982) and Craig and Vaughan (1994). Modal percentages of mineral composition determined using the standard modal percentage chart and point counting were

normalised and plotted on QAP diagram (Streckeisen, 1974). The mineral abbreviations (Appendix B) were after Whitney and Evans (2010).

3.3 Whole Rock Geochemical Analysis

Major and trace element (XRF) analysis of the rocks were used to ascertain the composition of the protolith, the altered and unaltered rocks and the environment of formation or deposition of these rocks were deduced.

Twelve (12) representative samples out of the thirty-six (36) samples were sent to Australian Laboratory Services (ALS) in Canada for whole rock geochemical analysis. Seven (7) out of the twelve (12) samples are unaltered whilst five (5) are altered.

Standard procedures were followed during the sample preparation and analysis. The samples were weighed, crushed using mechanical crusher to about 70% below 2 mm and split using the riffle splitter and then pulverised using the agate mortar to about 85% and made to pass through <75 µm to obtain powdered samples. Glass discs were prepared from each powdered samples using lithium borate flux composed of 50% lithium tetraborate ($Li_2B_4O_7$) and lithium borate ($LiBO_2$). 0.9g of ignited or calcined powdered samples were added to 9.0g of lithium borate flux, mixed well and fused in an auto fluxer between 1050^oC to 1100^oC. A flat molten glass disc was prepared from the resulting melt. The disc was then analysed by X-ray fluorescence spectrometry for major oxides using the XRF-06 machine with the upper and lower detection limits being 100% and 0.01% respectively.

Minor and trace elements were analysed using multi element-mass spectrometer. Prepared specimens (0.25 g) were digested using Perchloric ($HClO_4$), Hydrofluoric (HF), Nitric (HNO_3) and Hydrochloric (HCL) acids. The resultant constituents were topped up with dilute hydrochloric acid and analysed by inductively coupled plasma-atomic emission spectroscopy (ICP-AES). Following this analysis, the results were reviewed for high concentrations of bismuth, mercury, molybdenum silver and tungsten, and diluted accordingly. Samples were then analysed by inductively coupled plasma-mass spectrometry (ICP-MS). Results were corrected for spectral inter-element interferences. Standard reference samples were used in the quantitative analyses of the elements. Details of the analytical procedure, accuracy, precision and standards were available at the Australian Laboratory Services (ALS), Canada. Major, minor, trace and REE element compositions of the analysed rocks from Amoanda and Saddle pits are given in Appendix E. Thirteen (13)

major oxides (SiO_2, Al_2O_3, Fe_2O_3, CaO, MgO, Na_2O, K_2O, Cr_2O_3, TiO_2, MnO, P_2O_5, SrO, BaO) were analysed.

CHAPTER 4

RESULTS

4.1 Petrography

This involves field description of hand specimens and microscopic studies in transmitted light and reflected light of the banket footwall quartzite, banket conglomerate and mafic intrusives of the Damang gold deposit. Selection of the samples was done after pit mapping.

4.1.1 Banket Footwall Quartzite

In the Amoanda Pit, the banket footwall quartzite is found adjacent to the Western Birimian Fault and is structurally east dipping (Sharpe, 2005). Unaltered rock is medium to dark grey arenaceous metasedimentary rocks. It shows trough cross bedding defined by concentrations of heavy minerals (Fig. 4.1). The banket footwall quartzite is characterised by cross bed forsets marked by magnetite. Altered banket footwall quartzite is pink to pinkish grey with characteristic heavy mineral concentrations along foliation planes. The rock is also characterised by high quartz alteration mostly flat lying with milky quartz veins along foliation and occasional sulphides which occur in the rock (Fig. 4.2).

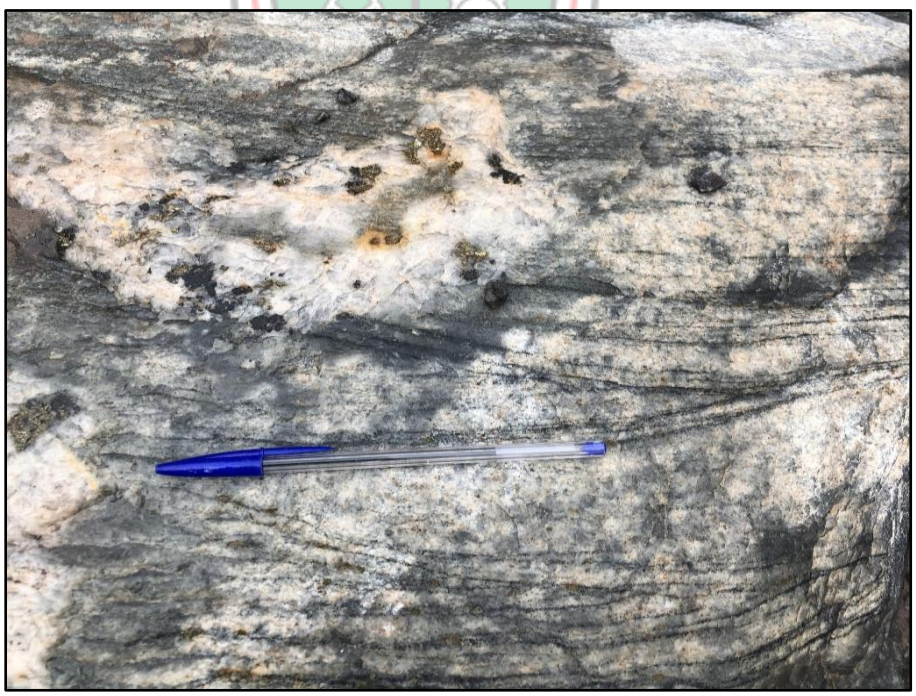

Fig. 4.1 Photograph of banket footwall quartzite showing trough cross bedding marked by heavy minerals

Fig. 4.2 Photograph of banket footwall quartzite showing quartz vein

In hand specimen, the rock is light grey to dark grey. Quartz grains are medium grained, moderately sorted, sub-rounded to rounded with a few sheared especially along foliation planes. Quartz grains range from 10mm to 25mm in diameter. The fragments are fine grained in the quartz dominant layers. The quartz grains are recrystallised into fine quartz veinlets at an angle to the bedding plane. These also offset a contoured plagioclase that cuts across the bedding plane and is disseminated throughout the rock. Some of these plagioclase occurs parallel to the bedding plane. Pebbly layers occur between sandstone units and are medium to coarse grained poorly sorted and comprise of glassy quartz with rare grey quartz. It contains fine to medium grained feldspars and sub-rounded quartz in the matrix. Foliation is associated with quartz due to recrystallisation. The quartz rich layer is boudinaged, showing deformation of the layer rich in quartz. Dark minerals appear to occur along a sugary quartz vein which is discontinuous. Sulphides occur in the pink fractured irregular vein section.

In thin section, quartz grains are fine to medium grained sub-rounded and moderately sorted with isolated plagioclase, opaque dust and chlorite films at the margins (Fig. 4.3A). Medium to coarse grained quartz is partially or weakly recrystallised into fine to medium grains. Recrystallisaton occurs at the margins of the pebbles into medium grains that appear to be weakly sheared, elongated which may be offset and recrystallised (Fig 4.3B). There is also a network of quartz vein due to recrystallisation into different generations recrystallised later into quartz veins. The grains form triple junction and show undulose extinction and weak intra-grain recrystallisation. Current bedding is also marked by opaque minerals which had

been transformed into amphiboles (Fig. 4.3C). These minerals which mark current bedding had been overprinted by aggregates of opaque minerals into medium grains that overprint recrystallised quartz which is in turn sheared by deformation (Fig. 4.3D).

Isoclinal folding occur. Medium to coarse grained quartz had been observed to occur at the limb of the isoclinal fold (Fig. 4.4A). Folded medium grained sandstone had been offset by coarser grained quartz. Amphiboles mark the margins of a fold and along cleavages. Opaque mineral 1 mostly marks the quartz and marks the margins of the fold. At the core of the fold, there is rounded recrystallised quartz. There is folding of foliation 1 which is an open fold with the axial plane nearly parallel to foliation 2 and marked by elongated quartz and amphiboles. Foliation 1 is isoclinal tight fold and strongly marked by elongated plagioclase with brecciated quartz. Quartz vein cuts across the recrystallised massive quartz and appears to be the axial plane of an anticlinal fold in the massive quartzite. This is a recrystallised version of the crenulated fold which probably occurs in the syncline. Recrystallised coarser grained quartz is limited to the fold and cuts across the initial crenulated fold (Fig. 4.4B). Opaque minerals overprint folds and its margins are corroded by further recrystallisation.

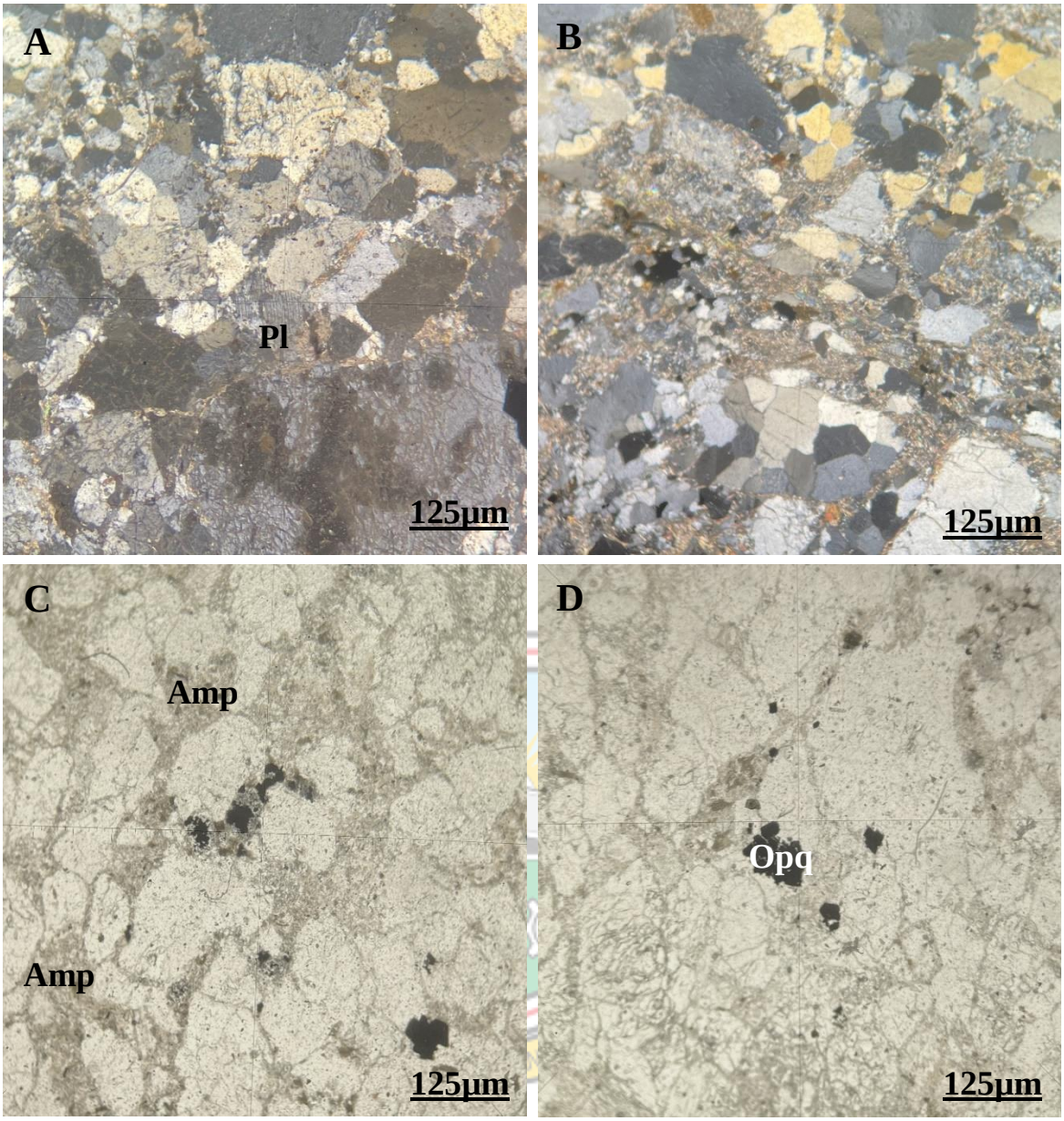

Figs. 4.3 (A to D) Photomicrograph of Thin Sections of Banket Footwall Quartzite showing:

A) Fine to medium quartz grains which are sub-rounded moderately sorted with isolated plagioclase in sample D10 (cross polars). B) Fractured quartz recrystallised into medium grained in sample D02 (cross polars). C) Bedding marked by fine opaque minerals which are deformed and marks the margins of quartz and partially replaced by secondary amphiboles in sample D03 (plane polarised light). D) Opaque minerals that mark current bedding which in turn are overprinted by aggregates of opaque minerals in sample D03 (plane polarised light).

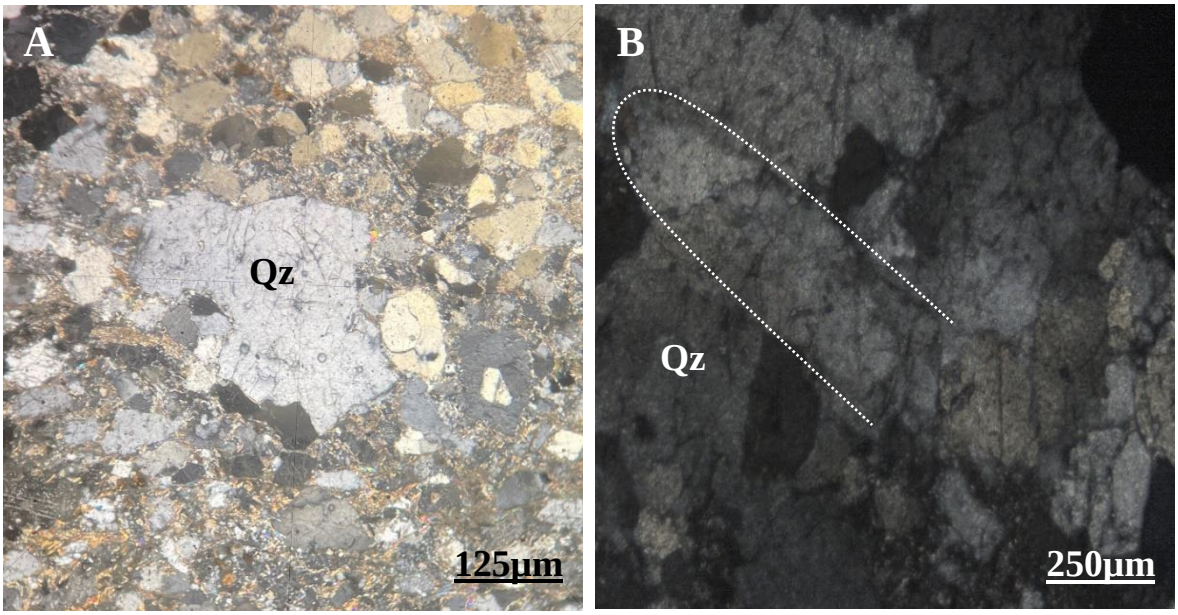

Figs. 4.4 (A and B) Photomicrograph of Thin Sections of Banket Footwall Quartzite showing: A) Medium to coarse grained quartz which is partially/weakly recrystallised into fine to medium grains in sample D05 (cross polars). B) Recrystallised coarser grained quartz cuts across fold in sample D13 (cross polars).

Three types of opaque minerals occur. Opaque mineral 1 which probably is a primary, is dusty and surrounds quartz pebbles and bedding (Fig. 4.5A). They mark the margins of medium grained quartz which is clustered into a coarser grain. These opaque minerals are aligned parallel to foliations (Fig. 4.5B). Fine opaque mineral 1 may also form at the margins of the inner ring of quartz grains possibly due to concretionary mode of formation. Secondary opaque minerals in the banket footwall quartzite is subhedral, corroded and clustered around cleavages. Secondary opaque minerals in the banket footwall quartzite are subhedral, corroded and clustered around cleavages.

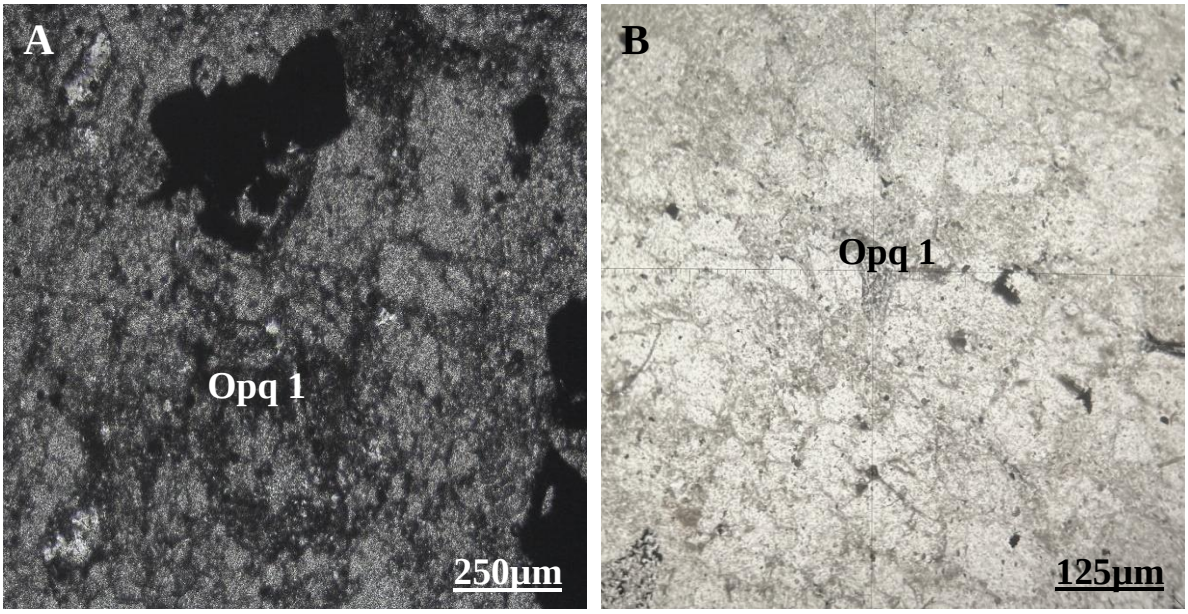

Figs. 4.5 (A and B) Photomicrograph of Thin Sections of Opaque Minerals in Banket Footwall Quartzite showing: A) Opaque mineral 1, dusty and surrounds quartz pebble in sample D10 (plane polarised light) B) Opaque mineral 1 which is fine grained and marks bedding in sample D23 (plane polarised light).

Opaque mineral 2 which may occur as elongated and sheared along recrystallised quartz; it normally overprints sheared quartz and is drawn out and smeared along grain margins. It overprints opaque mineral 1 and so is secondary (Fig. 4.6A). Opaque minerals 2 are corroded by third generation recrystallised quartz. Opaque mineral 2 appears to be aligned at a foliation marking axial plane of a fold (Fig. 4.6B).

Opaque mineral 3 is almost euhedral, cubic and mostly overprints recrystallised quartz. It also overprints foliations 1 and 2. Since it is secondary, it overprints the primary opaque mineral 1 (Fig. 4.6C). Modal composition of banket footwall quartzite is indicated in Table 4.1. Quartz-Feldspar-Rock fragments (QFR) diagram to show protoliths of this rock as sublitharenite, feldspathic litharenite and litharenite (Fig. 4.7).

Table 4.1 Modal percentage of Banket Footwall Quartzite

Minerals / Sample No	Quartz	Chlorite	Plagioclase	Sericite	Amphibole	Opaque Mineral	Epidote	TOTAL
D01	50	30	6	5	5	4	-	100
D02	57	15	10	5	10	3	-	100
D03	65	5	10	4	13	3	-	100
D04	66	5	1	3	20	5	-	100
D05	64	20	10	2	-	4	-	100
D06	77	3	5	2	10	3	-	100
D07	73	2	6	2	12	5	-	100
D08	40	10	20	5	15	10	-	100
D09	60	5	8	2	15	10	-	100
D10	67	15	5	3	-	10	-	100
D13	66	5	1	3	20	5	-	100
D14	65	5	15	3	10	1	1	100
D15	60	10	6	3	17	4	-	100
D16	50	15	10	5	10	10	-	100
D17	66	3	15	2	10	2	2	100
D18	45	10	15	3	24	3	-	100
D19	63	3	12	2	15	3	2	100
D20	72	10	10	3	-	5	-	100
D21	76	3	6	2	10	3	-	100
D22	53	10	10	2	20	5	-	100
D23	50	10	11	4	20	5	-	100
D24	40	5	30	3	17	5	-	100
D29	65	7	15	4	6	3	-	100
D30	64	6	6	1	20	3	-	100

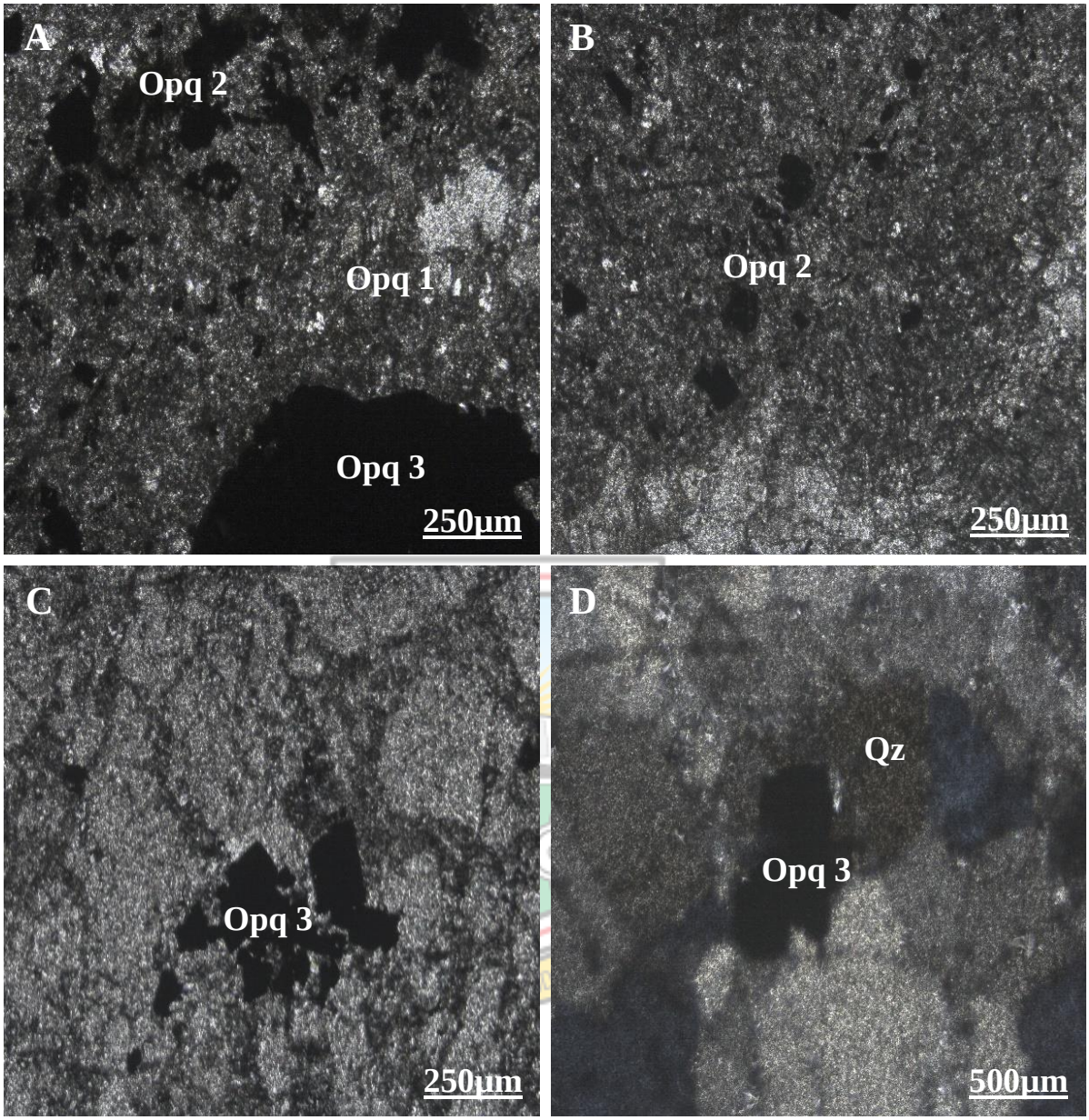

Figs. 4.6 (A to D) Photomicrograph of Thin Sections of Opaque Minerals of Banket Footwall Quartzite showing:

A) Opaque minerals 1, Opaque minerals 2 and Opaque minerals 3 in sample D16 (plane polarised light). B) Opaque mineral 2 which appears to be aligned to a foliation/marking a fold cleavage in sample D16 (plane polarised light). C) Opaque mineral 3 overprints foliation 1 and foliation 2 in sample D15 (plane polarised light). D) Opaque mineral 3 overprint recrystallised quartz in sample D20 (cross polars).

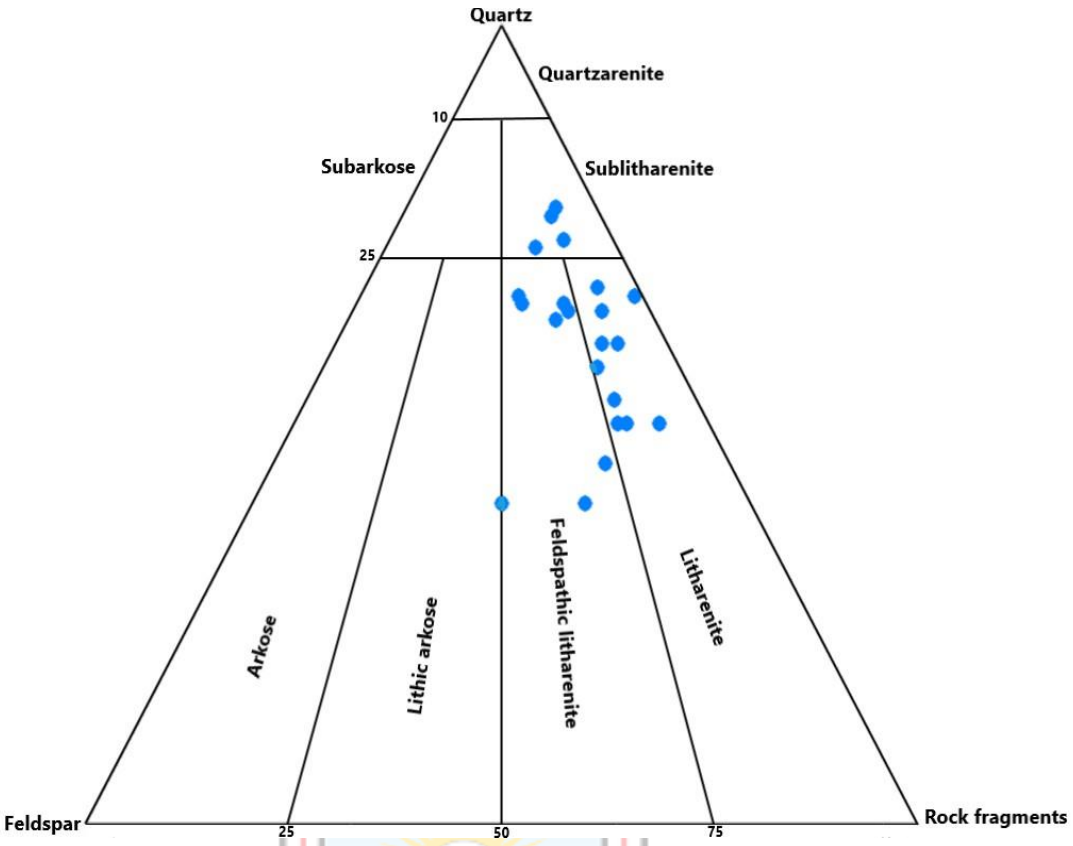

Figs. 4.7 QFR Diagram showing Protoliths of Quartzite Types from Damang

Chalcopyrite is coarse grained irregular with weak pleochroism. Under cross nicols, it shows exsolution of delafosite lamellae with pleochroism. It also shows bright extinction and exsolution of hematite. It is partially replaced by magnetite which is partially altered to hematite. Also magnetite shows thin fine exsolution of cream yellow pleochroic ilmenite with brownish grey tint and anisotropism. Pyrite is creamy white and shows pleochroism of greenish yellow. Under cross nicols, it shows anisotropism and appears to be partially altered to brownish black magnetite with cubic shape. The creamy white chalcopyrite is partially replaced by yellow sub-euhedral tabular mineral which in turn is replaced by black mineral. The yellowish variety of chalcopyrite has inclusions of whitish grey weakly pleochroic and anisotropic goethite. It also has bluish grey non pleochroic anisotropic mineral. The mineral also has exsolution of pleochroic grey to dark grey anisotropism. It changes from dark grey to black (Fig. 4.8A). Fine gold grain is granular and deep yellow. It is associated with hematite aggregates in the matrix of gangue minerals and some magnetite (Fig. 4.8B). Note that gold replaces pyrite which has been partially replaced by hematite.

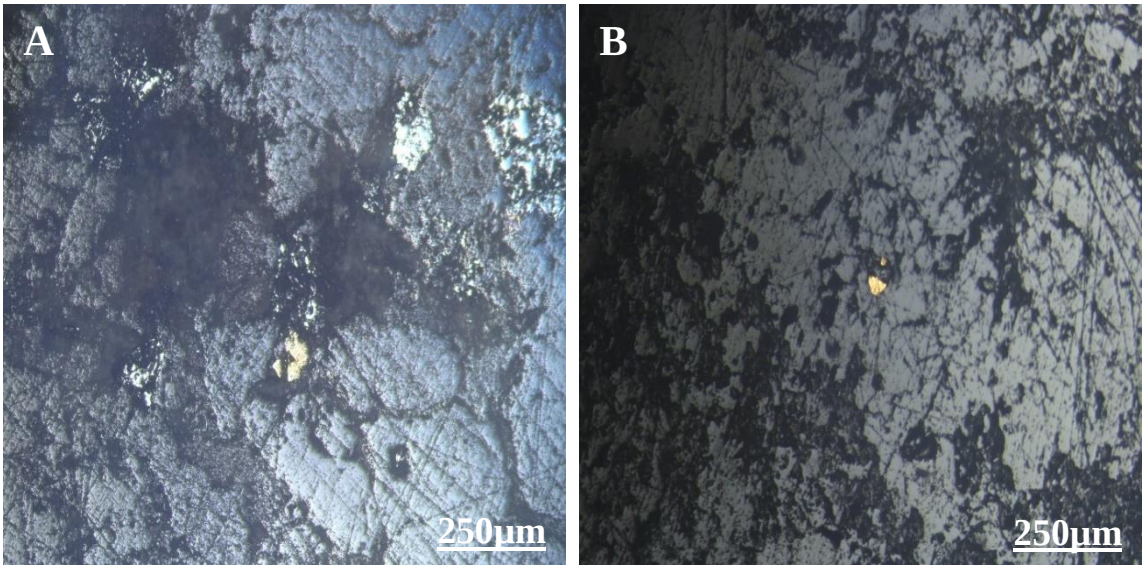

Figs. 4.8 (A and B) Photomicrograph of Polished Section of Banket Footwall Quartzite showing: A) Chalcopyrite partially replaced by magnetite with inclusions of hematite in sample D10 (plane polarised light). B) Gold inclusions in gangue Sample D30 (plane polarised light).

4.1.2 Banket Conglomerate

At Saddle Pit, the conglomerates were found between the banket footwall and banket hangingwall quartzites. Some of the conglomerates are oligomictic and moderately sorted whilst others are polymictic and poorly sorted (Fig. 4.9). There are quartz veins in part of the conglomerates with sulphides.

Fig. 4.9 Oligomictic Banket Conglomerate with sulphide alteration

In hand specimen, the rock is light to dark grey. Grains are medium grained quartz with isolated coarse grains. Generally, rounded to sub-rounded and moderately sorted. Lenticular quartz pebbles have diameters ranging from from 25 mm to 60 mm. Feldspar and sericite make up the matrix with dark minerals sometimes aligned parallel to bedding. The grains are recrystallised into sugary veins. Quartz veins cut conglomerate with sulphide alterations at the contact.

In thin section, quartz (40%) grain is medium grained with isolated coarse grains. Generally, rounded to sub-rounded, moderately sorted in a matrix of 60%. The quartz shows undulose extinction and recrystallised into fine grains with triple junction (Fig. 4.10A). Elongated quartz shows deformation lamellae and undulose extinction (Fig. 4.10B). This progresses into a sub-angular grain that is recrystallised into fine grains (Fig. 4.10C).

The rock is medium grained with quartz drawn out in two directions at right angles and partially recrystallised into finer grains with sutured and wormy shapes. Quartz shows undulose extinction. This occurs with amphiboles that have characteristic cleavages at 56^0 in two main directions. Amphibole shows pleochroism from greenish brown to brown with extinction angle of 38.5^0 (Fig. 4.10D). It is partially altered to chlorites releasing opaque oxide granules. Secondary amphibole is yellowish green to green, colloidal and also partially altered to fine chlorites and epidotes.

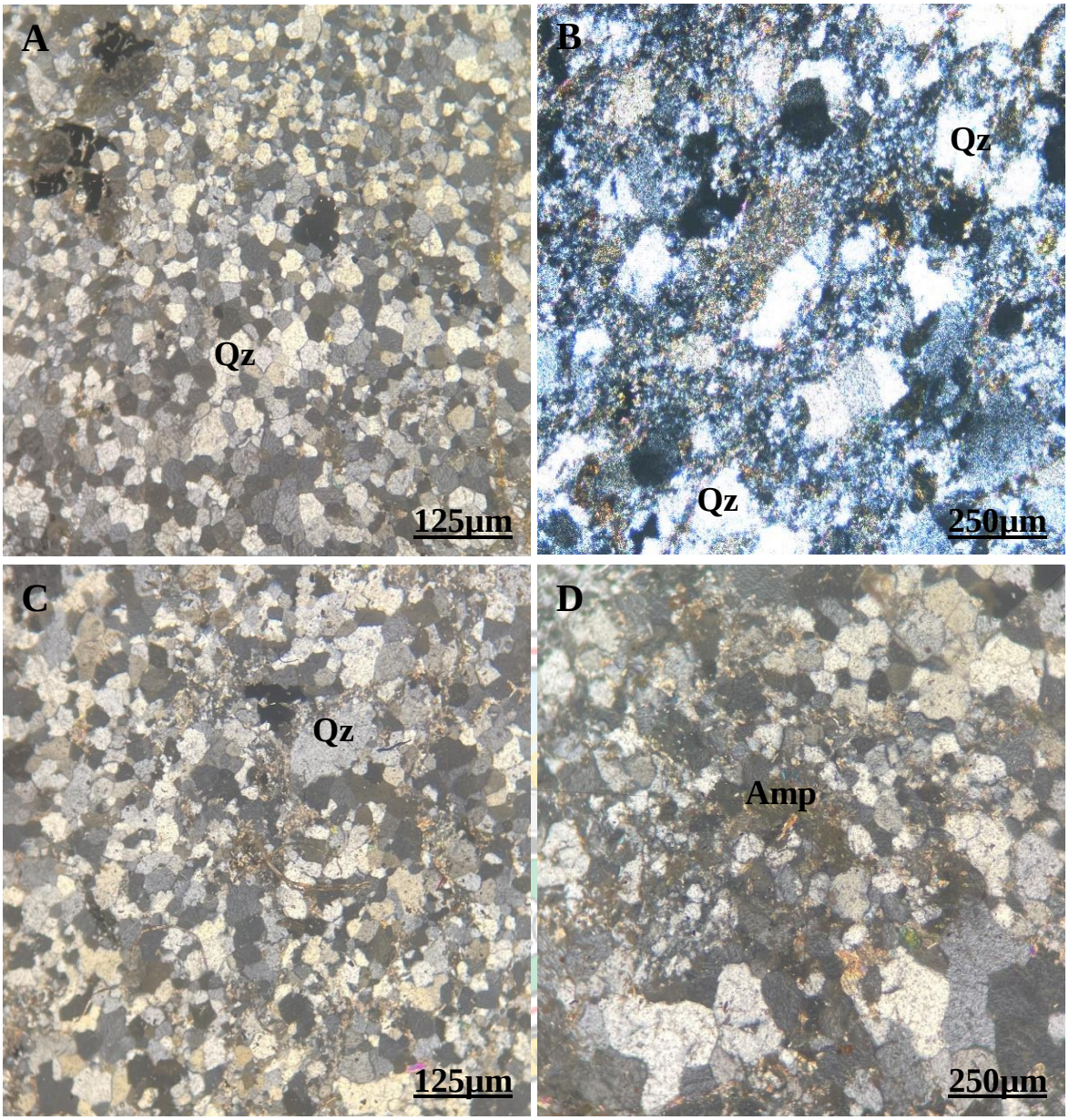

Figs. 4.10 (A to D) Photomicrograph of Thin Sections of Banket Conglomerate showing: A) Medium grained quartz partially recrystallised into sub-rounded finer grains in sample D36 (cross polars). B) Medium grained elongated quartz exhibiting deformation lamellae in sample D31 (cross polars). C) Recrystallised quartz in sample D33 (cross polars). D) Primary amphibole in sample D33 (cross polars)

There appears to be a fold with elongated quartz and sub-angular quartz which is recrystallised at the hinge (Fig. 4.11A). The apex of the fold is crystallised to fine grained quartz with sutured margins (Fig. 4.11B). Modal composition of banket conglomerate is indicated in Table 4.2.

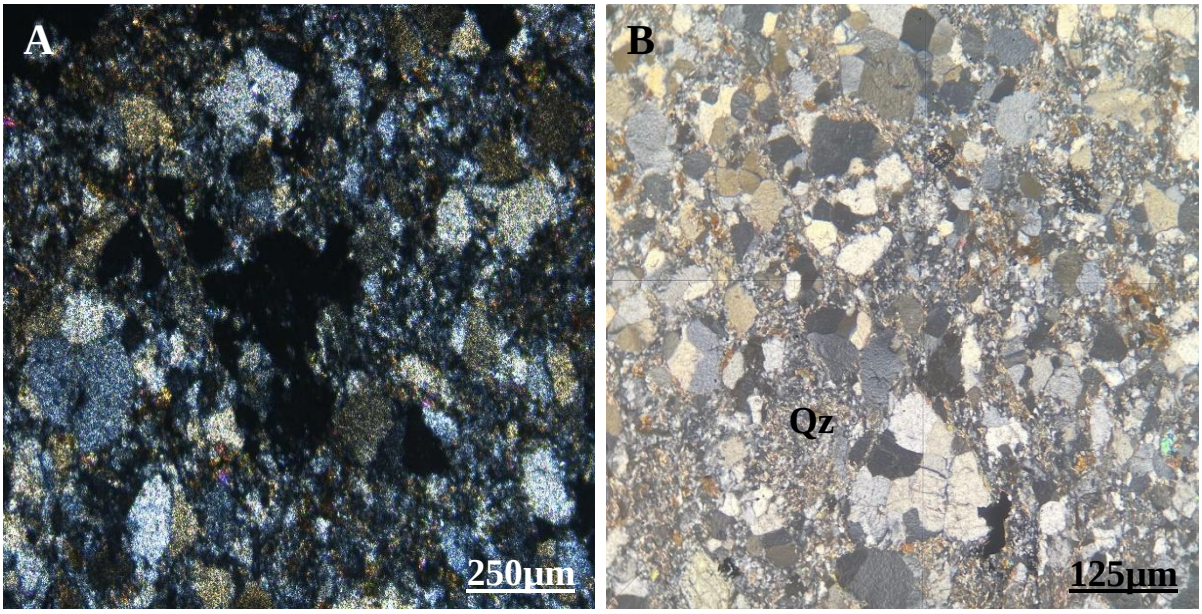

Figs. 4.11 (A and B) Photomicrograph of Thin Sections of Banket Conglomerate showing: A) Aggregate of garnets partially replaced by biotite and granular quartz in sample D31 (cross polars). B) Fine grained quartz in sample D31 (cross polars).

Table 4.2 Modal percentage of Banket Conglomerate

Sample No. / Minerals	D31	D32	D33	D34	D35	D36
Quartz	60	62	50	59	85	60
Chlorite	15	10	19	20	5	25
Plagioclase	10	20	1	1	4	1
Sericite	5	3	2	10	2	2
Amphibole	-	-	20	-	-	-
Opaque Mineral	3	2	4	10	4	2
Epidote	-	-	4	-	-	10
Biotite	5	3	-	-	-	-
Garnet	2	-	-	-	-	-
TOTAL	100	100	100	100	100	100

In polished section, pyrite is partially replaced by granular magnetite aggregates of dark grey non pleochroic with brownish tint anisotropy. Pyrite is subhedral, tabular with the margins destroyed by gangue and partially replaced by graphite which is also partially replaced earlier chalcopyrite (Fig. 4.12A). Gold is fine grained which aggregates into

irregular, bright yellow weakly pleochroic with green tint and isotropic. It is associated with greyish blue (magnetite), weakly pleochroic and magnetite is anisotropic. They are all partially overprinted by gangue and graphite. Elsewhere fine network of gold also occurs (Fig 4.12B).

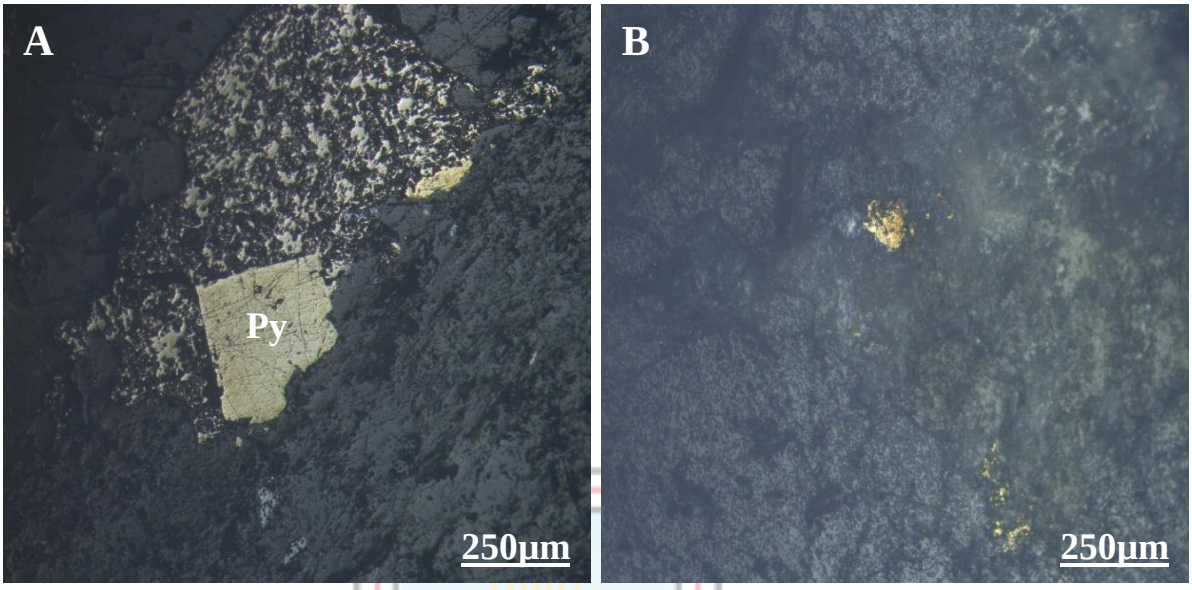

Figs. 4.12 (A and B) Photomicrograph of Polished Sections of Banket Conglomerate showing: A) Pyrite in sample D31 (plane polarised light). B) Gold in sample D33 (plane polarised light).

4.1.3 Mafic Intrusives

At Saddle Pit, the mafic intrusives intruded the Tarkwaian rocks (Fig. 4.13). They are dykes and sills which cut the Tarkwaian rocks. In hand specimen, the intrusives are dark grey to dark green, fine to medium grained from 2 mm to 8 mm.

Fig. 4.13 Photograph of Mafic Intrusive (Dyke) in Quartzite

In thin section, the rock is medium grained with amphibole and plagioclase irregularly aligned. Secondary amphibole overprints plagioclase. Plagioclase shows partial alteration to sericite and fine quartz whereas amphibole shows partial alteration to chlorite and epidote (Fig. 4.14A). Also, quartz vein is coarse grained, probably due to recrystallisation of quartz or corroded the margins of sheared versions. Recrystallised versions corrodes the margins of the amphiboles in the intrusive (Fig. 4.14B). Late amphibole which shows yellowish green to dark green pleochroism overprints both recrystallised quartz and earlier amphiboles (Fig 4.14C). Quartzite was probably intruded and later recrystallised. Opaque minerals are medium grained with irregular shapes and granular aggregates which occur as overprints on plagioclase and amphiboles. Late opaque minerals are also coarser grained with inclusions of amphiboles and plagioclase (Fig. 4.14D). Fine grained tabular plagioclase is partially altered to sericite and quartz whilst fine amphibole is partially altered to epidote. Modal composition of mafic intrusives is indicated in Table 4.3. Quartz-Alkali-Plagioclase (QAP) plot of this rock type is shown in Fig. 4.16

Table 4.3 Modal Percentage of Mafic Intrusives

Sample No. / Minerals	D12	D25	D26	D27	D28
Quartz	-	2	-	5	3
Chlorite	10	5	5	10	3
Plagioclase	30	30	44	20	20
Sericite	3	3	4	3	2
Amphibole	47	58	40	42	60
Opaque Mineral	10	2	6	3	1
Epidote	-	-	1	2	1
Pyroxene	-	-	-	15	10
TOTAL	100	100	100	100	100

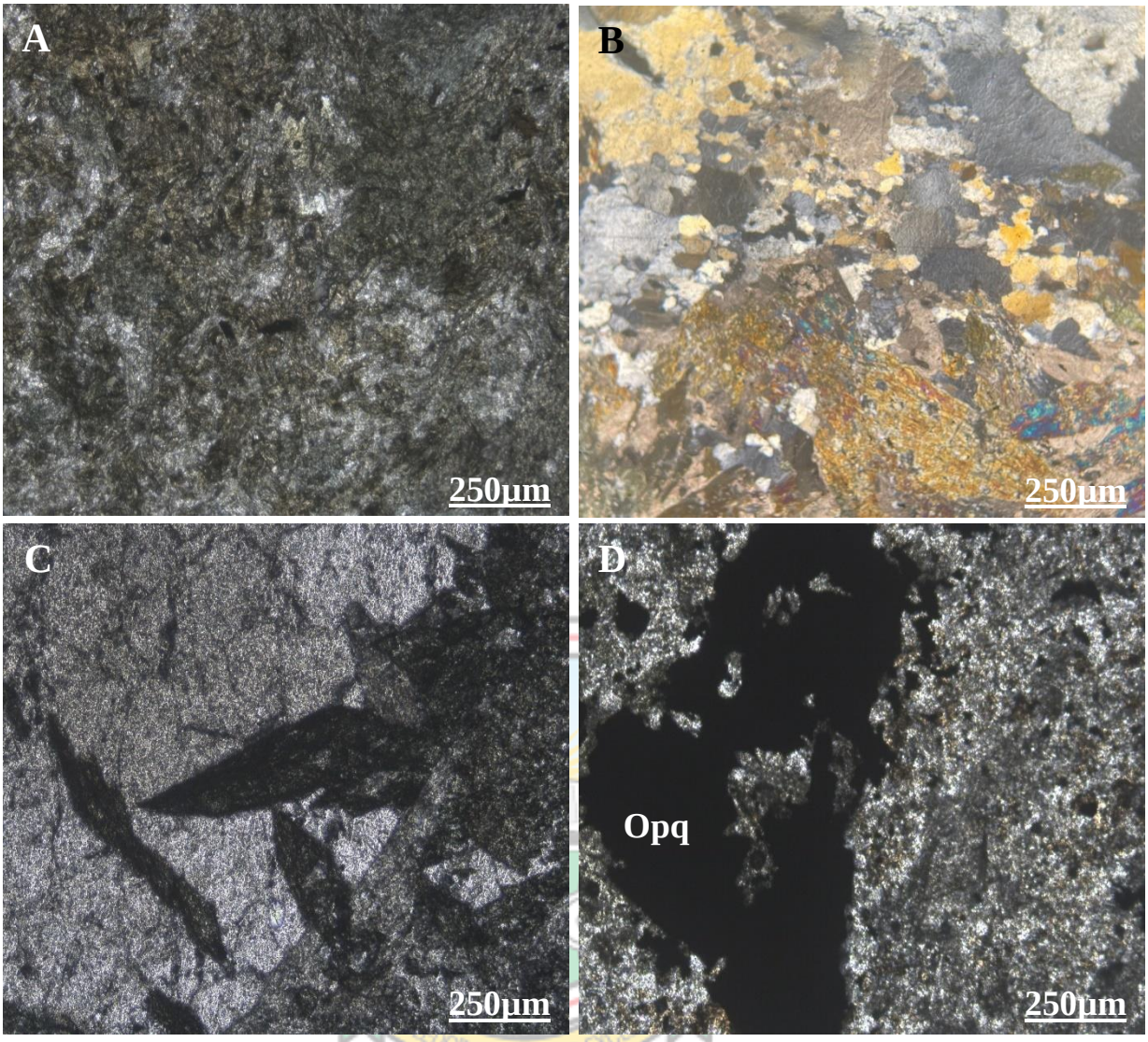

Figs. 4.14 (A to D) Photomicrograph of Thin Sections of Mafic Intrusives showing: A) Mafic intrusive with irregular alignment of amphiboles and plagioclase in sample D25 (plane polarised light). B) Quartzite intruded by mafic intrusives with quartzite being recrystallised at the margins in sample D28 (cross polars). C) Late amphiboles overprints the margins of mafic intrusives and quartz in sample D28 (plane polarised light). D) Late opaque minerals with inclusions of amphiboles and plagioclase in sample D26 (plane polarised light)

In polished section, delafosite is sub-eudral, tabular and pleochroic with straight extinction. Delafosite is then partially replaced by pyrrhotite and occurs at the fractures of quartz (Fig. 4.15A). Pyrite is also partially altered to hematite and magnetite. Pyrite 1 is disseminated with alteration of brownish black (goethite) and partially altered to hematite and magnetite. Pyrite 2 overprints pyrite 1 with replacement of hematite and magnetite. Replacements came

after the formation of pyrite 1 and pyrite 2. (Fig. 4.15B). Betekhtinite occurs along shear zone in matrix as medium grained creamy yellow pleochroic to yellowish grey to brownish grey, partially altered into pits. Chalcopyrite partially replaced and overprinted by bright yellow gold which is corroded at the margins by chalcopyrite (Fig. 4.15C). Gold is also associated with pyrite which is partially replaced by hematite and magnetite. It also appear as inclusions in the pyrite. Gold is pitted and filled with gangue (Fig. 4.15D).

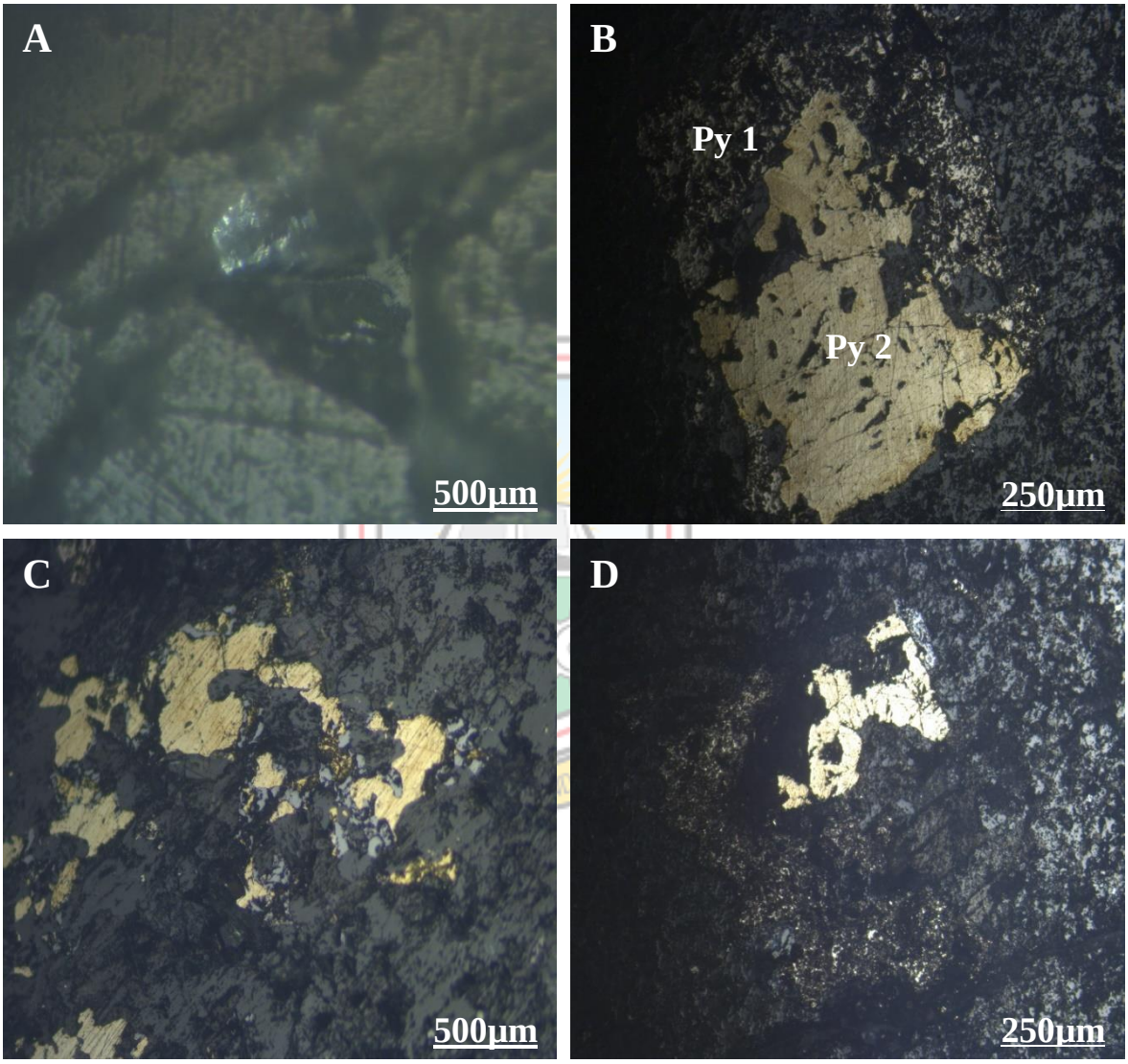

Figs. 4.15 (A to D) Photomicrograph of Polished Section of Mafic Intrusives showing: A) Delafosite, sub-euhedral and tabular and partially altered to pyrrhotite which occurs at the fractures of quartz in sample D28 (plane polarised light). B) Pyrite 1 overprinted by pyrite 2 also replaced by hematite and magnetite in sample D26 (plane polarised light). C) Chalcopyrite partially replaced by gold and overprinted by magnetite and hematite in sample D28 (plane polarised light) D) Gold marks foliation and associated with hematite in sample D26 (plane polarised light)

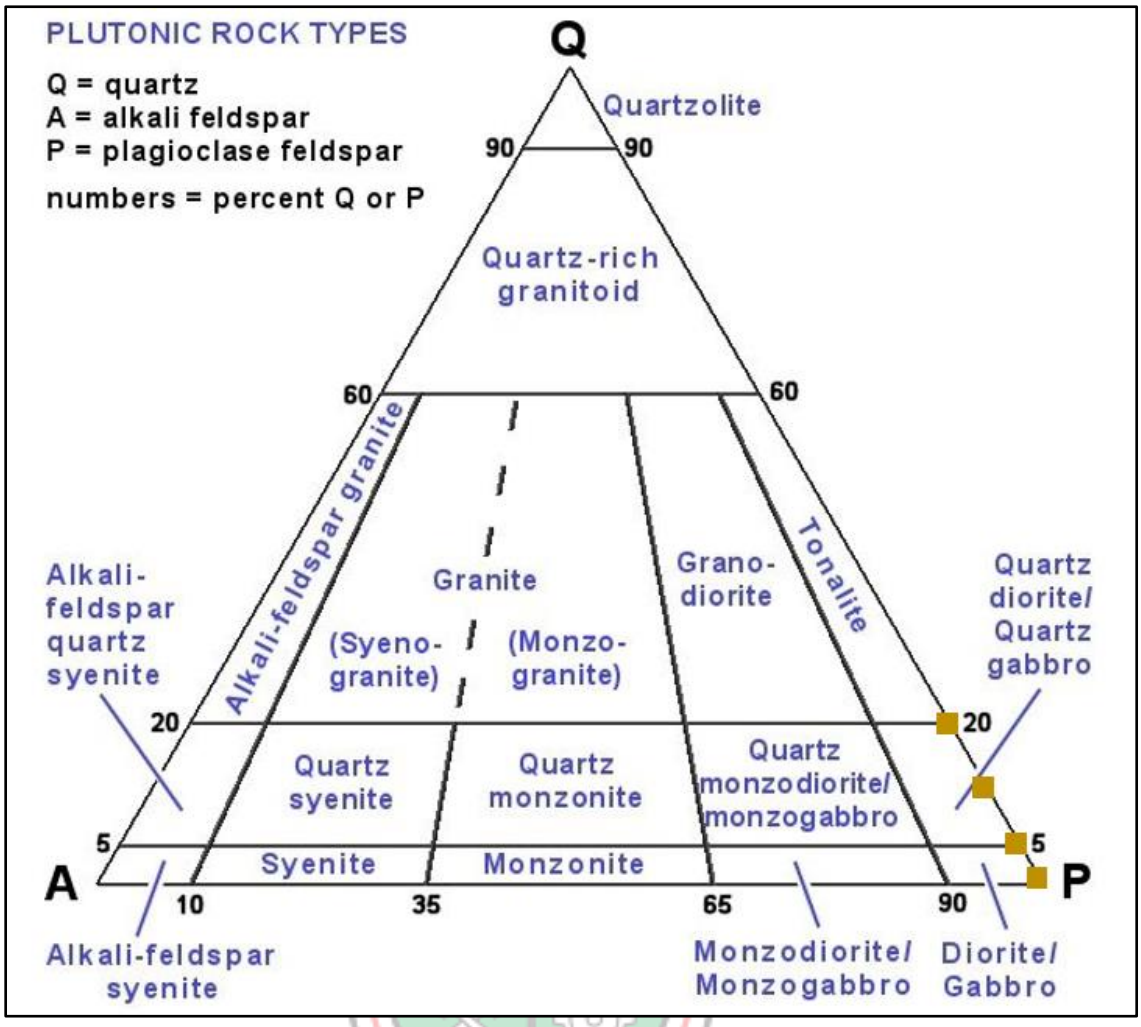

Figs. 4.16 QAP Diagram showing Mafic Intrusives from Damang

4.2 Geochemistry

Twelve (12) samples of the three (3) rock types: banket footwall quartzite, banket conglomerate and mafic intrusive were geochemically analysed with the results presented below.

4.2.1 Summary of Major Oxide Composition of Banket Footwall Quartzite

Major oxide composition of four samples (D01, D06, D16 and D22) of the banket footwall quartzite at the Amoanda Pit were analysed. D01 and D16 which are are altered whilst D06 and D22 are unaltered. Altered banket footwall quartzite has SiO_2 content ranges from 50.1 - 74.6 wt%, Al_2O_3 10.55 - 26.6 wt%, FeO_t 5.24 – 9.08 wt%, CaO 1.1 - 1.3 wt%, MgO 0.57 - 0.61 wt%, Na_2O 1.16 - 1.46 wt%, K_2O 2.25 - 7.06 wt%, Cr_2O_3 0.013 - 0.02 wt%, TiO_2

0.36 - 0.93 wt%, MnO 0.05 - 0.07 wt%, P_2O_5 0.03 - 0.16 wt%, SrO 0.02 - 0.08 wt% and BaO ranges from 0.09 to 0.32 wt% whilst gold values are up to 0.18 g/t. Unaltered banket footwall quartzite has SiO_2 content ranges from 76.7 – 78.4 wt%, Al_2O_3 9.92 – 10.8 wt%, FeO_t 3.97 – 4.79 wt%, CaO 1.23 - 1.33 wt%, MgO 0.53 - 0.66 wt%, Na_2O 1.58 - 1.82 wt%, K_2O 1.8 – 2.01 wt%, Cr_2O_3 0.011 - 0.014 wt%, TiO_2 0.26 - 0.29 wt%, MnO 0.08 - 0.09 wt%, P_2O_5 0.02 wt%, SrO 0.03 wt% and BaO ranges from 0.09 to 0.11 wt% whilst gold values are up to 0.03 g/t.

4.2.2 Summary of Major Oxide Composition of Banket Conglomerate

Major oxides composition of five rock samples (D31, D32, D33, D34 and D36) of the banket conglomerate rocks at the Saddle pit were analysed. D31 and D33 are altered whilst D32, D34 and D36 are unaltered. Altered banket conglomerate has SiO_2 content ranges from 66.7 – 85.5 wt%, Al_2O_3 6.86 - 13.6 wt%, FeO_t 3.54 - 9.98 wt%, CaO 0.53 - 1.14 wt%, MgO 0.5 - 0.99 wt%, Na_2O 0.99 - 1.89 wt%, K_2O 0.9 - 1.85 wt%, Cr_2O_3 0.012 - 0.022 wt%, TiO_2 0.23 - 0.63 wt%, MnO 0.08 - 0.12 wt%, P_2O_5 0.02 - 0.07 wt%, SrO 0.01 - 0.02 wt% and BaO ranges from 0.05 to 0.1 wt%. Gold values in the altered zone are up to 24.77 g/t. Unaltered banket conglomerate has SiO_2 content ranges from 82 – 89.1 wt%, Al_2O_3 3.96 – 7.15 wt%, FeO_t 3.17 – 4.79 wt%, CaO 0.26 – 0.94 wt%, MgO 0.34 - 0.53 wt%, Na_2O 0.4 – 0.9 wt%, K_2O 0.72 - 1.38 wt%, Cr_2O_3 0.009 - 0.018 wt%, TiO_2 0.23 - 0.32 wt%, MnO 0.09 - 0.11 wt%, P_2O_5 0.02 - 0.05 wt%, SrO <0.01 - 0.01 wt% and BaO ranges from 0.04 to 0.05 wt% whilst gold values in the unaltered zone are up to 0.3g/t.

4.2.3 Summary of Major Oxide Composition of Mafic Intrusive

Major oxides composition of three rock samples (D25, D26 and D27) of the mafic intrusive rocks at the Saddle pit were analysed. D26 is altered whilst D25 and D27 are unaltered. Altered mafic intusive has SiO_2 50.4 wt%, Al_2O_3 14.05 wt%, FeO_t 8.26 wt%, CaO 10.25 wt%, MgO 6.93 wt%, Na_2O 2.52 wt%, K_2O 0.27 wt%, Cr_2O_3 0.047 wt%, TiO_2 0.42 wt%, MnO 0.14 wt%, P_2O_5 0.03 wt%, SrO 0.08 wt% and BaO 0.01 wt%. Gold value in the altered zone is 10.1 g/t. Unaltered mafic intusive has SiO_2 content ranges from 46.3 - 51.5 wt%, Al_2O_3 15.6 – 16.75 wt%, FeO_t 9.41 - 10.15 wt%, CaO 7.79 – 8.33 wt%, MgO 6.72 - 10.45 wt%, Na_2O 2.19 - 2.46 wt%, K_2O 1.1 - 1.23 wt%, Cr_2O_3 0.032 - 0.064 wt%, TiO_2 0.52 - 0.53 wt%, MnO 0.12 - 0.18 wt%, P_2O_5 0.09 - 0.1 wt%, SrO 0.03 - 0.05 wt% and BaO ranges from 0.04 to 0.06 wt%. Gold value in the unaltered zone is up to 0.07 g/t.

4.2.4 Major Oxides Plots

From Appendix E, SiO_2 contents of banket conglomerate are very high, followed by banket footwall quartzite then mafic intrusive. MgO, and CaO and Al_2O_3 contents are generally high in the mafic intrusive to the banket footwall and banket conglomerates. Al_2O_3 contents are higher in the altered (Alt) rocks of the various units than the unaltered (UnAlt) rocks.

Fig. 4.17 to 4.22 are binary plots of some major oxides against SiO_2, MgO and Total FeO for the various rock (banket footwall (B_FW), banket conglomerate (B_CB) and mafic Intrusive (MI) were done to analyse the geochemical composition of the various rock units under investigation. The plots give an idea of major oxides concentrations and elemental relationships that are between or amongst the elements, the environment of formation or deposition of the rocks and the alteration patterns of the rocks.

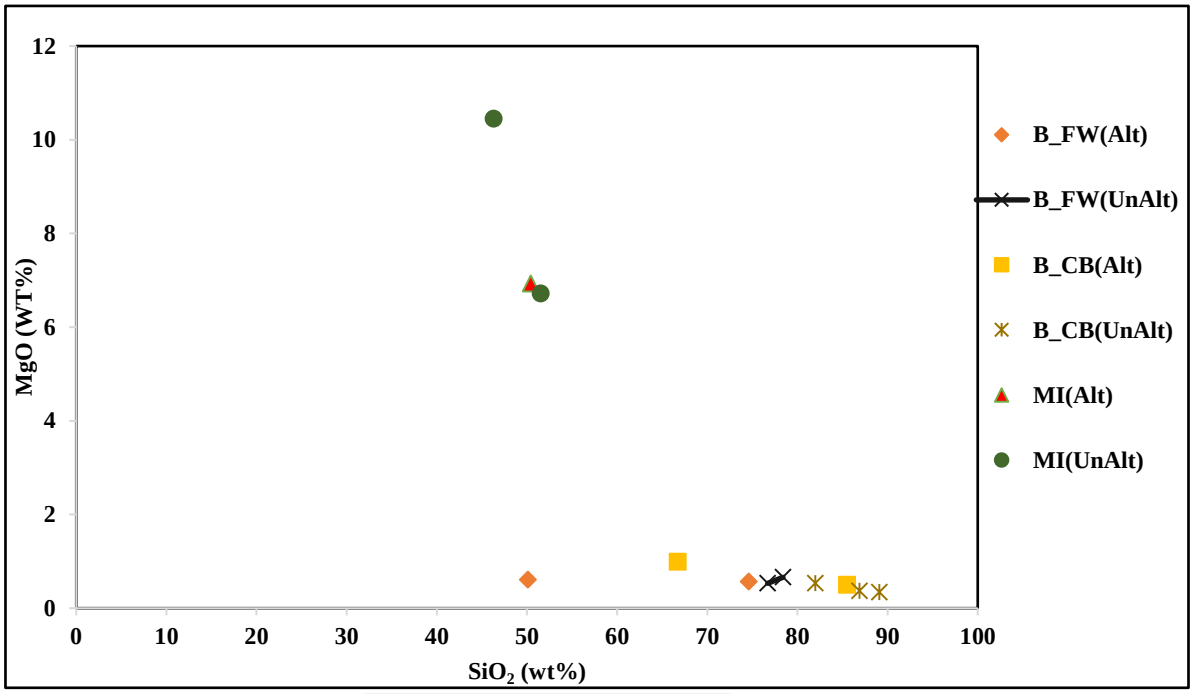

Fig. 4.17 Binary Plot of MgO (wt%) against SiO_2 (wt%) for the Three (3) Rock Types

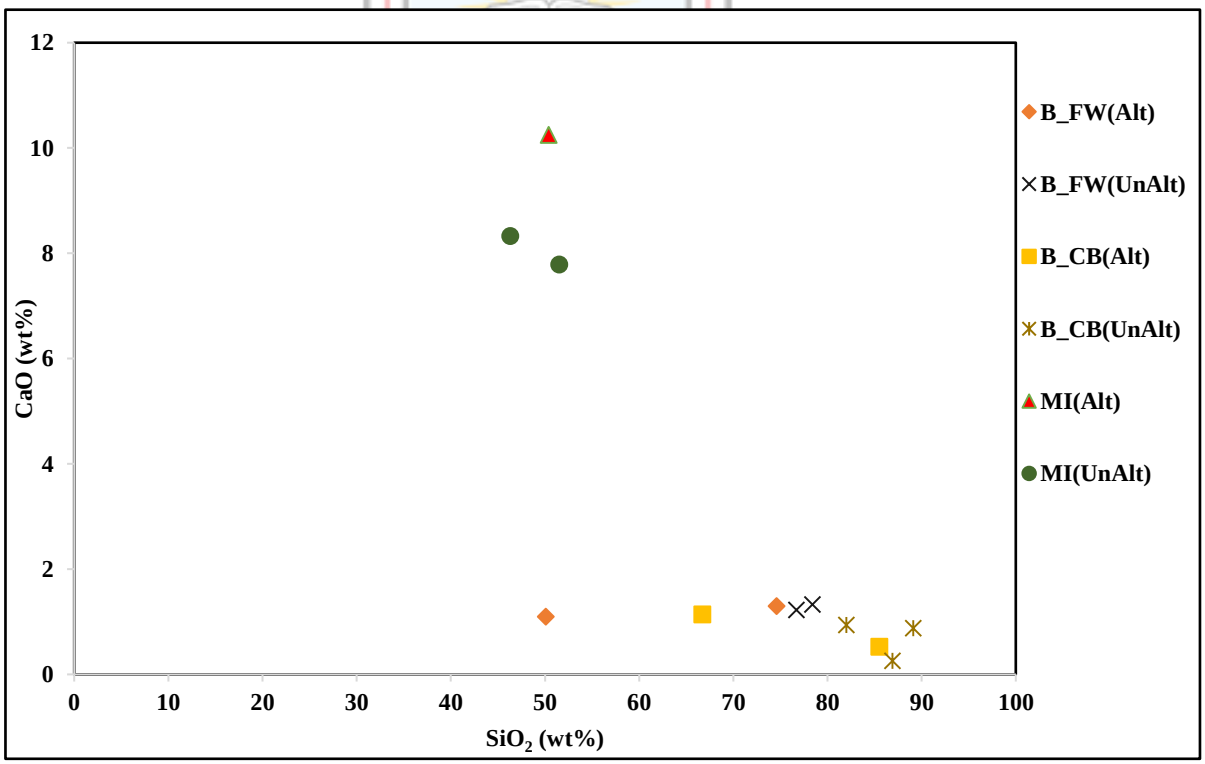

Fig. 4.18 Binary Plot of CaO (wt%) against SiO_2 (wt%) for the Three (3) Rock Types

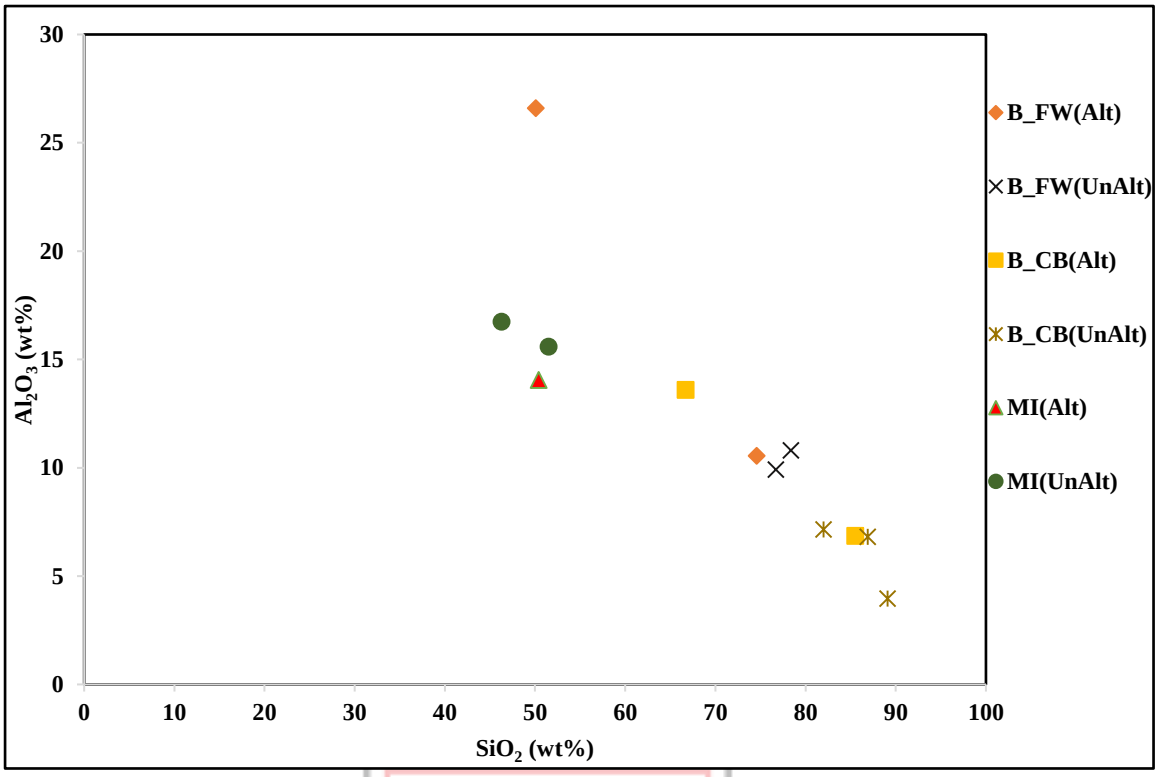

Fig. 4.19 Binary Plot of Al_20_3 (wt%) against SiO_2 (wt%) for the Three (3) Rock Types

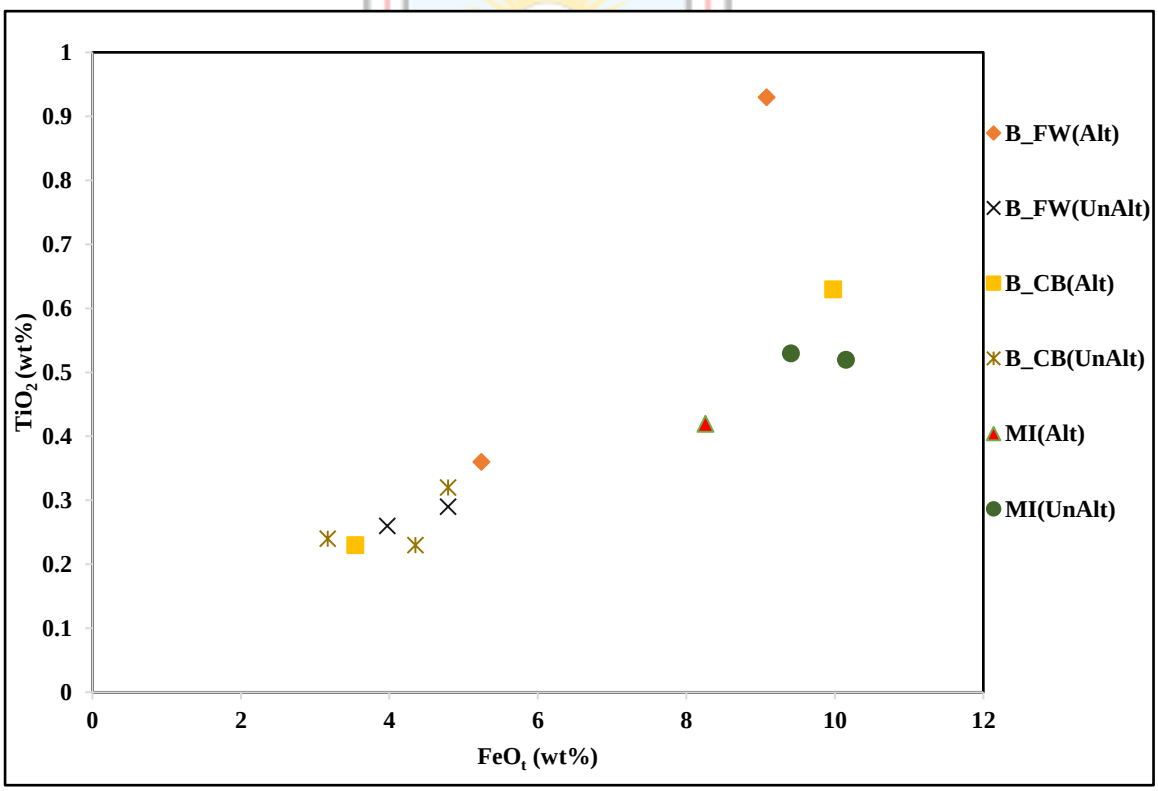

Fig. 4.20 Binary Plot of TiO_2 (wt%) against Total FeO (wt%) for the Three (3) Rock Types

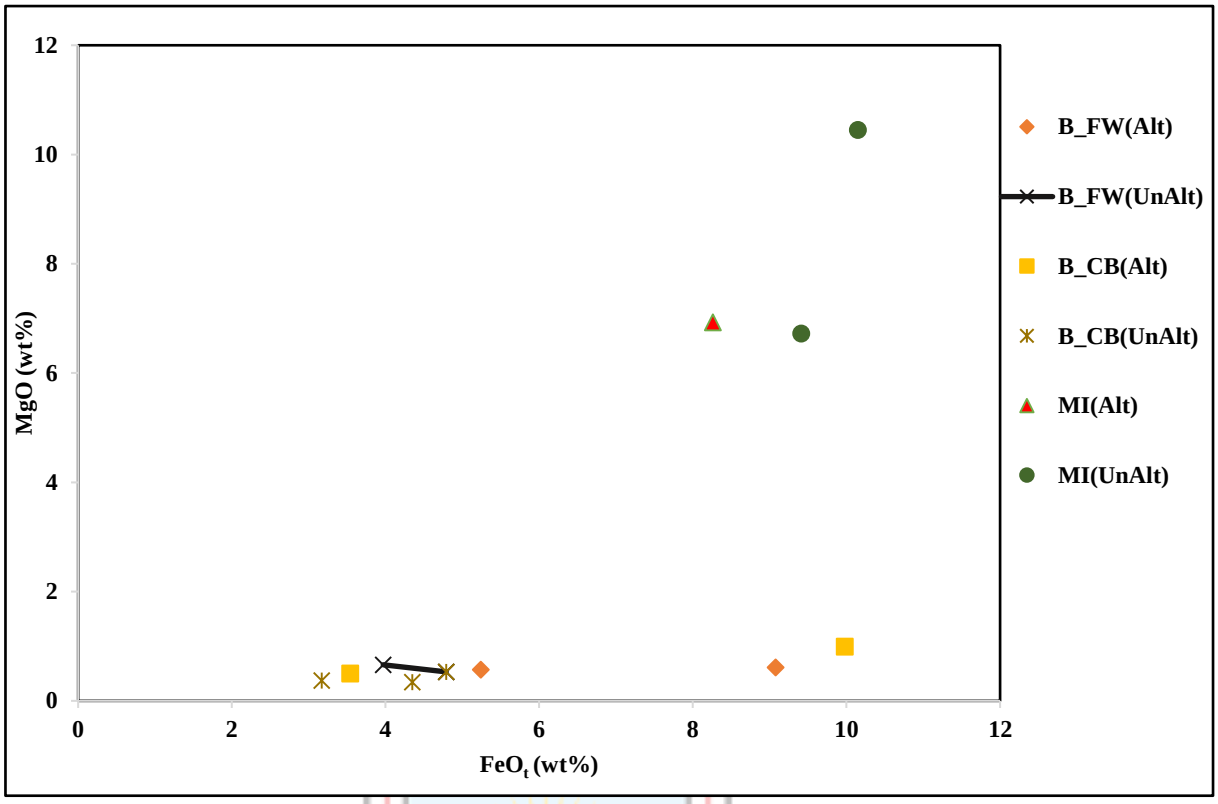

Fig. 4.21 Binary Plot of MgO (wt%) against Total FeO (wt%) for the Three (3) Rock Types

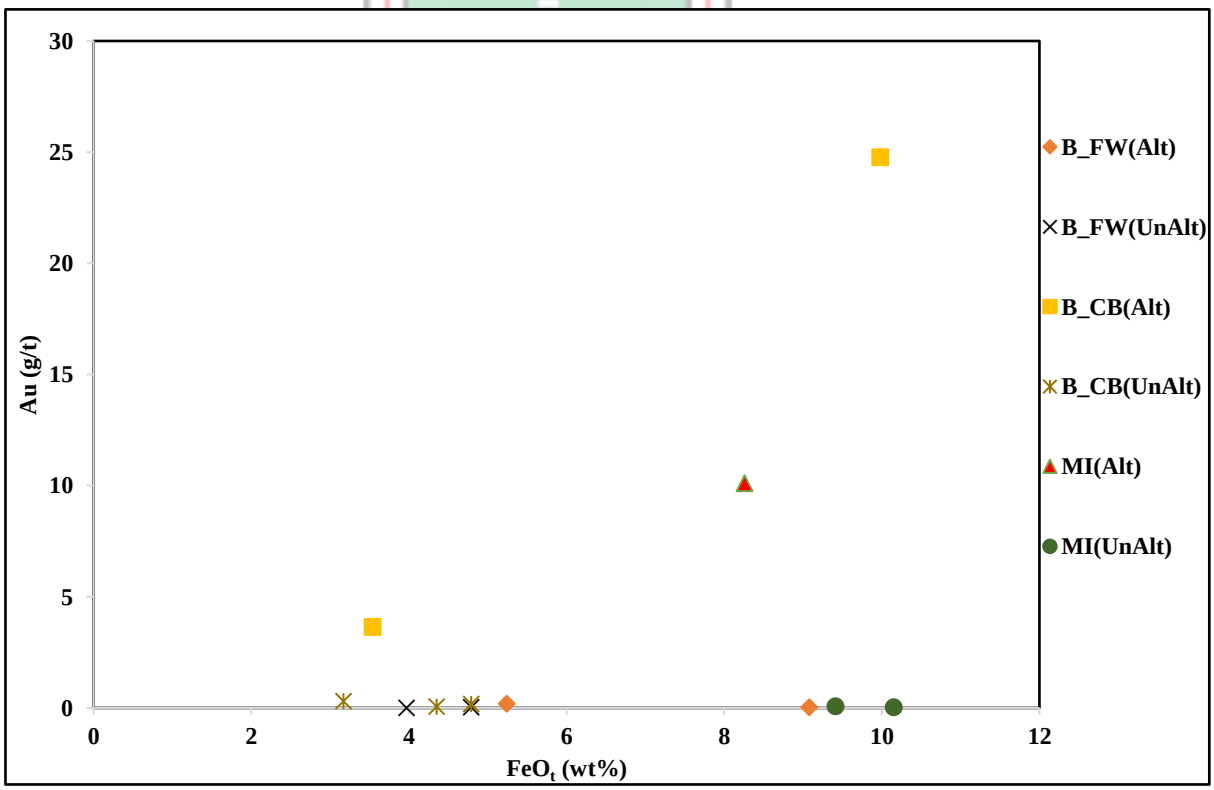

Fig. 4.22 Binary Plot of Au (g/t) against Total FeO (wt%) for the Three (3) Rock Types

From Fig. 4.17 and Fig. 4.18, MgO and CaO contents are higher in the mafic intrusive whilst relatively low in the banket footwall quartzite and banket conglomerate and also altered banket footwall quartzite. Banket conglomerate rocks have lower SiO_2 content than other unaltered rocks.

In Fig. 4.19, Al_2O_3 content in both banket footwall quartzite and banket conglomerate decreases with increasing SiO_2 content. The correlation coefficient of the banket footwall and banket conglomerate are -0.99 and -0.97 respectively. Al_2O_3 in the mafic intrusives are approximately the same in both the altered and unaltered rocks (16.75 wt% and 15.6 wt% in unaltered and 14.05 wt% in altered).

Between the total FeO and TiO_2 contents TiO2 increases with increasing FeO_t content in the banket footwall quartzite, banket conglomerate and mafic intrusive hence a positive correlation of 0.99, 0.98 and 0.89 respectively (Fig. 4.20).

The MgO and Fe_2O_3 content in the banket footwall quartzite and banket conglomerate remains low except in the more altered rocks (Fig. 4.21). Higher MgO and FeO_t occur in the mafic intrusives.

In Fig. 4.22, altered rocks of the three (3) rocks under observation have high FeO_t and gold (Au) content. Unaltered rocks of banket footwall quartzite and banket conglomerate have low FeO_t content and subsequently very low gold (Au) values. Unaltered mafic intrusives have higher FeO_t content but very low gold (Au) values. Altered mafic intrusive have high FeO_t and higher gold content. Sample D31of altered banket conglomerate has very high FeO_t of 9.98 wt% and high gold content of 24.77 g/t.

4.2.5 Rare Earth Element (REE) Plots

The rare earth elements (REE) are generally considered to be highly insoluble, immobile, exhibiting only minor changes during sedimentary processes or often remain unchanged during low grade metamorphism, weathering and hydrothermal alteration (Rugh, 2014). Hence REE patterns can provide information on the premetamorphic history of a rock. Rare earth patterns have been used to identify the source of sedimentary rocks (Rugh, 2014). REE concentrations in the banket footwall quartzite and banket conglomerates were normalised using Post-Archean Average Australian Sedimentary rock (PAAS) values in Appendix C after McLennan (1989) as shown in Table 4.4 and 4.5 respectively. Similarly, mafic

intrusive concentrations were normalised using Primitive Mantle Values (PMV) in Appendix D as shown in Table 4.6.

From Figs. 4.23 and 4.24 plots of the rare earth elements (REE) of banket footwall quartzite and banket conglomerate respectively show a flat pattern of light rare earth elements (LREE) and heavy rare earth elements (HREE). Furthermore, from Table 4.4, sample D01 and sample D16 which are altered samples of the banket footwall quartzite have their total REE values being very high that is 141.37 and 230.65 respectively and therefore are plotted above the unaltered samples (Fig. 4.23). Similarly, altered banket conglomerate has total REE values higher than the unaltered samples except for D36 which is unaltered but still has high value (Table 4.5). Eu anomaly values (Eu/Eu*) of both the banket footwall quartzite and banket conglomerate are all greater than one (1) and the Eu plots all lie above the general trend which indicates a positive europium anomaly.

Table 4.4 Normalisation of REE Concentration of Banket Footwall Quartzite using PAAS

Elements	Raw Values				Normalised Values			
	D01 (ppm)	D06 (ppm)	D16 (ppm)	D22 (ppm)	D01	D06	D16	D22
La	27.00	27.80	39.40	23.00	0.71	0.73	1.04	0.61
Ce	52.00	52.40	83.30	43.30	0.65	0.66	1.04	0.54
Pr	6.01	5.93	9.71	4.89	0.68	0.67	1.09	0.55
Nd	21.50	21.00	36.20	17.50	0.67	0.66	1.13	0.55
Sm	3.75	3.25	6.45	3.03	0.67	0.58	1.15	0.54
Eu	1.05	0.90	1.67	0.78	0.95	0.82	1.52	0.71
Gd	3.27	1.92	6.00	2.51	0.70	0.41	1.28	0.53
Tb	0.51	0.24	0.91	0.34	0.66	0.31	1.18	0.44
Dy	3.11	1.23	5.48	1.93	0.71	0.28	1.25	0.44
Ho	0.68	0.23	1.19	0.38	0.68	0.23	1.19	0.38
Er	1.88	0.70	3.34	1.17	0.65	0.24	1.15	0.40
Tm	0.27	0.10	0.52	0.16	0.54	0.20	1.04	0.32
Yb	1.84	0.67	3.37	1.08	0.66	0.24	1.20	0.39
Lu	0.30	0.12	0.51	0.17	0.60	0.24	1.02	0.34
Y	18.20	6.90	32.60	10.60	0.65	0.25	1.16	0.38
∑REE	141.37	123.39	230.65	110.84	10.17	6.50	17.44	7.11
∑LREE	110.26	110.38	175.06	91.72	3.38	3.29	5.45	2.78
∑HREE	11.86	5.21	21.32	7.74	5.19	2.15	9.31	3.24

Table 4.5 Normalisation of REE Concentration of Banket Conglomerate using PAAS

Elements	Raw Values					Normalised Values				
	D31 (ppm)	D32 (ppm)	D33 (ppm)	D34 (ppm)	D36 (ppm)	D31	D32	D33	D34	D36
La	43.00	17.10	16.70	19.40	28.70	1.13	0.45	0.44	0.51	0.76
Ce	88.70	34.50	32.80	39.90	58.00	1.11	0.43	0.41	0.50	0.73
Pr	9.13	3.88	3.80	4.20	6.24	1.03	0.44	0.43	0.47	0.70
Nd	32.60	14.30	13.80	14.30	21.70	1.02	0.45	0.43	0.45	0.68
Sm	5.38	2.57	2.53	2.42	3.95	0.96	0.46	0.45	0.43	0.71
Eu	1.43	0.71	0.67	0.63	1.01	1.30	0.65	0.61	0.57	0.92
Gd	4.45	2.37	2.49	1.99	3.28	0.95	0.50	0.53	0.42	0.70
Tb	0.50	0.30	0.30	0.20	0.40	0.65	0.39	0.39	0.26	0.52
Dy	3.87	2.33	2.27	1.73	2.72	0.88	0.53	0.52	0.39	0.62
Ho	0.77	0.51	0.48	0.35	0.53	0.77	0.51	0.48	0.35	0.53
Er	2.37	1.57	1.44	1.01	1.64	0.82	0.54	0.50	0.35	0.57
Tm	0.36	0.25	0.22	0.13	0.22	0.72	0.50	0.44	0.26	0.44
Yb	2.43	1.53	1.46	0.88	1.53	0.87	0.55	0.52	0.31	0.55
Lu	0.38	0.22	0.22	0.16	0.22	0.76	0.44	0.44	0.32	0.44
Y	22.40	14.20	12.80	9.60	15.20	0.80	0.51	0.46	0.34	0.54
∑REE	217.77	96.34	91.98	96.90	145.34	13.76	7.34	7.04	5.94	9.38
∑LREE	178.81	72.35	69.63	80.22	118.59	5.25	2.22	2.16	2.36	3.56
∑HREE	15.13	9.08	8.88	6.45	10.54	6.41	3.96	3.81	2.67	4.36

Table 4.6 Normalisation of REE Concentration of Mafic Intrusive using PMV

Elements	Raw Values			Normalised Values		
	D25 (ppm)	D26 (ppm)	D27 (ppm)	D25	D26	D27
La	9.00	7.40	8.70	12.95	10.65	12.52
Ce	19.30	15.30	18.30	10.72	8.50	10.17
Pr	2.43	1.90	2.28	8.87	6.93	8.32
Nd	9.70	7.90	9.40	7.24	5.90	7.01
Sm	2.07	1.68	2.10	4.75	3.85	4.82
Eu	0.74	0.67	0.82	4.48	4.06	4.97
Gd	2.25	2.11	2.62	3.85	3.61	4.49
Tb	0.38	0.31	0.43	3.55	2.90	4.02
Dy	2.44	2.04	2.80	3.38	2.83	3.88
Ho	0.53	0.45	0.64	3.29	2.80	3.98
Er	1.64	1.26	1.79	3.47	2.66	3.78
Yb	1.59	1.33	1.86	3.35	2.80	3.92
Lu	0.26	0.20	0.29	3.59	2.76	4.01
Y	14.50	12.10	17.40	3.24	2.71	3.89
Tm	0.23	0.19	0.27	0.33	0.27	0.38
∑REE	66.83	54.65	69.43	76.74	62.96	79.77
∑LREE	42.50	34.18	40.78	44.53	35.83	42.84
∑HREE	9.32	7.89	10.70	24.81	20.63	28.45

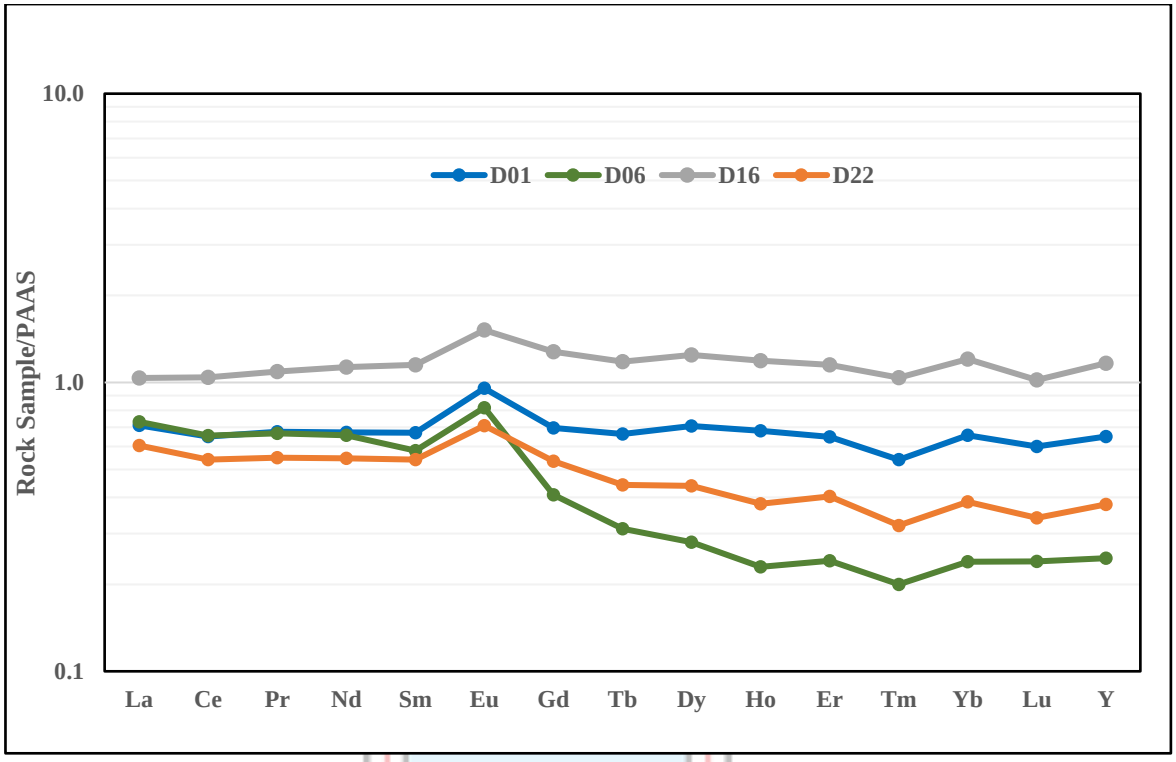

Fig. 4.23 Plot of REE of Banket Footwall Quartzite Normalised to PAAS

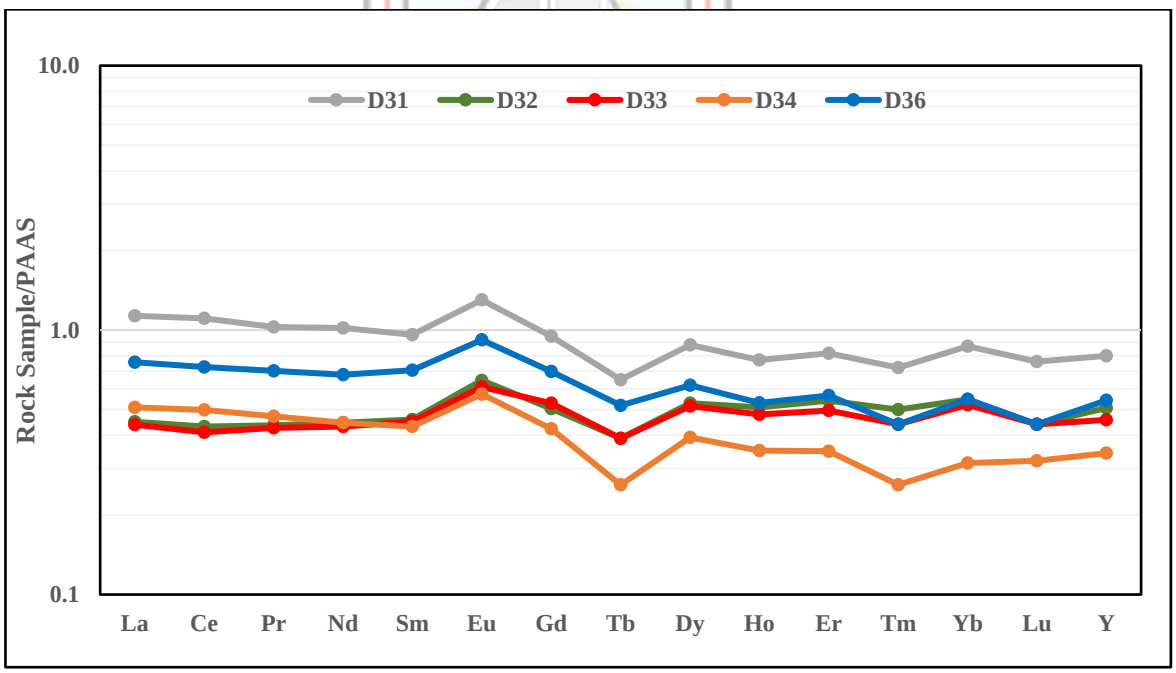

Fig. 4.24 Plot of REE of Banket Conglomerate Normalised to PAAS

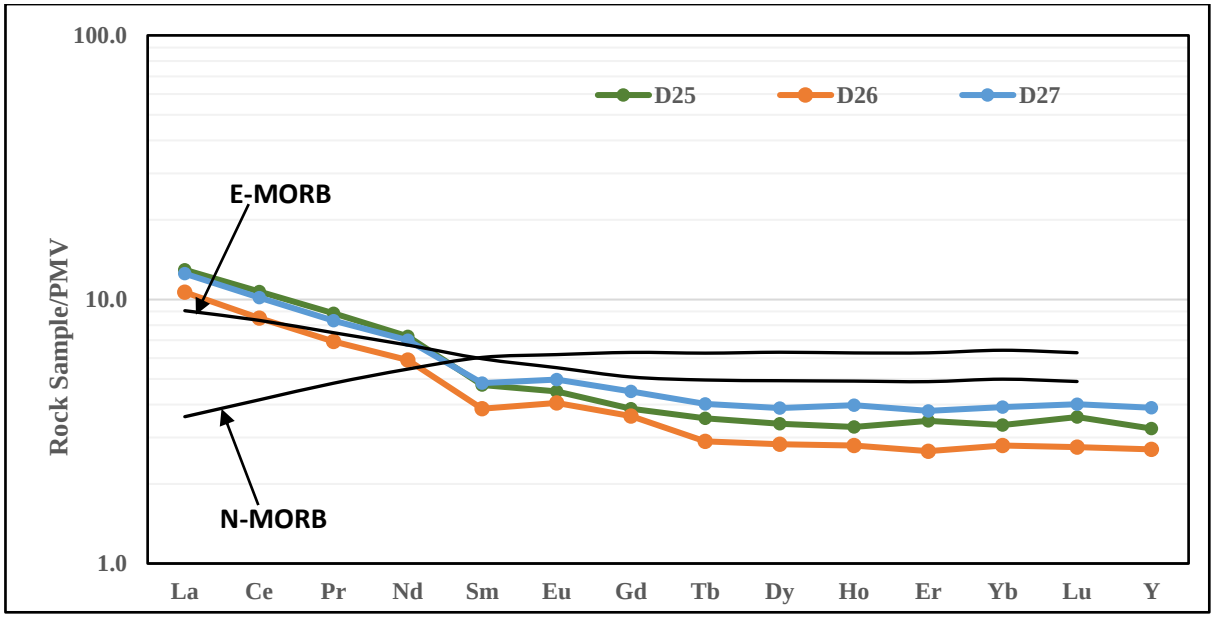

Fig. 4.25 Plot of REE of Mafic Intrusive Normalised to Primitive Mantle Values (PMV)

Fig. 4.25 depicts a uniform pattern in the samples being analysed where the light rare earth elements (LREE) are enriched and the high rare earth elements (HREE) are depleted. The unaltered rocks (D25 and D27) of the mafic intrusive has similar pattern as E-MORB (Enriched- Mid Ocean Rich Basalt).

4.3 Mass Balance Calculations

To determine the relative gains and losses of constituents during alteration, representative samples of the three (3) rock types were chemically analysed and compared. Average composition of unaltered and altered form of the various rock types are presented in Table 4.7. These averages were compared with one another using a computational and graphical method revised by Grant (1986). This is called the "isocon method" which provides a simple and direct means of considering changes in mass, volume and concentration within equivalent units during alteration. The isocon is simply a graphical simultaneous solution to Gresens' equation (1967). This method involves the establishment of a reference line corresponding to zero concentration change (an isocon) as determined statistically by a best fit to the geochemical data (Osterberg, 1985). The advantage of the isocon method is that the isocon may be established on the immobility of one component, a group of components, or on mass or volume chosen, then the determination of chemical gains and losses relative to concentration in the precursor rock can be determined graphically or mathematically by

the amount of displacement away from the reference isocon. It also provides the means of comparing a single precursor to different alteration types within the same lithologic unit on one isocon plot (Osterberg, 1985). Table 4.8, 4.9 and 4.10 shows the computational method used to obtain the gains and losses of the three (3) rocks.

Table 4.7 Average Chemical Concentrations of Unaltered and Altered Rock Types Analysed.

Components	Banket Footwall Quartzite		Banket Conglomerate		Mafic Intrusive	
	Unaltered	Altered	Unaltered	Altered	Unaltered	Altered
SiO_2 (wt%)	77.55	62.35	69.95	66.15	68.05	68.05
Al_2O_3 (wt%)	10.36	18.58	14.47	16.52	15.49	15.49
FeO_t (wt%)	4.38	7.16	5.77	6.47	6.12	6.12
CaO (wt%)	1.28	1.20	1.24	1.22	1.23	1.23
MgO (wt%)	0.60	0.59	0.59	0.59	0.59	0.59
Na_2O (wt%)	1.70	1.31	1.51	1.41	1.46	1.46
K_2O (wt%)	1.91	4.66	3.28	3.97	3.62	3.62
Cr_2O_3 (wt%)	0.01	0.02	0.01	0.02	0.02	0.02
TiO_2 (wt%)	0.28	0.65	0.46	0.55	0.51	0.51
MnO (wt%)	0.09	0.06	0.07	0.07	0.07	0.07
P_2O_5 (wt%)	0.02	0.10	0.06	0.08	0.07	0.07
SrO (wt%)	0.03	0.05	0.04	0.05	0.04	0.04
BaO (wt%)	0.10	0.21	0.15	0.18	0.17	0.17
Ba (ppm)	901.00	1862.50	1381.75	1622.13	1501.94	1501.94
V (ppm)	62.50	122.00	92.25	107.13	99.69	99.69
Cr (ppm)	95.00	125.00	110.00	117.50	113.75	113.75
Y (ppm)	8.75	25.40	17.08	21.24	19.16	19.16
W (ppm)	5.00	8.00	6.50	7.25	6.88	6.88

Table 4.8 Computation of Gains and Losses of Banket Footwall Quartzite

Components	C_iO (UA)	C_iA (A)	Slope to data point (C_iA/C_iO)	Gain/Loss relative to C_iO ($\Delta C_i/C_iO$)	Gain/Loss in weight % or ppm (ΔC_i)
SiO_2 (wt%)	77.55	62.35	0.80	-0.20	-15.20
Al_2O_3 (wt%)	10.36	18.58	1.79	0.79	8.22
FeO_t (wt%)	4.38	7.16	1.63	0.63	2.78
CaO (wt%)	1.28	1.20	0.94	-0.06	-0.08
MgO (wt%)	0.60	0.59	0.99	-0.01	-0.01
Na_2O (wt%)	1.70	1.31	0.77	-0.23	-0.39
K_2O (wt%)	1.91	4.66	2.44	1.44	2.75
Cr_2O_3 (wt%)	0.01	0.02	1.32	0.32	0.00
TiO_2 (wt%)	0.28	0.65	2.35	1.35	0.37
MnO (wt%)	0.09	0.06	0.71	-0.29	-0.03
P_2O_5 (wt%)	0.02	0.10	4.75	3.75	0.08
SrO (wt%)	0.03	0.05	1.67	0.67	0.02
BaO (wt%)	0.10	0.21	2.05	1.05	0.11
Ba (ppm)	901.00	1862.50	2.07	1.07	961.50
V (ppm)	62.50	122.00	1.95	0.95	59.50
Cr (ppm)	95.00	125.00	1.32	0.32	30.00
Y (ppm)	8.75	25.40	2.90	1.90	16.65
W (ppm)	5.00	8.00	1.60	0.60	3.00

Table 4.9 Computation of Gains and Losses of Banket Conglomerate

Components	C_iO (UA)	C_iA (A)	Slope to data point (C_iA/C_iO)	Gain/Loss relative to C_iO ($\Delta C_i/C_iO$)	Gain/Loss in weight % or ppm (ΔC_i)
SiO_2 (wt%)	86.00	76.10	0.88	-0.12	-9.90
Al_2O_3 (wt%)	5.98	10.23	1.71	0.71	4.25
FeO_t (wt%)	4.10	6.76	1.65	0.65	2.66
CaO (wt%)	0.69	0.84	1.20	0.20	0.14
MgO (wt%)	0.41	0.75	1.80	0.80	0.33
Na_2O (wt%)	0.57	1.44	2.53	1.53	0.87
K_2O (wt%)	1.05	1.38	1.32	0.32	0.33
Cr_2O_3 (wt%)	0.01	0.02	1.21	0.21	0.00
TiO_2 (wt%)	0.26	0.43	1.63	0.63	0.17
MnO (wt%)	0.10	0.10	1.00	0.00	0.00
P_2O_5 (wt%)	0.04	0.05	1.23	0.23	0.01
SrO (wt%)	0.02	0.02	1.00	0.00	0.00
BaO (wt%)	0.05	0.08	1.61	0.61	0.03
Ba (ppm)	437.67	661.50	1.51	0.51	223.83
V (ppm)	65.67	117.50	1.79	0.79	51.83
Cr (ppm)	106.67	125.00	1.17	0.17	18.33
Y (ppm)	13.00	17.60	1.35	0.35	4.60
W (ppm)	3.00	12.50	4.17	3.17	9.50

Table 4.10 Computation of Gains and Losses of Mafic Intrusive

Components	C_iO (UA)	C_iA (A)	Slope to data point (C_iA/C_iO)	Gain/Loss relative to C_iO ($\Delta C_i/C_iO$)	Gain/Loss in weight % or ppm (ΔC_i)
SiO_2 (wt%)	48.90	50.40	1.031	0.031	1.50
$Al2O_3$ (wt%)	16.18	14.05	0.869	-0.131	-2.13
FeO_t (wt%)	9.78	8.26	0.845	-0.155	-1.52
CaO (wt%)	8.06	10.25	1.272	0.272	2.19
MgO (wt%)	8.59	6.93	0.807	-0.193	-1.66
Na_2O (wt%)	2.33	2.52	1.084	0.084	0.20
K_2O (wt%)	1.17	0.27	0.232	-0.768	-0.90
Cr_2O_3 (wt%)	0.05	0.05	0.979	-0.021	0.00
TiO_2 (wt%)	0.53	0.42	0.800	-0.200	-0.11
MnO (wt%)	0.15	0.14	0.933	-0.067	-0.01
P_2O_5 (wt%)	0.10	0.03	0.316	-0.684	-0.07
SrO (wt%)	0.04	0.08	2.000	1.000	0.04
BaO (wt%)	0.05	0.01	0.200	-0.800	-0.04
Ba (ppm)	448.00	90.90	0.203	-0.797	-357.10
V (ppm)	160.00	118.00	0.738	-0.263	-42.00
Cr (ppm)	365.00	350.00	0.959	-0.041	-15.00
Y (ppm)	15.95	12.10	0.759	-0.241	-3.85
W (ppm)	11.50	13.00	1.130	0.130	1.50

To obtain the graphical representation of the gains and losses of elements and oxides, scaling of the concentrations of the unaltered and altered are done to distribute the data properly and for easy reading. It is important to realise that scaling is irrelevant to the slope of an isocon if the isocon is based on the slopes of CiA/CiO, of the rays from the origin to each point, because the scale factor cancels in the slope calculations (Grant, 2005). Table 4.11, 4.12 and 4.13 show the scaling of the concentrations of the three (3) rock types. The scaled concentrations have been used for the plotting of altered against unaltered as shown in figure 4.26 to 4.28. The isocon line of constant mass and constant volume is plotted. In plotting the second isocon line, immobile elements or oxides thus, Al_2O_3, TiO_2, Y and REE are tested together with those oxides and elements close to the constant mass and constant volume to see their correlation before they can be chosen to draw the isocon line. Fig. 4.29 to Fig 4.33 shows the correlation plots for the testing.

Table 4.11 Scaling concentrations of Banket Footwall Quartzite

Components	C_iO (UA)	C_iA (A)	Scale	CiO	CiA
SiO_2 (wt%)	77.55	62.35	0.64	50	40.2
Al_2O_3 (wt%)	10.36	18.58	4.63	48	86.06
FeO_t (wt%)	4.38	7.16	10.5	46	75.2
K_2O (wt%)	1.91	4.66	23.1	44	107.52
Na_2O (wt%)	1.7	1.31	24.71	42	32.36
CaO (wt%)	1.28	1.2	31.25	40	37.5
MgO (wt%)	0.6	0.59	63.87	38	37.68
TiO_2 (wt%)	0.28	0.65	65.45	18	42.22
BaO (wt%)	0.1	0.21	360	36	73.8
MnO (wt%)	0.09	0.06	400	34	24
SrO (wt%)	0.03	0.05	1066.67	32	53.33
P_2O_5 (wt%)	0.02	0.1	800	16	76
Cr_2O_3 (wt%)	0.01	0.02	2400	30	39.6
Ba (ppm)	901	1862.5	0.03	28	57.88
Cr (ppm)	95	125	0.27	26	34.21
V (ppm)	62.5	122	0.38	24	46.85
Y (ppm)	8.75	25.4	2.51	22	63.86
W (ppm)	5	8	4	20	32

Table 4.12 Scaling Concentrations of Banket Conglomerate

Components	C_iO (UA)	C_iA (A)	Scale	C_iO	C_iA
SiO_2 (wt%)	86	76.1	0.47	40	35.4
Al_2O_3 (wt%)	5.98	10.23	6.36	38	65.04
FeO_t (wt%)	4.1	6.76	8.77	36	59.31
K_2O (wt%)	1.05	1.38	32.48	34	44.83
CaO (wt%)	0.69	0.84	46.15	32	38.54
Na_2O (wt%)	0.57	1.44	10.53	6	15.16
MgO (wt%)	0.41	0.75	72.58	30	54.07
TiO_2 (wt%)	0.26	0.43	106.33	28	45.72
MnO (wt%)	0.1	0.1	260	26	26
BaO (wt%)	0.05	0.08	514.29	24	38.57
P_2O_5 (wt%)	0.04	0.05	600	22	27
SrO (wt%)	0.02	0.02	1333.33	20	20
Cr_2O_3 (wt%)	0.01	0.02	1285.71	18	21.86
Ba (ppm)	437.67	661.5	0.04	16	24.18
Cr (ppm)	106.67	125	0.13	14	16.41
V (ppm)	65.67	117.5	0.18	12	21.47
Y (ppm)	13	17.6	0.77	10	13.54
W (ppm)	3	12.5	2.67	8	33.33

Table 4.13 Scaling Concentrations of Mafic Intrusive

Components	C_iO (UA)	C_iA (A)	Scale	CiO	CiA
SiO_2 (wt%)	48.9	50.4	0.82	40	41.23
Al_2O_3 (wt%)	16.18	14.05	2.35	38	33.01
FeO_t (wt%)	9.78	8.26	3.68	36	30.4
MgO (wt%)	8.59	6.93	3.96	34	27.45
CaO (wt%)	8.06	10.25	1.99	16	20.35
Na_2O (wt%)	2.33	2.52	13.76	32	34.68
K_2O (wt%)	1.17	0.27	25.75	30	6.95
TiO_2 (wt%)	0.53	0.42	26.67	14	11.2
MnO (wt%)	0.15	0.14	186.67	28	26.13
P_2O_5 (wt%)	0.1	0.03	273.68	26	8.21
BaO (wt%)	0.05	0.01	480	24	4.8
Cr_2O_3 (wt%)	0.05	0.05	250	12	11.75
SrO (wt%)	0.04	0.08	250	10	20
Ba (ppm)	448	90.9	0.05	22	4.46
Cr (ppm)	365	350	0.02	8	7.67
V (ppm)	160	118	0.13	20	14.75
Y (ppm)	15.95	12.1	1.13	18	13.66
W (ppm)	11.5	13	0.52	6	6.78

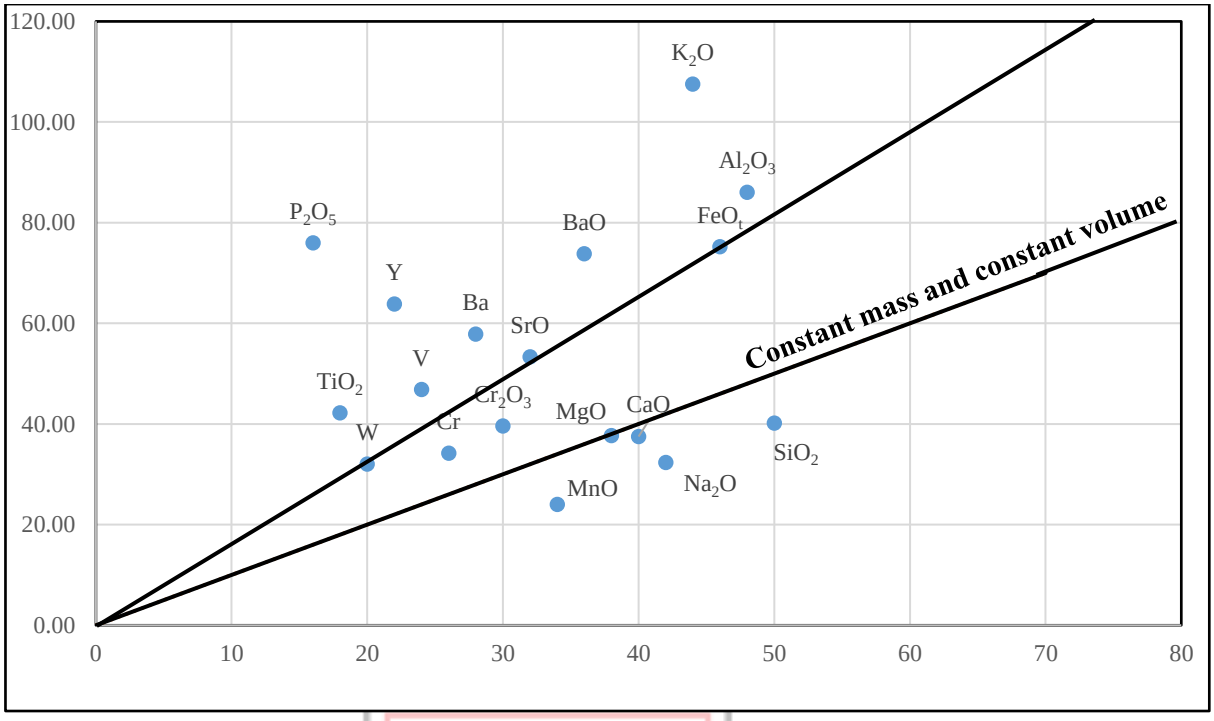

Fig. 4.26 Isocon Diagram of Banket Footwall Quartzite

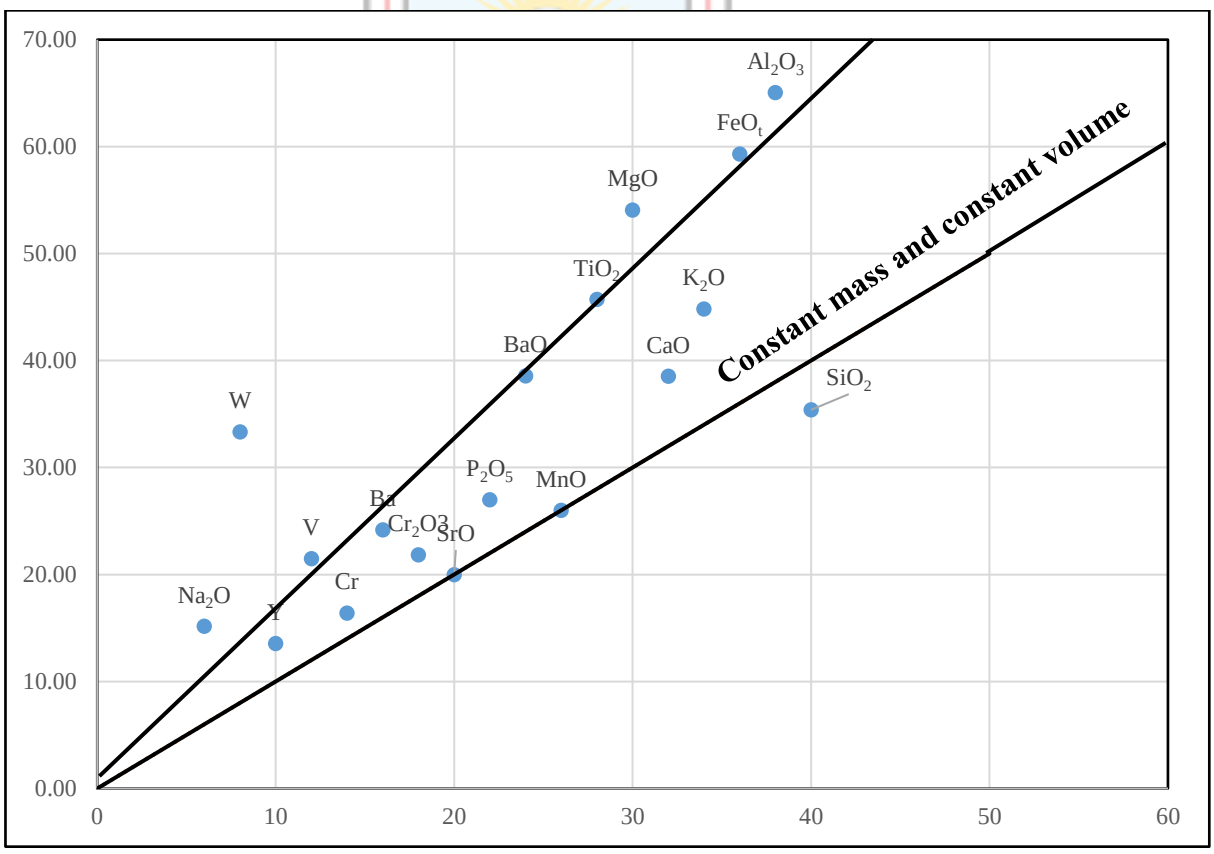

Fig. 4.27 Isocon Diagram of Banket Conglomerate

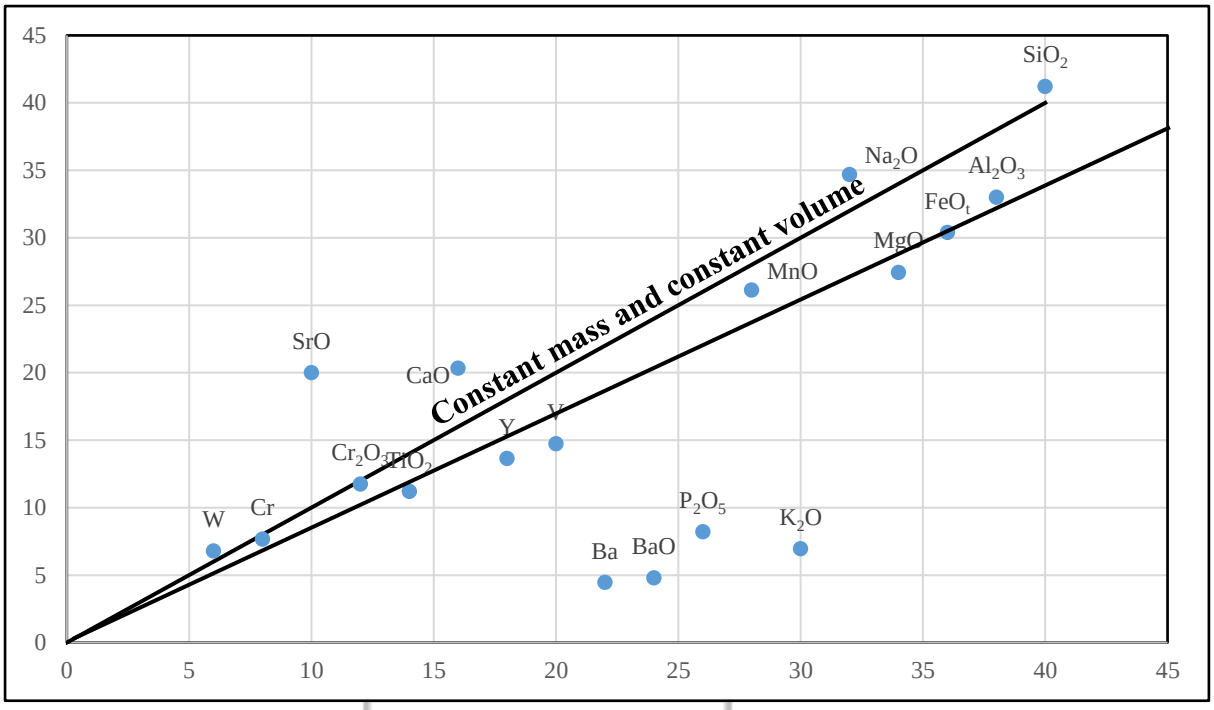

Fig. 4.28 Isocon Diagram of Mafic Intrusive

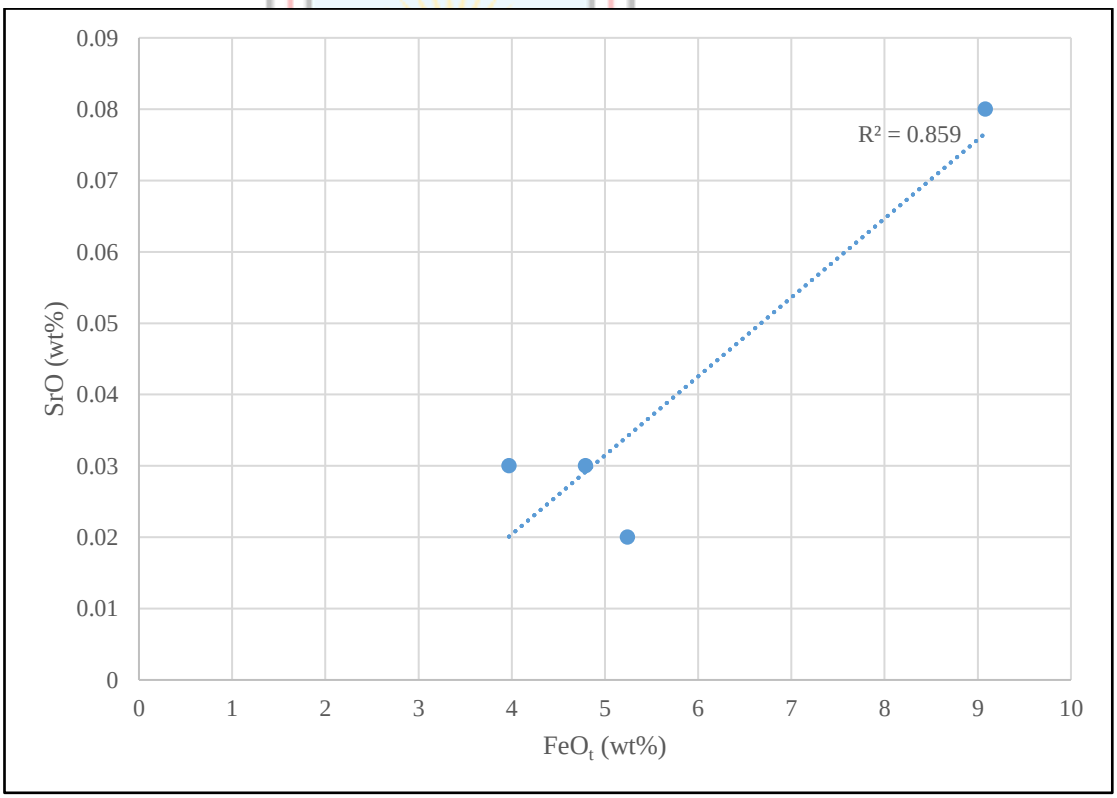

Fig. 4.29 Correlation Plot of SrO against Total FeO for Banket Footwall Quartzite

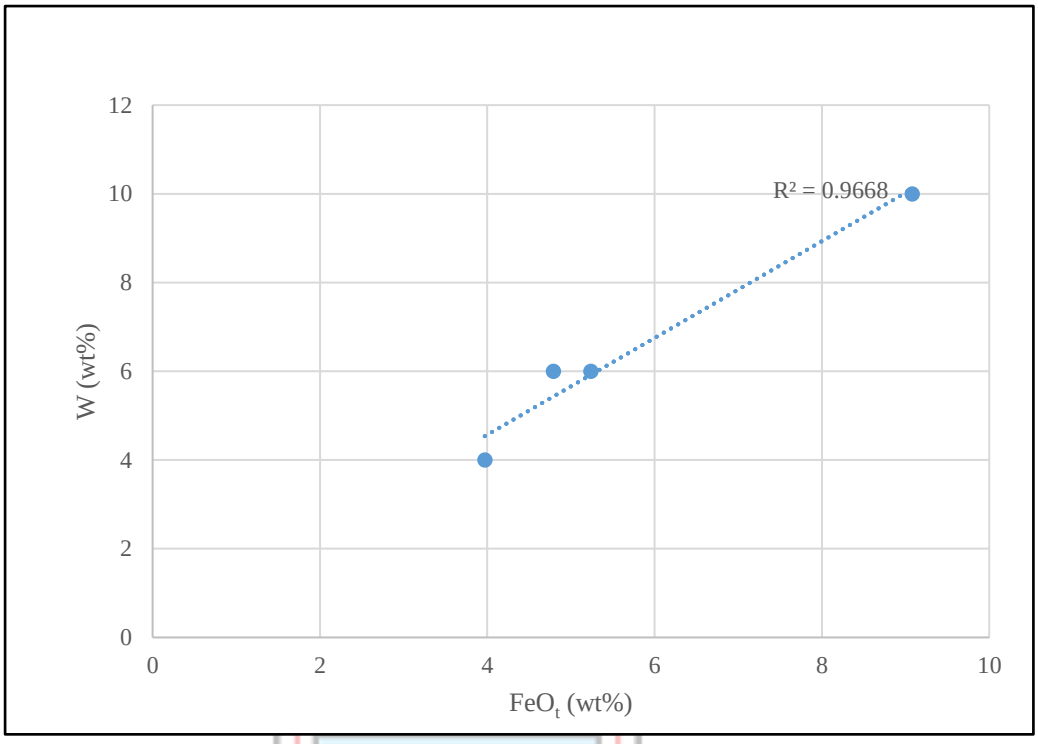

Fig. 4.30 Correlation Plot of W against Total FeO for Banket Footwall Quartzite

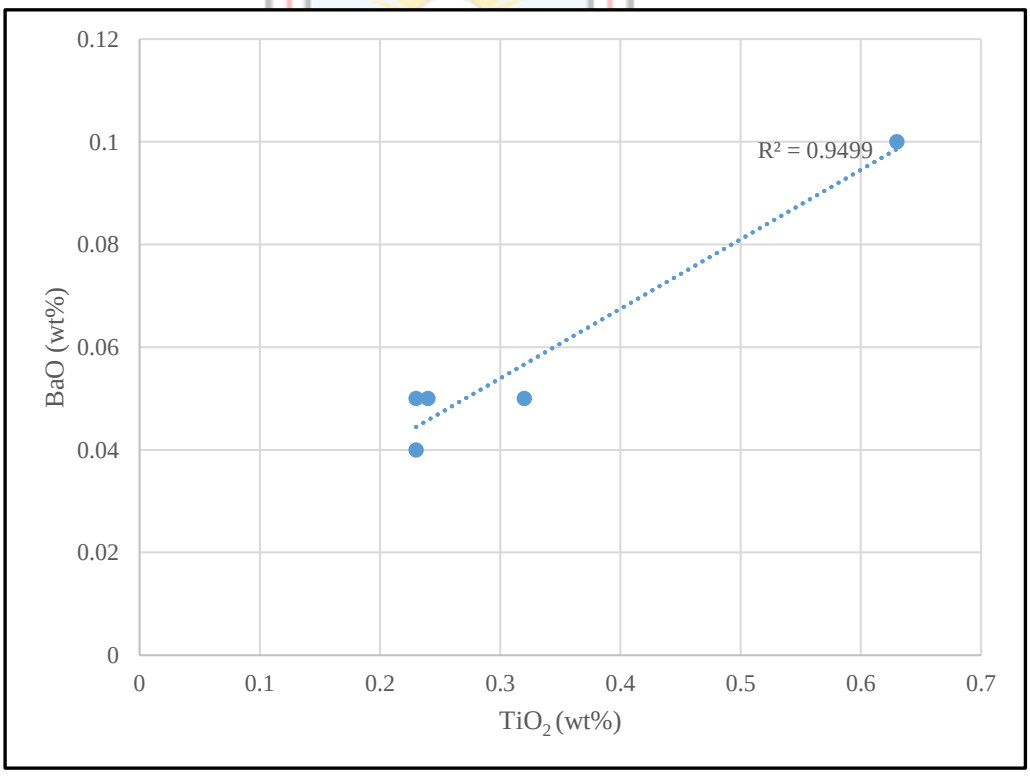

Fig. 4.31 Correlation Plot of BaO against TiO_2 for Banket Conglomerate

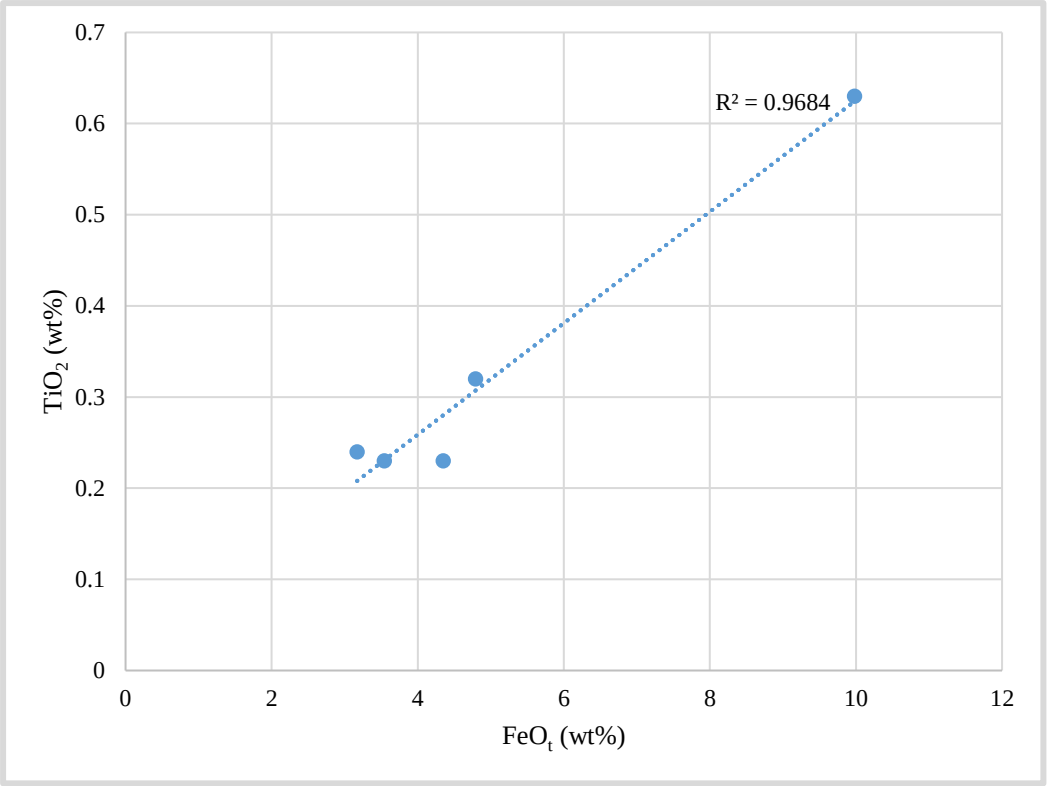

Fig. 4.32 Correlation Plot of TiO_2 against Total FeO for Banket Conglomerate

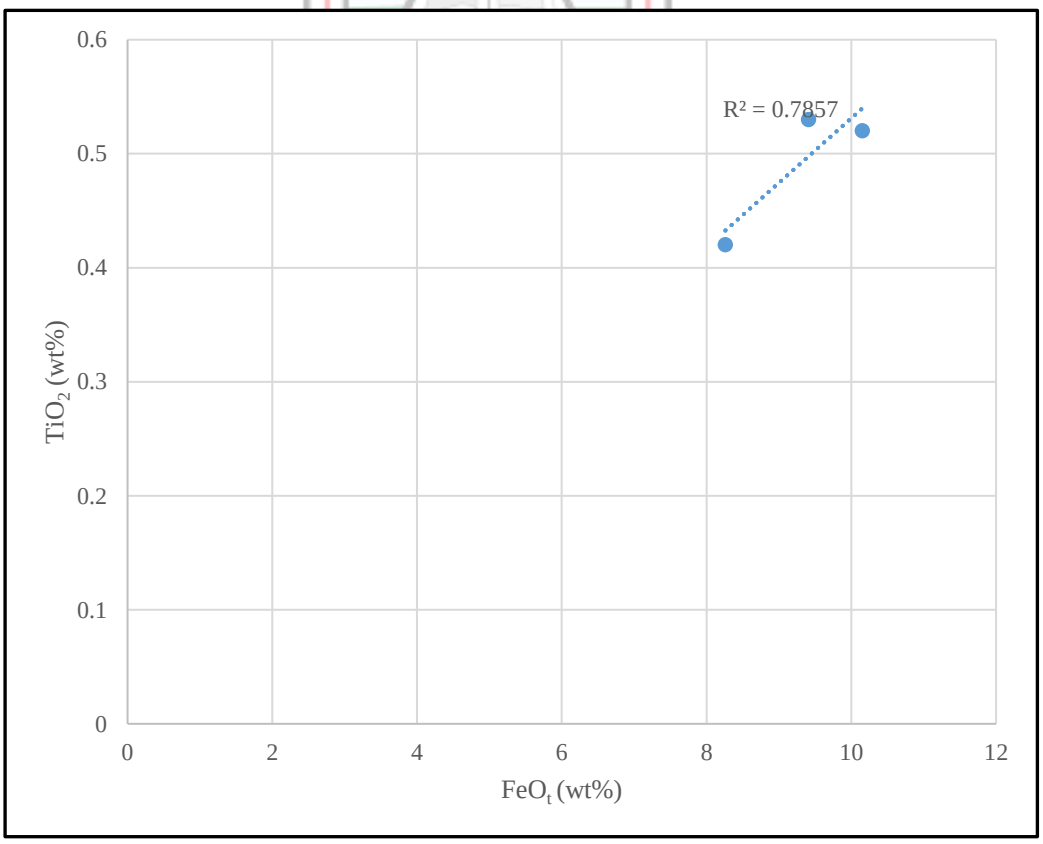

Fig. 4.33 Correlation Plot of TiO_2 against Total FeO for Mafic Intrusive

CHAPTER 5

DISCUSSION

5.1 Petrography

Amoanda Pit and Damang Cutback Pit are located in the Tarkwaian Group, north east of Tarkwa where banket footwall quartzites and banket conglomerates of the Banket Series host important gold deposits (Griffiths *et al.*, 2002). These quartzites are overlain by conglomerates (Sharpe, 2005). The quartzites at Amoanda Pit have quartz grains which are medium to coarse grained (10 mm to 25 mm), sub-rounded, sub-mature, moderately sorted and are dominated by monotonous succession of cross-beds (Fig. 4.1). Occasional oligomictic, sub-rounded quartz pebbles occur. The grains are associated with matrix of granular medium grained plagioclase feldspars, amphibole, magnetite, hematite and ilmenite (Fig. 4.3A, 4.8A and Table A). There are two (2) generations of magnetite and hematite where earlier versions are primary and associated with sedimentation and found at the margins of quartz pebbles (quartz 1) (Fig. 4.3C), the second generation types are associated with alteration and found with recrystallised quartz (quartz 2) which are also parallel to foliations (Fig. 4.3B). Primary chalcopyrite is partially replaced by secondary magnetite which shows exsolution of ilmenite and also partially altered and aggregate into cubic pyrite. Granular fine gold is associated with secondary hematite and magnetite (Fig. 4.8B). Other heavy minerals in the matrix are rutile, zircon and gold (Junner *et al.*, 1942; Kesse, 1985; Hirdes and Nunoo, 1994). Quartz-Feldspar-Rock fragments (QFR) plot after Folk (1974) was used to unravel the protoliths of the quartzite as sublitharenite, feldspathic litharenite and litharenite with differences in the protoliths due to varying quartz composition and feldspars (Fig. 4.7). There are two (2) generations of plagioclase feldspars which are associated with sedimentation. The primary plagioclase were mainly oligoclase composition (An_{14}) (Fig. 4.3A), secondary plagioclase is labradorite (An_{60}) shows no features of hydrothermal sources (Fig. 4.14D) but may be associated with mafic rock such as dolerite.

Banket conglomerate located at the Damang Cutback Pit overlies banket footwall quartzites (Fig. 3.3). It is coarse to medium grained (25mm to 60mm), oligomictic or polymictic with matrix made up of quartz, plagioclase feldspars and sericite and large pebble or matrix composed of rounded and moderately sorted quartz pebbles and lithic pebbles of chert,

schist, quartzites and hornstone (Fig. 4.9, Table 4.2). Pebble fabrics are clast supported in the well developed areas where there is parallel stratification of elongate clast and matrix supported in the poorly developed areas (Fig. 4.9). These sedimentary textures of the Tarkwaian Group are considered to be of shallow water continental origin derived from the Birimian and associated granitoids (Sestini, 1973). The sediments were deposited by high energy alluvial fans entering a steep-sided basin filled with fresh water which consist of coarse, poorly sorted, immature sediments with low roundness (Kesse, 1985). Associated with the matrix are chlorite, plagioclase feldspars, garnet and amphiboles. Two types of amphiboles occur; the amphiboles are either partially altered to chlorites or partially altered to chlorites and epidotes (Fig. 4.10D). Biotite which marks foliation is partially replaced by garnet (Fig. 4.11A). Plagioclase is euhedral of andesine composition (An_{44}) and labradorite (An_{58}).

Intrusives at the Damang Cutback Pit occur as a sill or dyke (Fig. 4.13). The rock contains plagioclase feldspars, amphibole, chlorite, sericite and quartz as dominant minerals with epidote, biotite, garnet and pyroxene as minor constituents. Primary plagioclase and amphiboles are overprinted by granular pyrite, pyrrhotite and chalcopyrite. (Fig. 4.14A). Primary plagioclase is partially altered to sericite and quartz whilst primary amphibole is partially altered to chlorite. Pyrite 1 is partially altered to secondary hematite and magnetite and overprinted by pyrite 2 (Fig. 4.15B). Quartz 2 also corrodes the margins of primary amphiboles whilst margins of chalcopyrite are also corroded and partially replaced by gold which is overprinted by secondary hematite and magnetite (Fig. 4.15C and D). Gold is also associated with pyrite. Quartz-Alkali-Plagioclase (QAP) plot after Streckeisen *et al.*, 2002 indicate diorite (Fig. 4.16). This was referred to as ‘epidiorite’ gabbro (Junner *et al.*, 1942).

The sill is also in contact with banket footwall quartzites or banket conglomerates with no significant change in the host rock fabric. Primary plagioclase in the dolerite is mainly oligoclase. With earlier amphiboles associated with plagioclase whilst late amphiboles overprint both quartz 2 and earlier amphiboles in the dolerite. Dolerite cut quartz 3 and corroded its margins. Secondary minerals such as goethite, pyrrhotite, chalcopyrite, pyrite, hematite and magnetite had partially been replaced by primary mineral pyrite which occur in fractures of quartz. Dolerite accompanied heat might have remobilised gold in the banket footwall quartzite and the banket conglomerate as there is the occurrence of contact metamorphism (Fig. 4.14B). According to Fiadonu (2019), hydrothermal alteration led to enrichments of gold. Banket footwall quartzite and banket conglomerate have sericite,

epidote, chlorite and garnet (Table 4.1; Table 4.2) and so affected by greenshist facies (Miyashiro, 1961). Amphiboles, epidote and plagioclase feldspars in the banket footwall quartzite and banket conglomerate suggests peak amphibolite facies metamorphism with subsequent greenschist facies metamorphism because of the presence of quartz and chlorite and late amphibolite facies in the dolerite described by Griffiths *et al.*, 2002 as having varying degrees of metamorphism up to greenschist facies. At Damang, all lithologies to the east of the Damang fault in the mine sequence, including the dolerites, have been affected by mid-amphibolite facies metamorphism with temperatures estimates based on garnet-biotite geothermometry of 5500 ^{o}C (Pigois *et al.*, 2003). The regional metamorphism is quite high and varies from middle amphibolite to greenschist facies (Brabham, 1998).

5.2 Geochemistry

The mafic intrusives contain chlorite and amphiboles (Fig. 4.14A) and these give rise to very high MgO (Fig. 4.17). Alternatively, banket footwall quartzites and banket conglomerates have very low chlorite $(Mg,Fe)_5Al(Si_3Al)O_{10}(OH)_8$ and amphibole $Mg_7Si_8O_{22}(OH)_2$ composition and therefore MgO values are relatively low. Mafic intrusives are ankerite-$CaFe(CO_3)$ rich and so CaO richer ranging from 7.79 to 10.25 wt% (Fig. 4.18). Banket footwall quartzites and banket conglomerates have relatively low values of CaO ranging from 0.26 to 1.33 wt%. Plagioclase is partially altered to sericite in all the rock types. Sericite alteration dominate the altered rock types and is depicted by their Al_2O_3 contents ranging from 6.86 to 26.6 wt% (Fig. 4.19). Banket footwall quartzite (sample D16) has very high Al_2O_3 content of 26.6 wt% than all the other samples probably due to very high sericitic alteration. Ilmenite which is a major heavy mineral is associated with the three rock types (Fig. 4.3A). This is evident in Fig. 4.20 with all the rock types having traces of TiO_2. Samples with high values of FeO_t have high values of TiO_2 as seen in Fig. 4.20. Rocks altered with magnetite and hematite also have high amount of ilmenite.

All the mafic intrusives (D25, D26 and D27) analysed are made up of mainly amphiboles, biotite $[K(Mg,Fe)_3AlSi_3O_{10}(OH)_2]$ and epidote $Ca_2(Al_2,Fe)(SiO_4)(Si_2O_7)O(OH)$ (Table 4.3, Fig. 4.21). Hence they have higher values of MgO and FeO_t than the banket footwall quartzites and banket conglomerate. Meta-dolerite consists of amphibole and plagioclase crystals with minor quartz, biotite, chlorite, epidote and accessory oxide phases (Sharpe, 2005).

Gold grade is associated with altered rocks. Palaeoplacer gold is the main source of gold in the banket conglomerate (Griffiths *et al.,* 2002) are associated with pyrite and sericite (Fig. 4.22). Unaltered mafic intrusives and banket footwall quartzite have little or no gold (Appendix E). Unaltered banket conglomerates also have less or no gold (Appendix E). Grades are significantly improved where quartz veins and alteration affect conglomerates. The banket conglomerates have the earliest gold mineralisation known in the area and are interpreted to be palaeoplacer gold deposits that have been slightly modified by subsequent metamorphism and deformation (Tunks *et al.,* 2004)

The flat pattern of the samples of banket footwall quartzite and banket conglomerate plots is an indication of the fact that alteration had no effect on the REE distribution pattern of the original rock. The Eu anomaly values being greater than 1 is an indication of plagioclase accumulation in the rock (Hugh, 1993) (Fig. 4.23 and Fig. 4.24). High total REE value are also indications of alteration in the rocks.

In Fig. 4.25, all the three (3) samples of the mafic intrusives (D25, D26 and D27) show similar patterns where the light rare earth elements (LREE) are enriched whilst the heavy rare earth elements (HREE) are significantly depleted. This results indicate that the mafic magma was a hydrous magma (Lesnov, 2010). Due to the alteration, D26 had not caused so much enrichment in the LREE and depletion in the HREE. Unaltered mafic intrusive samples (D25 and D27) which has the same pattern as E-MORB (Enriched-Mid Ocean Ridge Basalt) implies a similar tectonic setting for the mafic intrusives. E-MORB are normally formed in rifted zones on the ocean floor (Corcoran and Dostal, 2001).

From Fig. 4.26, FeO_t, SrO and W form a linear array through the origin. This suggests that these elements are considered immobile components of the banket footwall quartzite and so were used to define a best-fit isocon as they had little mass transfer of components (Grant, 1986). The other elements that fall above the isocon line mainly K_2O, P_2O_5, BaO, TiO_2 and Al_2O_3 which represent minerals of potassium feldspars, ilmenite and sericite have been significantly added due to alteration as seen in Table 4.9. Alternatively, components that fall below the isocon line are those minerals that have been significantly removed in the alteration process of banket footwall quartzite which are ankerite, amphibole and quartz. Subsequently, Fig. 4.27 also indicates that oxides such as Na_2O, MgO and Al_2O_3 which are rich in sericite, chlorite and amphibole had been significantly been added during alteration and CaO, K_2O, and SrO also representing ankerite, potassium feldspars and apatite had

significantly been removed during the alteration in the banket conglomerate. Similarly, the mafic intrusive plot in Fig. 4.28 also indicates elements such as SrO, SiO_2, Na_2O, CaO Cr_2O_3 representing mineral such as ankerite, has been significantly added during alteration and K_2O, P_2O_5, Ba and BaO had significantly been removed during the alteration process. According to Fiadonu (2019), gold enrichment was transported in solution as bisulphide complex ($Au(HS)_2^-$) at a temperature range of 250 ºC to 400 ºC and pressure range of 0.70 – 2.00 kbar based on fluid inclusion isochore calcualations.

CHAPTER 6

CONCLUSIONS AND RECOMMENDATIONS

6.1 Conclusions

- The banket footwall quartzites at Amoanda Pit have quartz grains which are medium to coarse grained, sub-rounded, sub-mature, moderately sorted and are dominated by monotonous succession of cross-beds. These contain two (2) generations of magnetite and hematite with the earlier versions associated with sedimentation and found at the margins of the quartz pebbles; the second generation minerals are related with alteration and found with recrystallised quartz. Primary Plagioclase is mainly of oligoclase composition and secondary plagioclase (labradorite composition) of hydrothermal sources. Granular fine gold is associated with secondary hematite and magnetite. The palaeoplacers were affected by peak amphibolite facies metamorphism with subsequent greenschist facies metamorphism.
- The mafic intrusive (dolerite) contains plagioclase feldspars, amphibole, chlorite, sericite and quartz as dominant minerals with epidote, biotite, garnet and pyroxene as minor constituents. Contact metamorphism occurs at the margins of dolerite and the banket footwall quartzite or the banket conglomerate. Dolerite intrusion accompanied heat might have remobilised gold in the banket footwall quartzite and the banket conglomerate to form secondary amorphous gold other than the palaeoplacer granular gold.
- Possibly, high MgO wt% in the mafic intrusives correspond to chlorite and amphibole constituents in the rock. Immobile components of FeO_t, SrO and W are found in the banket footwall quartzite whilst BaO and TiO_2 are in the banket conglomerate. However, K_2O, P_2O_5, BaO, TiO_2 and Al_2O_3 had been significantly added due to alteration of the banket footwall quartzite and Na_2O, MgO, Al_2O_3, CaO, K_2O, and SrO to the banket conglomerate. These elements/oxides may be associated with potassium feldspars, sericite, chlorite, amphibole, ankerite, ilmenite and apatite. Some ankerite was also added during alteration of the mafic intrusives.
- Alteration had no effect on the REE distribution pattern in the banket footwall quartzite and banket conglomerate. Mafic intrusive (diorite) show that light rare earth elements (LREE) are enriched whilst the heavy rare earth elements (HREE)

are significantly depleted which is an indication that the mafic magma was a hydrous magma.

6.2 Recommendations

- Exploration for post placer gold at the contacts between dolerite and banket footwall quartzite or banket conglomerate should target gold other than the palaeoplacer gold.
- Further petrological investigations using microprobe or scanning electron microscope (SEM) should find out the morphology and associated minerals and elements which accompanied the introduction of gold other than the palaeoplacer gold.
- Mass balance calculations should extensively be conducted with XRD examination to ascertain the minerals added and removed during alteration.

REFERENCES

Abouchami, W., Boher, M., Michard, A. and Albarède, F. (1990), "A Major 2.1 Ga Old Event of Mafic Magmatism in West Africa: An Early Stage of Crustal Accretion". *Journal of Geophysical Research*, Vol. 95, pp. 17605-17629.

Allibone, A., McCuaig T. C., Harris D., Etheridge, M., Munroe, S. and Byrne, D. (2002a), "Structural Controls on Gold Mineralisation at the Ashanti Gold Deposit", *Society of Economiic Geologists*, Special Publication, Obuasi, Ghana, Vol. 9, pp. 60-94.

Anon (1990), *Geocongress '90: 23rd Earth Science Congress of the Geological Society of South Africa: abstracts, University of Cape Town, Cape Town, (Johannesburg)*: Geological Society of South Africa, 768 pp.

Asihene, K. A. B. and Barning, K. (1975), "A Contribution to the Stratigraphy of the Birimian System of Ghana, West Africa", *Ghana Geological Survey Report 75/5, Accra*, 30 pp.

Assie, K. E. (2008), "Lode Gold Mineralisation in the Palaeoproterozoic (Birimian) Volcano-Sedimentary Sequence of Afema Gold District, Southeastern Côte d'Ivoire", *Journal of African Earth Sciences*, Vol. 57, No. (5), pp. 423-430.

Attoh, K. (1980), "Structure, Stratigraphy, and some Chemical characteristics of an Early Proterozoic (Birimian) Volcanic belt, northeastern Ghana", *Current Research*, Part C, Geological Survey Canada Paper 80-1C, pp. 69-80

Barnicoat, A., Henderson, I. H. C., Knipe, R. J., Yardley, B. W. D., Napier, R. W., Fox, N. P. C., Kenyon, A. K., Muntingh, D. J., Strydom, D., Winkler, K. S., Lawrence, S. R. and Cornford, C. (1997), "Hydrothermal gold mineralization in the Witwatersrand Basin." Nature, Vol. 386, pp. 820-823.

Bessoles, B. (1977), "Le Craton Ouest Africain Mémoire. Bureau Recherque Géologique Minière, Orléans", *Géologie de l'Afrique*, Vol. 1, 88, 402 pp.

Boher, M., Abouchami, W., Michard, A.F. and Arndt, N. T. (1992), "Crustal Growth in West Africa at 2.1 Ga", *Journal of Geophysical Research*, Vol. 97, pp. 345 - 369.

Brabham, G. (1998), “The Regional Geological Setting and Nature of The Damang Stockwork Gold Deposit - A New Type Of Gold Deposit in Ghana”, *Unpublished MSc Thesis,* Dept. of Geology and Geophysics, University of Western Australia, 101 pp.

Corcoran, P. L. and Dostal, J. (2001), “Development of an ancient back-arc basin overlying continental crust: the Archean Peltier Formation, Northwest Territories, Canada”, *The Journal of Geology*, Vol. 109, pp. 329-348.

Craig, J. R. and Vaughan, D. J. (1994), *Ore microscopy and ore petrography*, 2nd Edition, John Wiley and Sons, Inc., New York, 127 pp.

Davis, D. W., Hirdes, W., Schaltegger, U. and Nunoo, E. A. (1994), "U-Pb Age Constraints on Deposition and the Provenance of Birimian and Gold-Bearing Tarkwain Sediments in Ghana, West Africa." *Precambrian Research*, Vol. 67, pp. 89-107.

de Kock, G. S., Armstrong, R. A., Siegfried, H. P. and Thomas, E. (2011) “Geochronology of the Birim Supergroup of the West African Craton in the Wa-Bolé region of west-central Ghana: Implications for the stratigraphic framework”, *Journal of African Earth Sciences*, Vol. 59, pp. 1-40.

Doblas, M., López-Ruiz J., Cebriá, J.M., Youbi, N. and Degroote, E. (2002), “Mantle insulation beneath the West African Craton during the Precambrian-Cambrian transition” *The Geological Society of America*, Vol. 30 (9) pp. 839-842.

Dzigbodi – Adjimah, K. (1988), "On the Genesis of the Birimian Gold Deposits of Ghana", International. Conference on the Geology of Ghana, Accra Ghana pp. 123 - 167.

Fiadonu, E. B. (2019), “The Geology and Physico-chemical Characteristics of the Hydrothermal Gold Mineralisation at the Damang Gold Deposit, Ghana”, *Unpublished PhD Thesis*, Dept. of Geological Engineering, University of Mines and Technology, 203 pp.

Folk, R. L. (1974), *Petrology of Sedimentary Rocks*. Hemphill Publishing Co., Austin, 170 pp.

Grant, J. A. (2005), “Isocon analysis: A brief review of the method and applications”, *Physics and Chemistry of the Earth*, Vol. 30, pp. 997-1004.

Grant, J. A. (1986), “The isocon diagram - a simple solution to Gresens’ equation for metasomatic alteration”, *Economic Geology*, Vol. 81, pp. 1976-1982.

Gresens, R. L. (1967), “Composition–volume relationships of metasomatism”, *Chemical Geology*, Vol. 2, pp. 47-55.

Griffis, R. J., Barning, K., Agezo, F. L. and Akosah, F. K. (2002), *Gold deposits of Ghana*, Minerals Commission, Accra, 430 pp.

Hirdes, W. and Davis, D.W. (2002), “U–Pb geochronology of Palaeoproterozoic rocks in the southern part of the Keougou-Keneba inlier, Senegal, West Africa: evidence for diachronous accretionary development of the Birimain Province”, *Precambrian Research*, Vol. 118, pp. 83-99

Hirdes, W., Davis, D. W., Ludtke, G. and Konan, G. (1996), "Two Generations of Birimian (Palaeoproterozoic) Volcanic Belts in Northeastern Côte d’Ivoire (West Africa): Consequences for the Birimian Controversy". *Precambrian Research*, Vol. 80, pp. 173-191.

Hirdes, W. and Nunoo, B. (1994), “The Proterozoic Palaeoplacers at Tarkwa Gold Mine, SW Ghana: Sedimentology, Mineralogy, and Precise Age Dating of the Main Reef and West Reef, and Bearing of the Investigations on Source Area Aspects”, *Geologisches Jahrbuch*, D100, pp. 247-311

Hirdes, W., Davis, D. W. and Eisenlohr, B. N. (1992), "Reassessment of Proterozoic Granitoid Ages in Ghana on the Basis of U/Pb Zircon and Monazite Dating." *Precambrian Research*, Vol. 56, pp. 89-96.

Hugh, R. R. (1993), *Using Geochemical Data: Evaluation, Presentation, Interpretation*, John Wiley and Sons Press, 384 pp.

Hutchison, C. S. (1974), *Laboratory Handbook of Petrographic Techniques*, John Wiley and Sons Press, 527 pp.

Jessell, M. and Liégeois, J.-P. (2015), “100 years of research on the West African Craton”, *Journal of African Earth Sciences*, Vol. 112 pp. 377 – 381

Joảo, B. G. T., Jorge, A. B., Carlson, M. M. L., Johildo, S. F. B., Carlos, E. S. C. and Valter, M. C. F. (2001), “Gold mineralisation in the Serra de Jacobina region, Bahia Brazil:

tectonic frameworkand metallogenesis", *Springer-Verlag, Mineralium Deposita* Vol. 36 pp. 332-344

Junner, N. R., Hirst, T. and Service, H. (1942), "The Tarkwa Goldfield." *Gold Coast Geological Survey Memoir* 6.

Junner, N. R. (1940), "Geology of the Gold Coast and Western Togoland." *Gold Coast Geological Survey Bulletin* No.11, 40 pp.

Kesse, G. O. (1985), *The Mineral and Rock Resources of Ghana*. A. A. Balkema, Rotterdam, 610 pp.

Ledru, P., Milesi, J. P., Johan, V., Sabaté, P. and Maluski, H. (1997), "Foreland Basins and Gold-bearing Conglomerates: a new model for the Jacobina Basin São Francisco Province, Brazil." *Precambrian Research* 86. pp. 155-176.

Leube, A., Hirdes, W., Mauer, R. and Kesse, G. O. (1990), "The Early Proterozoic Birimian Supergroup of Ghana and Some Aspects of its Associated Gold Mineralisation", *Precambrian Research*, Vol. 46, pp. 136-165.

Lof, P. (1982), *Elsevier's Mineral and Rock Table*. Elsevier Science, 1 pp.

Marston, R. J., Woolrich, P. and Kwesie, J. (1992), "Closely associated stockwork and palaeoplacer gold mineralization in the early Proterozoic Tarkwaian System of Abosso, SW Ghana. In: Peters, J.W., Kesse, G.O. and Acquah. P.C. (Eds.), Regional Trends in African Geology, Proceedings of the 9th International Geological Conference, Accra. pp. 243-271.

McLennan, S. M. (1989), "Rare Earth Elements in Sedimentary Rocks: Influence of Provenance and Sedimentary Processes", *Rev. Mineral.*, Vol.2, pp. 169-200

Milesi, J. P., Ledru, P., Marcoux, E., Mougeot, R., Johan, V., Lerouge, C., Sabaté, P., Bailly, L., Respaut, J. P. and Skipwith, P. (2002) "The Jacobina Palaeoproterozoic gold-bearing conglomerates, Bahia, Brazil: a ''hydrothermal shear-reservoir'' model.", Ore Geology Reviews, pp. 95-136

Milesi, J. P., Ledru, P., Feybesse, J. L., Dommanget A. and Marcoux E. (1992), "Early Proterozoic Ore Deposits and Tectonics of the Birimian Orogenic Belt, West Africa". *Precambrian Research*, Vol. 58, pp. 305-344.

Milesi, J. P., Ledru, P., Ankrah, P., Johan V, Marcoux, E. and Vinchon, C. (1991), "The Metallogenetic Relationship Between Birimian And Tarkwaian Gold Deposits in Ghana." *Mineralium Deposita*, Vol. 26, pp. 228-238.

Miyashiro, A. (1961), “Evolution of metamorphic belts”, *Journal of Petrology*, Vol. 2, pp. 277-311

Molinari, L. and Scarpelli, W. (1988), “Depósitos de Ouro de Jacobina. In: Schobbenhaus C, Coelho CES (eds) Os Principais Depósitos Minerais do Brasil”, Departamento Nacional da Produção Mineral, Vol. 3, pp. 463 – 478.

Oberthür, T., Vetter, U., Davis, D. W. and Amanor, J. A. (1998), “Age constraints on gold mineralisation and Palaeoproterozoic Crustal Evolution in the Ashanti belt of Southern Ghana”, *Precambrian Research*, Vol. 80, pp. 129-143.

Osterberg, S. A. (1985), “Stratigraphy and hydrothermal alteration of the Headway Coulee massive sulphide prospect, Northern Onaman area, Northwestern Ontario”. Unpublished. M.Se. Thesis, University of Minnesota at Duluth, 114 pp.

Papon, A. (1973), “Geolgie et Dineralisation du Sun-Ouest de la Côte d’Ivoire”, *Mem BRGM*, Paris, France. 80, 284 pp.

Phillips, G. N. and Powell, R. (2015), “Hydrothermal Alteration in the Witwatersrand Goldfields”, Ore Geology Reviews, 65 (1), pp. 245-273.

Picot, P. and Johan, Z. (1982), *Atlas of Ore Minerals*, Adams Press, 275 pp.

Pigois, J. -P.; Groves, D. I.; Fletcher, I. R.; McNaughton, N. J. and Snee, L. W. (2003), “Age constraints on Tarkwaian Palaeoplacer and Lode-Gold Formation in the Tarkwa-Damang District, SW Ghana.” *Mineralium Deposita*, Vol. 38, pp. 695 - 714.

Robert, F., Poulsen, K. H. and Dubé, B. (1997), “Gold deposits and their geological classification” *Fourth Decennial International Conference on Mineral Exploration* pp. 209-220

Roscoe, S. M. and Card, K. D. (1992), “Early Proterozoic tectonics and metallogeny of the Lake Huron region of the Canadian Shield”, *Precambrian Research*, Vol.58, pp. 99-119.

Sestini, G. (1973), "Sedimentology of a Palaeoplacer: The Gold Bearing Tarkwaian of Ghana; in Amstutz, G. C. and A. J. Bernard (Eds): Ores in Sediments." *Springer-Verlag, Heidelberg* pp. 275-305.

Sharpe, R. (2005), "Stratigraphic and Structural Framework of Hydrothermal and Palaeoplacer Gold Deposits In the Damang District", Unpublished Internal Report, Abosso Gold Fields Limited, 91pp.

Streckeisen, A. L., Zanettin, B. A., Le Bas, M. J., Bonin, B., Bateman, P., Bellieni, G., Dude, A., Efremova, S., Keller, J., Lameyre, J., Sabine, P. A., Schmid, R., Sorensen, H. and Woodley, A. R. (2002), *Igneous rocks; a classification and glossary of terms; recommendations of the International union of Geological Science Subcommission on the Systematics of Igneous Rocks*. Cambridge University Press, Cambridge, U.K., 800 pp.

Streckeisen, A. (1974), "Classification and Nomenclature of Plutonic Rocks, Recommendation of the IUGS Subcommission on Systematics of Igneous Rocks", *Geologische Rundschau. Internationale Zeitschrift fur Geologie*, Stuttgart, Vol. 63, pp. 773-785.

Strogen, P. (1988) "The sedimentology, stratigraphy and structure of the Tarkwaian, Western Region, and its relevance to gold exploration and development. In: Kesse, G.O. (Ed.), Proceedings of the International Conference on the Geology of Ghana with Special Emphasis on Gold", *Geological Society of Ghana, Accra, 1988*, Vol. 3, pp. Hl–H31.

Tagini, B. (1971), "Esquisse Tructurale de la Côte d'Ivoire. Essai de Géotechnique Régionale", In Leube, A., Hirdes, W. Mauer, R. and Kesse, G.O. (eds), The Early Proterozoic Birimian Supergroup of Ghana and Some Aspects of its Associated Gold Mineralisation, *Precambrian Research*, Vol. 46, pp. 136-165.

Trashliev, S. S. (1972), *The geology of 1/4° field sheets 82 (Wiawso SE) and 46 (Asankrangwa NE)*. Ghana Geological Survey (unpublished), Accra. 88 pp.

Tunks, A., Selley D., Roggers, J. and Brabham, G. (2004), "Vein Mineralisation at the Damang Gold Mine, Ghana: Controls on Mineralisation", *Journal of Structural Geology*, Vol. 26 (6-7) pp. 1257-1273.

White, A. J. R. (2011), “The Nature and Origin of Gold Mineralisation at Damang Mine Ghana”, Unpublished PhD Thesis, University of Oxford, 358pp.

Whitney, D. L. and Evans, B. W. (2010), “Abbreviations for Names of Rock-Forming Minerals”, *American Mineralogist*, Vol. 95, pp. 185 - 187.

Wright, J. B., Hastings, D. A. and Jones, W. B. (1985), *Geology and Mineral Resources of West Africa*., G. Allen and Unwin, London, 187 pp.

APPENDIX A: SUMMARY OF HAND SPECIMEN DESCRIPTION

	SAMPLE ID	UTM_E	UTM_N	UTM_RL	GENERAL DESCRIPTION
AMOANDA PIT	D01	623789.472	604790.652	-21.005	Highly altered sandstone with sheared quartz veins.
	D02	623790.230	604791.102	-21.159	Weakly altered sandstone with glassy and milky quartz veins.
	D03	623790.481	604791.715	-20.934	Sandstone with irregular glassy veins and disseminated sulphides.
	D04	623790.392	604792.314	-20.129	Altered sandstone with milky quartz veins along foliation.
	D05	623790.997	604794.344	-19.662	Altered sandstone with milky quartz veins along foliation.
	D06	623790.479	604792.664	-19.693	Sandstone with sugary quartz veins cut by glassy quartz veins which is in turn cut by magnetite rich veins and disseminated sulphides.
	D07	623791.697	604795.952	-19.364	Highly altered sandstone with magnetite and weak disseminated sulphides.
	D08	623792.411	604797.147	-19.731	Highly altered sandstone with spots of glassy quartz and disseminated magnetite.
	D09	623794.823	604802.497	-19.451	Highly silicified sandstone with spots of glassy quartz with disseminated magnetite sulphides.
	D10	623795.904	604804.786	-19.529	Highly silicified sandstone with spots of glassy quartz with disseminated magnetite sulphides. Glassy quartz veins parallel to foliation and porphyritic sulphides with inclusions of magnetite.
	D11	623798.773	604810.066	-19.225	Altered sandstone with banded hematite with pods of glassy and milky quartz.

AMOANDA PIT	D12	623800.597	604813.829	-18.538	Altered sandstone with banded hematite with pods of glassy and milky quartz.
	D13	623801.503	604814.934	-18.786	Sandstone with glassy, tourmalitic quartz vein with pods of grey quartz and sulphides along cleavages.
	D14	623801.120	604814.503	-18.845	Sandsone with brecciated glassy quartz vein.
	D15	623802.899	604820.848	-17.730	Sandstone with disseminated magnetite cut by cubic glassy quartz.
	D16	623801.895	604819.150	-16.990	Altered Sandstone with pink feldspar cut by glassy and milky quartz.
	D17	623785.440	604745.856	-25.614	Sandstone cut by horizontal glassy quartz veins with occasional sulphide.
	D18	623807.180	604721.107	-25.774	Highly silicified current bedded with disseminated magnetite.
	D19	623846.198	604757.596	-31.044	Sandstone with glassy, fractured and tourmaline quartz vein.
	D20	623844.853	604756.629	-30.864	Quartzofeldspathic coarse grain sugary vein with disseminated magnetite.
	D21	623803.827	604717.387	-24.857	Altered quartzite with sugary glassy quartz and disseminated sulphides
	D22	623684.723	604515.259	27.847	Unaltered quartzite with no disseminated sulphides.
	D23	623683.984	604515.464	27.182	Unaltered quartzite with no disseminated sulphides.
	D24	623695.335	604529.852	25.662	Quartzite with lensitic glassy quartz vein.

SADDLE PIT	D25	628544.242	610094.862	-48.639	Unaltered mafic intrusive with no disseminated sulphides.
	D26	628548.266	610097.323	-48.379	Mafic Intrusive in contact with quartzite and vein with occasional sulphides.
	D27	628537.800	610161.270	-50.283	Mafic intrusive with carbonate alteration and irregular quartz veins.
	D28	628631.195	610210.489	-47.039	Mafic Intrusive in association quartz veins.
	D29	628495.214	610195.894	-49.100	Pink altered quartzite with quartz veins and disseminated sulphides.
	D30	628510.214	610085.051	-59.121	Pink altered quartzite with quartz veins, magnetite and disseminated sulphides.
	D31	628480.312	610071.800	-59.851	Well matured banket conglomerate with smoky quartz veins and disseminated sulphides.
	D32	628479.769	610042.268	-59.813	Altered banket conglomerate with disseminated sulphides.
	D33	628470.731	610034.151	-58.166	Altered banket conglomerate with quartz veins and disseminated sulphides.
	D34	628554.603	610190.219	-52.578	Poorly matured unaltered banket conglomerate with no veins and no sulphides.
	D35	628564.436	610199.817	-51.522	Unaltered banket conglomerate with no veins and no sulphides
	D36	628571.659	610206.660	-50.940	Mediumly matured banket conglomerate with sulphides

APPENDIX B: MINERAL ABBREVIATIONS
(After Whitney and Evans, 2010)

SYMBOL	MINERAL
Amp	Amphibole
Opq	Opaque Mineral
Pl	Plagioclase
Py	Pyrite
Qz	Quartz

APPENDIX C: POST-ARCHEAN AVERAGE AUSTRALIAN SEDIMENTARY ROCK (PAAS) VALUES

Elements	Post-Archean Average Australian Sedimentary rock (PAAS) (ppm)
La	38
Ce	80
Pr	8.9
Nd	32
Sm	5.6
Eu	1.1
Gd	4.7
Tb	0.77
Dy	4.4
Ho	1
Er	2.9
Tm	0.5
Yb	2.8
Lu	0.5
Y	28

APPENDIX D: PRIMITIVE MANTLE VALUES (PMV)

Elements	Primitive Mantle Values (ppm)
La	0.695
Ce	1.8
Pr	0.274
Nd	1.34
Sm	0.436
Eu	0.165
Gd	0.584
Tb	0.107
Dy	0.721
Ho	0.161
Er	0.473
Yb	0.475
Lu	0.0724
Y	4.47
Tm	0.7027

APPENDIX E: WHOLE ROCK ANALYSIS

SAMPLE ID	D01	D06	D16	D22	D25	D26	D27	D31	D32	D33	D34	D36
Oxide wt%												
SiO_2	74.6	76.7	50.1	78.4	46.3	50.4	51.5	66.7	86.9	85.5	89.1	82
Al_2O_3	10.55	9.92	26.6	10.8	16.75	14.05	15.6	13.6	6.82	6.86	3.96	7.15
FeO_t	5.24	4.79	9.08	3.97	10.15	8.26	9.41	9.98	3.17	3.54	4.35	4.79
CaO	1.3	1.23	1.1	1.33	8.33	10.25	7.79	1.14	0.26	0.53	0.88	0.94
MgO	0.57	0.53	0.61	0.66	10.45	6.93	6.72	0.99	0.37	0.5	0.34	0.53
Na_2O	1.16	1.58	1.46	1.82	2.19	2.52	2.46	1.89	0.41	0.99	0.4	0.9
K_2O	2.25	1.8	7.06	2.01	1.23	0.27	1.1	1.85	1.38	0.91	0.72	1.04
Cr_2O_3	0.013	0.014	0.02	0.011	0.064	0.047	0.032	0.022	0.009	0.012	0.018	0.015
TiO_2	0.36	0.29	0.93	0.26	0.52	0.42	0.53	0.63	0.24	0.23	0.23	0.32
MnO	0.07	0.08	0.05	0.09	0.12	0.14	0.18	0.12	0.09	0.08	0.1	0.11
P_2O_5	0.03	0.02	0.16	0.02	0.1	0.03	0.09	0.02	0.04	0.07	0.02	0.05
SrO	0.02	0.03	0.08	0.03	0.03	0.08	0.05	0.02	<0.01	0.01	0.01	0.02
BaO	0.09	0.09	0.32	0.11	0.06	0.01	0.04	0.1	0.05	0.05	0.04	0.05
LOI	1.85	1.91	4.19	2.24	3.82	7.26	5.05	2.85	0.87	0.87	1.09	1.43
Total	**98.10**	**98.98**	**101.76**	**101.75**	**100.11**	**100.67**	**100.55**	**99.91**	**100.61**	**100.15**	**101.26**	**99.35**
Au (g/t)	0.18	0.03	0.03	<0.01	0.03	10.10	0.07	24.77	0.30	3.64	0.05	0.17

APPENDIX E: WHOLE ROCK ANALYSIS (CONT'D)

SAMPLE ID	D01	D06	D16	D22	D25	D26	D27	D31	D32	D33	D34	D36
Trace Elements (ppm)												
Ba	815	819	2910	983	496	90.9	400	872	454	451	389	470
Ce	52	52.4	83.3	43.3	19.3	15.3	18.3	88.7	34.5	32.8	39.9	58
Cr	100	110	150	80	480	350	250	160	70	90	130	120
Cs	3.08	2.07	6.67	2.64	4.09	0.92	2.83	2.86	1.82	1.8	1.53	2.07
Dy	3.11	1.23	5.48	1.93	2.44	2.04	2.8	3.87	2.33	2.27	1.73	2.72
Er	1.88	0.7	3.34	1.17	1.64	1.26	1.79	2.37	1.57	1.44	1.01	1.64
Eu	1.05	0.9	1.67	0.78	0.74	0.67	0.82	1.43	0.71	0.67	0.63	1.01
Ga	13.1	11.1	35.8	11.9	14.9	12.9	14.8	17.7	8.2	9.1	5.5	9.2
Gd	3.27	1.92	6	2.51	2.25	2.11	2.62	4.45	2.37	2.49	1.99	3.28
Hf	3.3	3	10.8	2	1.7	1.3	1.6	6.9	2.2	2.1	3.2	3.5
Ho	0.68	0.23	1.19	0.38	0.53	0.45	0.64	0.77	0.51	0.48	0.35	0.53
La	27	27.8	39.4	23	9	7.4	8.7	43	17.1	16.7	19.4	28.7
Lu	0.3	0.12	0.51	0.17	0.26	0.2	0.29	0.38	0.22	0.22	0.16	0.22
Nb	4	3.1	8.6	2.9	2	1.6	2.1	6.6	2.8	2.7	2.1	3.2
Nd	21.5	21	36.2	17.5	9.7	7.9	9.4	32.6	14.3	13.8	14.3	21.7
Pr	6.01	5.93	9.71	4.89	2.43	1.9	2.28	9.13	3.88	3.8	4.2	6.24
Rb	53.1	41.7	158.5	46.3	40.1	4.8	36	58.6	36.2	28.2	24.5	37.9
Sm	3.75	3.25	6.45	3.03	2.07	1.68	2.1	5.38	2.57	2.53	2.42	3.95
Sn	1	1	2	1	1	<1	1	1	1	1	<1	1
Sr	238	257	679	329	330	665	491	218	67.5	96.9	69.6	198.5
Ta	0.4	0.4	0.7	0.4	0.3	0.1	0.1	0.5	0.3	0.3	0.2	0.4
Tb	0.51	0.24	0.91	0.34	0.38	0.31	0.43	0.65	0.43	0.38	0.29	0.47
Th	3.45	3.87	9.06	4.18	1.29	1.03	1.26	10.95	2.76	2.41	5.03	6.77
Tm	0.27	0.1	0.52	0.16	0.23	0.19	0.27	0.36	0.25	0.22	0.13	0.22
U	0.77	0.86	1.99	0.6	0.57	0.46	0.53	2.38	0.82	0.85	0.86	1.27
V	72	68	172	57	146	118	174	166	59	69	62	76
W	6	6	10	4	6	13	17	19	5	6	2	2
Y	18.2	6.9	32.6	10.6	14.5	12.1	17.4	22.4	14.2	12.8	9.6	15.2
Yb	1.84	0.67	3.37	1.08	1.59	1.33	1.86	2.43	1.53	1.46	0.88	1.53
Zr	127	125	457	86	64	51	62	278	91	82	128	145

INDEX

C

Q